INTEGRATION OF EXPERIMENTAL AND COMPUTATIONAL APPROACHES TO PHYSIOLOGICALLY BASED PHARMACOKINETIC MODELING OF TRIADIMEFON AND TRIADIMENOL

by

SUSAN RITGER CROWELL

(Under the Direction of Jeffrey W. Fisher)

ABSTRACT

A physiologically based pharmacokinetic (PBPK) model was experimentally parameterized and constructed for the conazole fungicides triadimefon and triadimenol. *In vitro* metabolic parameters for reduction of triadimefon to its primary metabolite, triadimenol, were measured in male and female Sprague-Dawley rats and CD-1 mice. Partition coefficients for triadimefon and triadimenol were measure *in vitro* in Sprague-Dawley rat tissues. A pharmacokinetic study of triadimefon and triadimenol disposition was performed following intravenous exposure to 50 mg/kg triadimefon in male Sprague-Dawley rats. Measured *in vitro* metabolic parameters and partition coefficients were incorporated into a PBPK model for triadimefon and triadimenol, and model simulations were compared to the pharmacokinetic data. The model could not adequately predict the complex distribution of both parent and metabolite during the clearance phase. Two possible explanations for this behavior were explored using alternate PBPK models: blood and tissue binding of triadimefon and triadimenol, and reverse metabolism of triadimenol to triadimefon. While the model with blood and tissue binding provided the best simulations of pharmacokinetic data, the individual binding parameters for

each tissue were fit to the single pharmacokinetic data set, and the model lacked parsimony. The model with bidirectional metabolism (i.e. triadimefon reduction to triadimenol, and triadimenol oxidation to triadimefon) provided an improved fit relative to the original model, as well as a probable explanation supported by the available literature for the observed behavior. All three models were extrapolated to humans using human metabolic parameters, and human equivalent doses were calculated for dosimetrics from simulation of rat no observed adverse effects level (NOAEL) oral exposure. Comparison to oral reference dose for triadimefon in humans indicated that the value was sufficiently protective of human health.

Finally, three methods of partition coefficient determination were compared for triadimefon and triadimenol: *in vitro* measurement, calculation from area under the curve for chemical concentration in *in vivo* pharmacokinetic data, and calculation by algorithm incorporating chemical- and tissue-specific information. The reverse metabolism model was employed to illustrate the differences between these methods. It was found that the algorithm method may over-estimate partition coefficient values, while *in vitro* and *in vivo* methods provided similar outcomes.

INDEX WORDS: PBPK, Pesticides, Conazoles, Triadimefon, Triadimenol, Metabolism, Risk assessment, Human equivalent dose, Partition coefficients

INTEGRATION OF EXPERIMENTAL AND COMPUTATIONAL APPROACHES TO PHYSIOLOGICALLY BASED PHARMACOKINETIC MODELING OF TRIADIMEFON AND TRIADIMENOL

by

SUSAN RITGER CROWELL

B.S.A., The University of Georgia, 2005

A Dissertation Submitted to the Graduate Faculty of The University of Georgia in Partial Fulfillment of the Requirements for the Degree

DOCTOR OF PHILOSOPHY

ATHENS, GEORGIA

2009

INTEGRATION OF EXPERIMENTAL AND COMPUTATIONAL APPROACHES TO PHYSIOLOGICALLY BASED PHARMACOKINETIC MODELING OF TRIADIMEFON AND TRIADIMENOL

by

SUSAN RITGER CROWELL

Major Professor: Jeffrey W. Fisher

Committee: Marsha Black
Julie Coffield
John F. Kenneke
W. Matthew Henderson

Electronic Version Approved:

Maureen Grasso
Dean of the Graduate School
The University of Georgia
December 2009

ACKNOWLEDGEMENTS

Innumerable people have assisted with the design and completion of this research, and I am incredibly grateful for their support, patience, and encouragement, all of which has been instrumental in making this work a success. First, I would like to thank Dr. Roger Wyatt, who believed in me from day one, and illuminated the path forward. My sincere thanks go to my graduate committee members, Drs. John F. Kenneke, W. Matthew Henderson, Marsha Black, and Julie Coffield. I am particularly indebted to my advisor, Dr. Jeffrey W. Fisher, without whose confidence in my capability as a modeler and scientist, and ability to find funding in nooks and crannies (not to mention kindness to displaced graduate students), I would not have completed this research or this degree.

To my beloved husband and dear friends, thank you for teaching me computer speak, helping to edit esoteric passages on computational modeling, for feeding me when I forgot, and for making the years spent working towards this degree the most joyous I have yet had the pleasure of experiencing.

I am grateful for the unending support of my family, who by and large have been *here* before. Thank you for the love of science and learning you instilled in me, and the encouragement you have provided as I have pursued this degree and everything that came before it. And Dad, thanks for telling me so long ago that artists and English majors can most often be found delivering pizzas – the message, while delivered sarcastically (our language, I suppose), did in fact hit home.

TABLE OF CONTENTS

LIST OF TABLES

Page

LIST OF FIGURES

Page

CHAPTER 1

INTRODUCTION

Physiologically based pharmacokinetic (PBPK) models are increasingly important to the chemical risk assessment process. PBPK models are mathematical descriptions of chemical disposition within an organism that facilitate the estimation of internal dose, or the amount of chemical that reaches target tissues. Traditional paradigms for chemical risk assessment rely on extrapolation from *in vivo* rodent toxicity studies for estimates of relevant human exposure levels; PBPK models provide a quantitative tool for this extrapolation. Additionally, PBPK models allow for the synthesis of *in vitro, in vivo,* and mechanistic data, whereas traditional approaches relied only upon *in vivo* rodent studies for derivation of regulatory exposure limits. This dissertation includes the measurement of metabolic parameters and partition coefficients for triadimefon and its primary metabolite triadimenol, and the incorporation of these into a PBPK model.

Purpose of the Study

The purpose of this study was to address the hypothesis that an iterative approach synthesizing computational modeling and experimental research will result in a robust PBPK model for triadimefon and triadimenol, and that this model will be useful for the design of future research. Thus, this research was undertaken to provide a proof-of-concept illustration of the harmonization of experimental and computational approaches to chemical risk assessment, and to develop the first PBPK model for the conazole fungicides. The experimental portion of this research included the measurement of *in vitro* metabolic kinetic parameters in rodent hepatic

microsomes, and of *in vitro* partition coefficients in various tissues of adult male Sprague Dawley rats. Additionally, a study of triadimefon and triadimenol disposition following intravenous (IV) triadimefon exposure in adult male Sprague Dawley rats was undertaken to provide pharmacokinetic data for PBPK model parameterization and partial validation. On these experimental foundations, a PBPK model was developed for the Sprague Dawley rat, and based on available physiological and chemical specific data, the model was extrapolated to humans. The extrapolated human model was used for the derivation of human equivalent doses (HEDs) for the no observed adverse effects level (NOAEL) dose from the relevant regulatory study in rats. Subsequently, different approaches for the determination of partition coefficients were investigated and compared as they relate to PBPK modeling efforts.

Scope of the Dissertation

This dissertation includes a literature review (Chapter 2) of available experimental research on conazole fungicides and triadimefon and triadimenol in particular, as well as computational modeling efforts for non-volatile pesticides. While the conazole family of fungicides has been heavily researched, there is little data appropriate for inclusion in PBPK models for triadimefon or triadimenol; indeed, no PBPK models have yet been reported in the literature for any of the conazoles.

Chapter 3 focuses on the influence of gender of species on the metabolism of triadimefon to triadimenol by rodent hepatic microsomes. This chapter has been submitted to *Toxicology Letters* as of October, 2009. Portions of Chapter 3 were presented at the Society of Toxicology annual conference (March, 2007; Seattle, WA). Chapter 4 reports the development of the PBPK model for triadimefon and triadimenol, as well as experimental measurement of partition coefficients and the pharmacokinetic data set of triadimefon in Sprague Dawley rats; this will be

submitted to *Toxicology and Applied Pharmacology*. In Chapter 5, three different methods of partition coefficient determination are explored with respect to triadimefon and triadimenol. Chapter 6 summarizes the conclusions and importance of these studies, and identifies future research that will build upon this body of work.

CHAPTER 2

LITERATURE REVIEW

Conazole Fungicides

Conazoles (1,2,4 triazoles and imidazoles) are a large class of agricultural and pharmaceutical fungicides. The mechanism of fungicidal action centers upon the inhibition of 14-lanosterol α demethylase (cytochrome P450 51), thereby disrupting ergosterol biosynthesis (Buchenauer, 1977). Ergosterol is a major constituent of fungal cell walls, contributing to their integrity and fluidity; its absence leads to fungal death. In vertebrates, which have neither cell walls nor ergosterol, lanosterol demethylase participates in the biosynthetic pathway of cholesterol. This biomolecule is important not only to cell membrane integrity, but also as a precursor to steroid hormones and other endogenous compounds. Because of their effect on cholesterol biosynthesis, it has been proposed that conazoles may interfere with steroid homeostasis and related aspects of normal mammalian physiology (Vinggaard et al., 2000; Zarn et al., 2003). In exposed mammals, conazoles have also been illustrated to modulate the activity and expression of cytochrome P450 (CYP) enzymes (Allen et al., 2006; Barton et al., 2006; Goetz et al., 2006; Ronis et al., 1994; Sun et al., 2006), potentially affecting the metabolism of a wide variety of xenobiotics and endogenous compounds. Additionally, several conazole fungicides are tumorigenic in rodents, causing thyroid follicular cell tumors in rats and mice, as well as liver adenomas in mice (FAO/WHO, 2004; Hurley et al., 1998).

Triadimefon and Triadimenol

Triadimefon is a broad-spectrum conazole fungicide with applications in agriculture and landscaping. It is a lipophilic, non-volatile pesticide with pre-planting, foliar, and post-harvest applications. The application of triadimefon to food products was recently limited to pineapples, though previously it was also applied to grapes, apples, pears, and raspberries (U.S. EPA, 2006). Non-food uses are now limited to commercial landscaping, pine seedlings, Christmas trees, and golf courses, though prior to the recent re-registration eligibility decision, it was also used for residential applications (U.S. EPA, 2006). The United States Environmental Protection Agency (U.S.EPA) estimates an application rate of approximately 135,000 lbs/year with an upper-end estimate of 266,000 lbs/year (U.S. EPA, 2006).

In vertebrates, triadimefon is metabolized by 11β-hydroxysteroid dehydrogenase type 1 (11β-HSD1) to the carbonyl reduction product and primary metabolite, triadimenol (Kenneke et al., 2008). Triadimenol retains the fungicidal activity of the parent compound and is sold as a commercial fungicide, applied at a rate of 24,000 lbs/year (U.S. EPA, 2006). Triadimenol is used a seed treatment for cotton and grains, including barley, corn, oats, rye, sorghum, and wheat (U.S. EPA, 2006). Oxidation of the *t*-butyl group of triadimenol results in alcohol and carboxylic acid derivatives (Roberts and Hutson, 1999). Triadimenol and subsequent metabolites are also conjugated via phase II metabolism, yielding mainly glucuronide conjugates (FAO/WHO, 1981). A proposed metabolic pathway for triadimefon and triadimenol in mammals appears in Figure 2.1.

Human exposures to triadimefon and its metabolite triadimenol occur most frequently via inhalation and dermal absorption for occupational and residential handlers, as well as through oral ingestion of contaminated food products or drinking water (U.S.EPA, 2006). The oral

reference doses (RfD) for human exposure to triadimefon or triadimenol are both 0.034 mg/kg/day (U.S. EPA, 2006).

A range of toxic effects have been observed following exposure to triadimefon and triadimenol in laboratory animals. Observed reproductive and developmental toxicity, as well as tumorigenicity, are held in common with other members of the conazole class (Zarn et al., 2003). Teratogenic effects observed subsequent to *in vivo* exposure to non-maternotoxic doses (300 mg/kg) of triadimefon by oral gavage included craniofacial and axial skeletal defects in the mouse (Menegola et al., 2005a). In *in vitro* studies of whole Sprague-Dawley rat embryos, triadimefon and triadimenol (125 – 250 µM) have been observed to induce changes in neural crest cell migration and subsequent malformations in branchial arches and branchial nerves (Menegola et al., 2005b). These *in vitro* results support the hypothesized teratogenic mechanism involving triadimefon and triadimenol interaction with retinoic acid levels in the developing embryo (Di Renzo et al., 2009). Delayed reproductive development in Wistar rats after exposure to triadimefon has been attributed to the perturbation of steroid homeostasis (Goetz et al., 2007), as has reduced male/female sex ratio and female fertility index (FAO/WHO, 1985; Zarn et al., 2003). In 24 month feeding studies with 0, 50, 300, and 1800 ppm triadimefon, male, but not female, CF_1/W mice showed a dose dependent increase in liver adenomas (FAO/WHO, 2004).

Triadimefon and its primary metabolite triadimenol are unique among conazoles in eliciting neurotoxic effects (Crofton, 1996), and indeed regulatory decisions center on neurotoxicity as the sensitive endpoint (U.S. EPA, 2006). In the critical study for regulatory standards, which was performed by the registrant of the pesticide, male and female rats respectively received 54.6 or 68.7 mg/kg/day triadimefon in the diet for 4 weeks, and displayed hyperactivity (U.S. EPA, 2006). The NOAEL from this study, 3.4 mg/kg/day, has been used with

an applied uncertainty factor of 100 for derivation of the oral RfD for human exposure of 0.034 mg/kg/day (U.S. EPA, 2006). Neurotoxicity consisting of stereotyped behavior and hyperactivity has also been observed in Sprague Dawley rats following single administration oral gavage of 50 – 200 mg/kg bw triadimefon. Subsequent necropsy of the central nervous system indicated the mechanism of triadimefon induced neurotoxicity may involve alteration of monoamine (*e.g.* dopamine and/or serotonin) metabolism (Walker et al., 1990; Crofton et al., 1996), likely as a monoamine oxidase inhibitor (Gagnaire and Micillino, 2006). Notably, female rats were found to recover from triadimefon induced intoxication more slowly than males, with some effects lingering for several days (Moser and MacPhail, 1989).

There is limited data available on human exposure to triadimefon or its metabolite, triadimenol. Triadimefon and triadimenol were measured in the urine and serum of occupationally exposed volunteers (Fernandez et al., 2001; Vazquez et al., 2002). Tissues were analyzed for each chemical, but metabolism of triadimefon to triadimenol was not assessed; volunteers were exposed separately to each of the fungicides. Both studies were mainly qualitative explorations of methodological approaches to measuring azole pesticides in human biological samples. For urine, there is a time course of triadimefon and triadimenol concentration, indicating that by 13 hours post-exposure, all measureable quantities of both pesticides had been eliminated (Fernandez et al., 2001). There is no time course available for serum concentrations.

Gender and Species Comparisons

There has been a great deal of research focused on the differences in metabolism of endogenous compounds and xenobiotics between males and females of common laboratory species. The consensus is that, in general, male and female rats display the greatest differences in

rates of xenobiotics metabolism, with males having higher maximum metabolic rates than females. This applies generally to substrates of CYP enzymes, especially 2A and 2C isoforms (Mugford and Kedderis, 1998). Similar gender differences are much less pronounced in other organisms, including mice, and are difficult to observe in humans due to intraspecies variation (Mode and Gustafsson, 2006). This itself speaks to possible differences in metabolism of endogenous compounds and xenobiotics between different species.

Recently, our laboratory focused on elucidation of the enzyme responsible for triadimefon metabolism in hepatic microsomes. It was found that a microsomal carbonyl reductase, 11β-hydroxysteroid dehydrogenase type 1 (11β-HSD1), is responsible for the reduction of triadimefon to triadimenol (Kenneke et al., 2008). Together with 11β-hydroxysteroid dehydrogenase type 2, 11β-HSD1 is responsible for the regulation of the availability of active glucocorticoids to localized steroid receptors, and has been observed to metabolize both reduction and oxidation of xenobiotics *in vitro* (Diederich et al., 2000; Kenneke et al., 2008; Maser and Bannenberg, 1994; Seckl and Walker, 2001). Whether or not there are differences in activity or expression of this enzyme between common laboratory animals and humans is not known. In order to provide a basis for extrapolation using a PBPK model of triadimefon ADME, understanding these differences between species, in a common assay, would be a valuable asset.

PBPK Modeling

In the past two decades, physiologically based pharmacokinetic (PBPK) modeling has come to play an increasingly important role in hypothesis driven toxicity research and in chemical risk assessment, a fact which has been reviewed previously (Clewell and Clewell, 2008; Leung and Paustenbach, 1995; Thompson et al., 2008). PBPK models are mathematical

representations of the anatomical and physiological features of an organism, as well as chemical specific information on a compound of interest, which together dictate a chemical's absorption, distribution, metabolism, and elimination (ADME) in that organism. Models are informed by the breadth of the scientific literature on pharmacokinetics and toxicity. PBPK models facilitate quantitatively based estimation of internal exposure, or the amount of a chemical of interest that reaches a target organ or tissue depot subsequent to a defined exposure scenario. Because they attempt to explain chemical disposition by mathematical description of physiological and ADME processes, the resulting models can be extrapolated to different exposure scenarios including high-to-low dose, route-to-route, and animal-to-human extrapolations.

Currently, there are no published PBPK models for any of the conazole fungicides. Additionally, there are no adequately detailed pharmacokinetic data available for triadimefon or triadimenol in any laboratory species or in humans. While a time course of triadimefon in human urine has been reported, the focus of the research was largely methodological and qualitative, and the data lacks sufficient identifying information, rendering it unusable for modeling purposes (Fernandez et al., 2001).

Partition Coefficient Determination

Partition coefficients describe the distribution of a chemical between two adjacent phases at equilibrium, such as blood and air, or blood and tissue. Partition coefficients are a critical facet of PBPK models, and there are a variety of published methods for their measurement or estimation. For non-volatile compounds, such as triadimefon and triadimenol, methods for *in vitro* partition coefficient determination have been published (Jepson et al., 1994). This approach has been used in several PBPK models, including for ethylene glycol and its metabolites (Corley et al., 2005), the metabolites of trichloroethylene (Fisher et al., 1998), and

bisphenol A (Kawamoto et al., 2007). Alternatively, an empirical proxy to partition coefficients can be calculated from pharmacokinetic data sets as the ratio of area under the concentration curve (AUC) in tissue to AUC in blood (Gallo et al., 1987; King et al., 1983; Lam et al., 1981); this approach has been used for PBPK models of deltamethrin (Mirfazaelian et al., 2006). An entirely computational method of partition coefficient determination is calculation by algorithm incorporating tissue composition information and chemical specific octanol-water partition coefficients (Poulin and Krishnan, 1996). This method has been used for a number of PBPK models, including other pesticides (Pelekis and Emond, 2009; Campbell, 2009; Timchalk and Poet, 2007; Zhang et al., 2000). Despite the availability of methods, there are currently no published data on partition coefficients for any of the conazole fungicides.

References

Allen, J.W., D.C. Wolf, M.H. George, S.D. Hester, G. Sun, S.F. Thai, D.A. Delker, T. Moore, C. Jones, G. Nelson, B.C. Roop, S. Leavitt, E. Winkfield, W.O. Ward, and S. Nesnow (2006). Toxicity profiles in mice treated with hepatotumorigenic and non-hepatotumorigenic triazole conazole fungicides: propiconazole, triadimefon, and myclobutanil. *Toxicologic Pathology* 34, 853 – 862.

Barton, H.A., J. Tang, Y.M. Sey, J.P. Stanko, R.N. Murrell, J.C. Rockett, and D.J. Dix (2006). Metabolism of myclobutanil and triadimefon by human and rat cytochrome P450 enzymes and liver microsomes. *Xenobiotica* 36, 793 – 806.

Buchenauer, H. (1977). Mode of action of triadimefon in *Ustilago avenae*. *Pesticide Biochemistry and Physiology* 7, 309 – 320.

Campbell, A. (2009). Development of PBPK model of molinate and molinate sulfoxide in rats

and humans. *Regulatory Toxicology and Pharmacology* 53, 195-204.

Clewell, R.A., and H.J. Clewell (2008). Development and specification of physiologically based pharmacokinetic models for use in risk assessment. *Regulatory Toxicology and Pharmacology* 50, 129 – 143.

Corley, R.A., M.J. Bartels, E.W. Carney, K.K. Weitz, J.J.Soelberg, R.A. Gies, and K.D. Thrall (2005). Development of a physiologically based pharmacokinetic model for ethylene glycol and its metabolite, glycolic acid, in rats and humans. *Toxicological Sciences* 85, 476 – 490.

Crofton, K.M. (1996). A structure-activity relationship for the neurotoxicity of triazole fungicides. *Toxicology Letters* 84, 155 – 59.

Di Renzo, F., E. Corsin, M.L. Broccia, M. Marinovich, C.L.Galli, E. Giavini, and E. Menegola (2009). Molecular mechanisms of teratogenic effects induced by the fungicide triadimefon: study of the expression of TGF-β mRNA and TGF-β and CRABPI proteins during rat *in vitro* development. *Toxicology and Applied Pharmacology* 234, 107 – 116.

Diederich, S., E. Eigendorff, P. Burkhardt, M. Quinkler, C. Bumke-Vogt, M. Rochel, D. Seidelmann, P. Esperling, W. Oelkers, and V. Bahr (2000). 11β-Hydroxysteroid dehydrogenase types 1 and 2: an important pharmacokinetic determinant for activity of synthetic mineralo- and glucocorticoids. *The Journal of Clinical Endocrinology & Metabolism* 87, 5695 – 5701.

FAO/WHO (1981). Pesticide Residues in Food: 1981 evaluations. http://www.inchem.org/documents/jmpr/jmpmono/v81pr32.htm

FAO/WHO (1985). Pesticide Residues in Food: 1985 evaluations. http://www.inchem.org/documents/jmpr/jmpmono/v85pr18.htm

FAO/WHO (2004). Pesticide Residues in Food 2004, Evaluations, FAO Plant Production and Protection Paper, 178 pp. 231 – 241. World Health Organization and Food and Agriculture Organization of the UN, Rome.

Fernandez, J.M., J.L.M. Vidal, P.P. Vazquez, and A.G. Frenich (2001). Application of restricted-access media column in coupled-column RPLC with UV detection and electrospray mass spectrometry for determination of azole pesticides in urine. *Chromatographia* 53, 503 – 509.

Fisher, J.W., D. Mahle, and R. Abbas (1998). A human physiologically based pharmacokinetic model for trichloroethylene and its metabolites, trichloroacetic acid and free trichloroethanol. *Toxicology and Applied Pharmacology* 152, 339 – 359.

Gagnaire, F. and J.C. Micillino (2006). Effects of triadimefon on extracellular dopamine, DOPAC, HVA and 5-HIAA in adult rat striatum. *Toxicology* 217, 91 – 104.

Gallo, J.M., F.C. Lam, and D.G. Perrier (1987). Area method for the estimation of partition-coefficients for physiological pharmacokinetic models. *Journal of Pharmacokinetics and Biopharmaceutics* 15, 271 – 280.

Goetz, A.K., W. Bao, H. Ren, J.E. Schmid, D.B. Tully, C. Wood, J.C. Rockett, M.G. Narotsky, G. Sun, G.R. Lambert, S.F. Thai, D.C. Wolf, S. Nesnow, and D.J. Dix (2006). Gene expression profiling in the liver of CD-1 mice to characterize the hepatotoxicity of triazole fungicides. *Toxicology and Applied Pharmacology* 215, 274 – 284.

Goetz, A.K., H. Ren, J.E. Schmid, C.R. Blystone, I. Thillainadarajah, D.S. Best, H.P. Nichols, L.F. Strader, D.C. Wolf, M.G. Narotsky, J.C. Rockett, and D.J. Dix (2007). Disruption of testosterone homeostasis as a mode of action for the reproductive toxicity of triazole fungicides in the male rat. *Toxicological Sciences* 95, 227 – 239.

Hurley, P.M., R.N. Hill, and R.J. Whiting (1998). Mode of carcinogenic action of pesticides inducing thyroid follicular cell tumors in rodents. *Environmental Health Perspectives* 106, 437 – 445.

Jepson, G.W., D.K. Hoover, R.K. Black, J.D. McCafferty, D.A. Mahle, and J.M. Gearhart (1994). A partition coefficient determination method for nonvolatile chemicals in biological tissues. *Fundamental and Applied Toxicology* 22, 519 – 524.

Kawamoto, Y., W. Matsuyama, M. Wada, J. Hishikawa, M.P.L. Chan, A. Nakayama, and S. Morisawa (2007). Development of a physiologically based pharmacokinetic model for bisphenol A in pregnant mice. *Toxicology and Applied Pharmacology* 224, 182 – 191.

Kenneke, J.F, C.S. Mazur, S.E. Ritger, and T.J. Sack (2008). Mechanistic investigation of the non-cytochrome P450-mediated metabolism of triadimefon to triadimenol in hepatic microsomes. *Chemical Research in Toxicology* 21, 1997 – 2004.

King, F.G., R.L. Dedrick, J.M. Collins, H.B. Matthews, and L.S. Birnbaum (1983). Physiological model for the pharmacokinetics of 2,3,7,8-tetrachlorodibenzofuran in several species. *Toxicology and Applied Pharmacology* 67, 390 – 400.

Lam, G., M. Chen, and W.L. Chiou (1981). Determination of tissue to blood partition coefficients in physiologically-based pharmacokinetic studies. *Journal of Pharmaceutical Sciences* 71, 454 – 456.

Leung, H.W. and D.J. Paustenbach (1995). Physiologically based pharmacokinetic and pharmacodynamic modeling health risk assessment and characterization of hazardous substances. *Toxicology Letters* 79, 55 – 65.

Maser, E., and G. Bannenberg (1994). 11β-Hydroxysteroid dehydrogenase mediates reductive

metabolism of xenobiotic carbonyl compounds. *Biochemical Pharmacology* 47, 1805 – 1812.

Menegola, E., M.L. Broccia, F. Di Renzo, V. Massa, and E. Giavini (2005). Craniofacial and axial skeletal defects induced by the fungicide triadimefon in the mouse. *Birth Defects Research (Part B)* 74, 185 – 195.

Menegola, E., M.L. Broccia, F. Di Renzo, V. Massa, and E. Giavini (2005). Study on the common teratogenic pathway elicited by the fungicides triazole-derivatives. *Toxicology in Vitro* 19, 737 – 748.

Mirfazaelian, A., K.B. Kim, S.S. Anand, H.J. Kim, R. Tornero-Velez, J.V. Bruckner, and J.W. Fisher (2006). Development of a Physiologically Based Pharmacokinetic Model for Deltamethrin in the Adult Male Sprague Dawley Rat. *Toxicological Sciences* 93, 432-442.

Mode, A. and Gustafsson, J.A. (2006). Sex and the liver – a journey through five decades. *Drug Metabolism Reviews* 38, 197 – 207.

Moser, V.C. and MacPhail, R.C. (1989). Neurobehavioral effects of triadimefon, a triazole fungicide, in male and female rats. *Neurotoxicology and Teratology* 11, 285 – 293.

Mugford, C.A. and Kedderis, G.L. (1998). Sex-dependent metabolism of xenobiotics. *Drug Metabolism Reviews* 30, 441 – 498.

Pelekis, M. and C. Emond (2009). Physiological modeling and derivation of the rat to human toxicokinetic uncertainty factor for the carbamate pesticide aldicarb. *Environmental Toxicology and Pharmacology* 28, 179 – 191.

Poulin, P. and K. Krishnan (1996). A tissue composition-based algorithm for predicting

tissue:air partition coefficients of organic chemicals. *Toxicology and Applied Pharmacology* 136, 126 – 130.

Roberts, T. and Hutson, D. (1999). Triadimefon. In Metabolic Pathways of Agrochemicals Part Two: Insecticides and Fungicides. (T. Roberts and D. Hutson, Eds.), pp. 1090 – 1094. The Royal Society of Chemistry, Cambridge, UK.

Ronis, M.J.J., Ingelman-Sundberg, M., and Badger, T.M. (1994). Induction, suppression and inhibition of multiple hepatic cytochrome P450 isozymes in the male rat and bobwhite quail *(Colinus virginianus)* by ergosterol biosynthesis inhibiting fungicides (EBIFs). *Biochemical Pharmacology* 48, 1953 – 1965.

Seckl, J.R. and B.R. Walker (2001). Minireview: 11β-hydroxysteroid dehydrogenase type 1 – a tissue-specific amplifier of glucocorticoid action. *Endocrinology* 142, 1371 – 1376.

Sun, G., S.F. Thai, G.R. Lambert, D.C. Wolf, D.B. Tully, A.K. Goetz, M.H. George, R.D. Grindstaff, D.J. Dix, and S. Nesnow (2006). Fluconazole-induced hepatic cytochrome P450 gene expression and enzymatic activities in rats and mice. *Toxicology Letters* 164, 44 – 53.

Thompson, C.M., B. Sonawane, H.A. Barton, R.S. DeWoskin, J.C. Lipscomb, P. Schlosser, W. A. Chiu, and K. Krishnan (2008). Approaches for applications of physiologically based pharmacokinetic models in risk assessment. *Journal of Toxicology and Environmental Health Part B* 11, 519 – 547.

Timchalk, C. and T.S. Poet (2007). Development of a physiologically based pharmacokinetic and pharmacodynamic model to determine dosimetry and cholinesterase inhibition for a binary mixture of chlorpyrifos and diazinon in the rat. *Neurotoxicology* 29, 428 – 443.

United States Environmental Protection Agency (2006). Re-registration eligibility decision for

triadimefon and triadimenol and tolerance reassessment for triadimenol. Washington D.C.: Office of Pesticide Programs, U.S. Environmental Protection Agency.

Vazquez, P.P, J.M. Fernandez, and M.D.G. Garcia (2002). Determination of azole pesticides in human serum by coupled column reversed-phase liquid chromatography using ultraviolet absorbance and mass spectrometric detection. *Journal of Liquid Chromatography & Related Technologies* 25, 3045 – 3058.

Vinggaard, A.M., C. Hnida, V. Breinholt, and J.C. Larsen (2000). Screening of selected pesticides for inhibition of CYP19 aromatase activity in vitro. *Toxicology in Vitro* 14, 227 – 234.

Walker, Q.D., Lewis, M.H., Crofton, K.M., and Mailman, R.B. (1990). Triadimefon, a triazole fungicide, induces stereotyped behavior and alters monoamine metabolism in rats. *Toxicology and Applied Pharmacology* 102, 474 – 485.

Zarn, J.A., Bruschweiler, B.J, and Schlatter, J.R. (2003). Azole fungicides affect mammalian steroidogenesis by inhibiting sterol 14a-demethylase and aromatase. *Environmental Health Perspectives* 111, 255 – 261.

Zhang, X., A.M. Tsang, M.S. Okino, F.W. Power, J.B. Knaak, L.S. Harrison, and C.C. Dary (2000). A physiologically based pharmacokinetic/pharmacodynamic model for carbofuran in Sprague-Dawley rats using the exposure-related dose estimating model. *Toxicological Sciences* 100, 345 – 359.

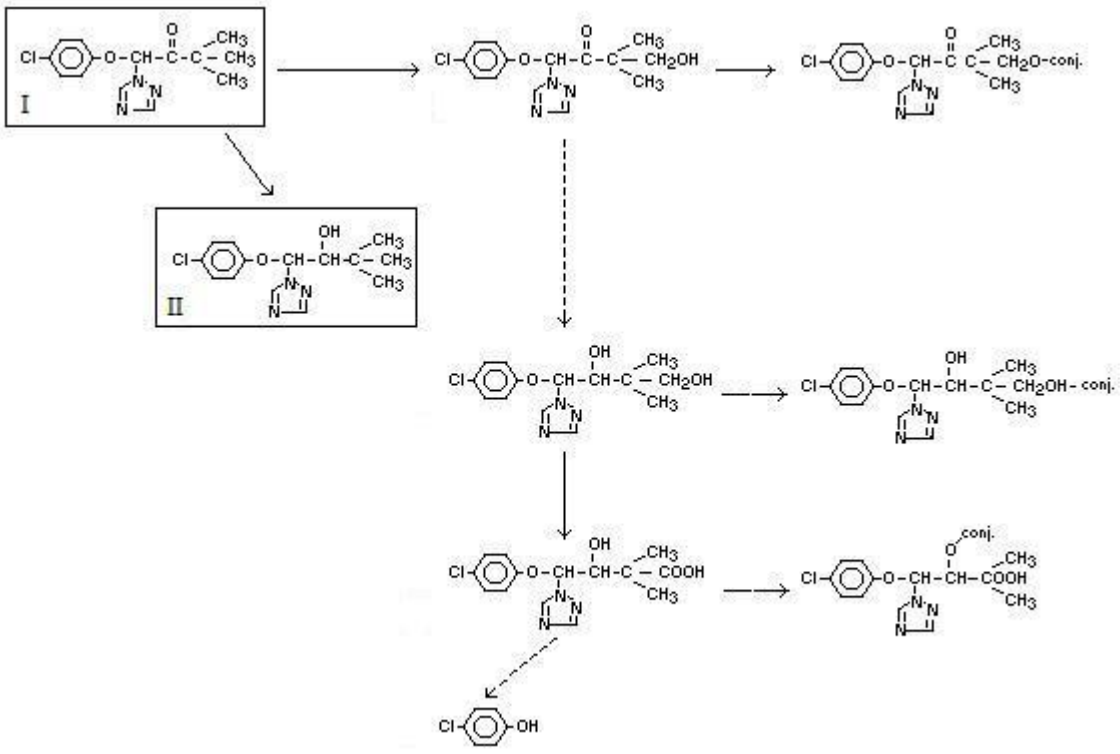

Figure 2.1. Proposed metabolic pathway for triadimefon (I) and triadimenol (III) in mammals. Solid arrows represent verified reactions, while dashed arrows represent unverified reactions. Adapted from FAO/WHO (1981).

CHAPTER 3

GENDER AND SPECIES DIFFERENCES IN METABOLISM OF TRIADIMEFON BY RODENT HEPATIC MICROSOMES[1]

[1]Crowell, S.R., W.M Henderson, J.F. Kenneke, and J.W. Fisher. Submitted to *Toxicology Letters*, 10/27/2009

Abstract

Understanding the potential differences in metabolic capacity and kinetics between various common laboratory species as well as between genders is an important facet of chemical risk assessment that is often overlooked, particularly for chemicals that undergo non-cytochrome P450 mediated metabolism. The use of physiologically based pharmacokinetic (PBPK) models to better describe chemical exposure is made more powerful by incorporation of high quality *in vitro* kinetic data. To this end, metabolism of the conazole fungicide triadimefon was studied in hepatic microsomes of both genders of SD rats and CD-1 mice. Triadimefon depletion and triadimenol formation were measured in each type of microsomes. Michaelis-Menten regressions were applied to metabolic data and V_{MAX} and the Michaelis constant (K_M) values calculated. Male SD rats metabolized triadimefon more rapidly than female SD rats or either gender of CD-1 mouse. K_M values were in the micromolar range, indicating the possibility of competitive inhibition with endogenous substrates. Intrinsic clearances derived from kinetic parameters indicate that triadimefon metabolism is blood-flow limited in all organisms studied with the possible exception of female rat. The *in vitro* half-life method was investigated as a less resource intensive method for the derivation of intrinsic clearance, and was found to be useful as a complement to the traditional Michaelis-Menten approach.

Key Words: Triadimefon, Michaelis-Menten, V_{MAX}, K_M, Rodent hepatic microsomes, *In vitro* half-life, Gender

Introduction

Conazoles (1,2,4 triazoles and imidazoles) are a class of agricultural and medicinal fungicides that inhibit 14α-lanosterol demethylase (Buchenauer, 1977) and disrupt the conversion of lanosterol to ergosterol, which is a major constituent of fungal cell walls. In vertebrates, lanosterol demethylase is involved in cholesterol synthesis, which is important not only to cell membrane integrity, but also as a precursor to steroid hormones and other biomolecules. Conazoles may interfere with steroid biosynthesis and related aspects of normal mammalian physiology (Zarn et al., 2003). Besides acting as enzyme inhibitors, conazoles are also known to modulate the expression of many cytochrome P450 (CYP) enzymes (Allen et al., 2006; Barton et al., 2006; Goetz et al.; 2006, Ronis et al. 1994), potentially affecting the metabolism of a wide variety of xenobiotics and endogenous compounds. Additionally, several conazole fungicides are carcinogenic, causing thyroid and/or liver tumors in rodents (Hurley et al., 1998).

Triadimefon is a broad-spectrum conazole fungicide with applications in agriculture and landscaping. It is a lipophilic, non-volatile pesticide with pre-planting, foliar, and post-harvest applications. The U.S. Environmental Protection Agency (U.S. EPA) estimates an application rate of approximately 135,000 lbs/year with an upper-end estimate of 266,000 lbs/year (U.S. EPA, 2006). The primary metabolite of triadimefon is the carbonyl reduction product, triadimenol (Figure 3.1), which we have previously shown is catalyzed via 11β-hydroxysteroid dehydrogenase type 1 (11β-HSD1) (Kenneke et al., 2008). Triadimenol retains the fungicidal activity of the parent compound, and is sold as a commercial fungicide, applied at a rate of 24,000 lbs/year (U.S. EPA, 2006). Oxidation of the *t*-butyl group of triadimenol results in alcohol and carboxylic acid derivatives (Roberts and Hutson, 1999). Triadimenol and

subsequent metabolites are also conjugated via phase II metabolism, yielding mainly glucuronide conjugates (FAO/WHO, 1980).

A variety of toxicities are associated with exposure to triadimefon and triadimenol, though the mechanisms underlying these effects are not clear. Triadimefon and triadimenol are unique among conazoles in eliciting neurotoxic effects (Crofton, 1996); indeed, regulatory decisions center on neurotoxicity as the sensitive endpoint for toxicity (U.S.EPA, 2006). Teratogenic activity has been observed in both *in vitro* and *in vivo* studies, and despite administration of high doses, it is thought the effects in the developing animal do not result from maternal toxicity (Menegola et al., 2000; 2005a; 2005b). Toxic effects on the developing reproductive systems of male and female rats have been attributed to perturbation of reproductive hormones, including testosterone (Goetz et al., 2007; Rockett et al., 2006; Zarn et al., 2003). Triadimefon has also been found to be tumorigenic, causing a dose-dependent increase in liver adenomas in male, but not female, CF_1/W mice in a 24 month feeding study (FAO/WHO, 2004).

For both triadimefon and triadimenol, there is an insufficient understanding of mechanisms of known toxicity to vertebrates, and whether potential differences in triadimefon metabolism between males and females confer greater vulnerability (e.g. reproductive toxicity). Much research has focused on the differences in metabolism of other xenobiotics and endogenous compounds between males and females of common laboratory species, though the focus has largely been on CYP-mediated metabolism. The consensus of the literature is that, generally, male and female rats display the greatest disparity in rates of metabolism, with males having higher maximum metabolic rates than females. This applies to many CYP substrates, especially 2A and 2C isoforms (Mugford and Kedderis, 1998). Similar gender differences are

much less pronounced in other organisms, including mice, and have been difficult to observe in humans due to intraspecies variation (Mode and Gustafsson, 2006).

Understanding gender and species differences in metabolism and toxicity enhances the utility of physiologically based pharmacokinetic (PBPK) modeling, an increasingly important tool for chemical risk assessment, by providing a quantitative basis for extrapolation between different organisms and sensitive subpopulations. PBPK models facilitate the estimation of internal dose metrics (i.e. internal exposure to relevant tissues), which are ultimately used to derive acceptable limits of exposure and thus have far reaching implications in chemical regulation. PBPK modeling is a powerful tool for generating precise and scientifically informed extrapolations of exposure between organisms, but its utility is limited by the quality and availability of physiological and chemical parameters (e.g., kinetic data). By using hepatic microsomal assays to address differences in metabolism between two common laboratory animals, CD-1 mice and Sprague Dawley (SD) rats, as well as between the males and females of these species, this research aims to elucidate mechanistic differences and to provide *in vitro* kinetic data for the development of PBPK models for the improvement of risk assessment.

Materials and Methods

Reagents

Triadimefon and triadimenol were obtained from the EPA National Pesticide Standard Repository (Fort Meade, MD). β-Nicotinamide adenine dinucleotide phosphate (NADP), glucose 6-phosphate (G6P), glucose 6-phosphate dehydrogenase (G6PDH), magnesium chloride ($MgCl_2$), and phosphate buffer were purchased from Sigma Chemical Co. (St. Louis, MO). Acetonitrile from Fisher Chemicals (Fair Lawn, NJ) was of analytical grade. Perchloric acid (60-62%) was obtained from J. T. Baker (Phillipsburg, NJ).

Microsomal Incubation Procedure

Microsomal metabolic assays were performed according to methods detailed in Mazur, et al. (2007). Frozen hepatic microsomes from male and female SD rats and male and female CD-1 mice were obtained from In Vitro Technologies (Baltimore, MD) and stored at -80°C until use. Triadimefon and triadimenol standards were dissolved in acetonitrile and stored in amber vials at 4°C. The final assay concentration of acetonitrile was less than 1% v/v, and appropriate control experiments were conducted to establish that these concentrations did not affect microsomal metabolism. All incubations were carried out in a total reaction volume of 1000 µL in microcentrifuge tubes, held in a 37°C heating block. Microsomal suspensions of 0.125 mg microsomal protein (MSP) were prepared in a 0.1 M potassium phosphate buffer (pH 7.4). Varying triadimefon stock solutions were added to the suspensions to achieve final substrate concentrations of 0 – 170 µM; acetonitrile was used as a substrate-free control. The samples were vortexed and allowed to stand in the heating block for five minutes to allow for temperature equilibration. An NADPH regenerating system (NRS) was prepared in a 0.1 M phosphate buffer containing NADP, G6P, $MgCl_2$, and G6PDH and held at 37°C. The reaction was initiated by the addition of 250 µL NRS to the microsomal suspension, with final assay concentrations of 0.5 mM NADP, 7 mM G6P, 1.25 mM $MgCl_2$, and 1.5 U of G6PDH. Assays were incubated for 0 – 30 minutes and then quenched with 100 µL of 60% perchloric acid, vortexed, and immediately placed on ice. The samples were centrifuged at 4°C for 10 minutes at 10,600 x *g*, and the supernatant transferred to seal cap high-performance liquid chromatography (HPLC) vials for analysis.

Intrinsic clearance (CL_{INT}) was determined using the *in vitro* half-life ($T_{½}$) method (Obach, 1999) for comparison to values determined from classic Michaelis-Menten regressions

of substrate depletion and product formation. Microsomal suspensions with a final reaction concentration of 0.4 µM triadimefon were incubated for 0 – 90 minutes (male rat), 0 – 120 minutes (male and female mouse), and 0 – 240 minutes (female rat) before quenching, centrifugation, and HPLC analysis. Kinetics were shown to be linear with respect to time and protein concentration in preliminary experiments (data not shown).

Analytical Procedure

Triadimefon and triadimenol calibration standards were prepared in 990 µL of 0.1 M phosphate buffer with 10 µL stock solution and 100 µL perchloric acid. Ten or more standards of varying concentrations (0 – 170 µM) were used for initial calibration curves (ICAL). Subsequent instrument calibration was verified by analyzing a standard of intermediate concentration of both triadimefon and triadimenol prior to sample analysis and after every tenth sample. Sample quantification was considered valid if the standards varied by less than 5% from the ICAL.

Analysis of microsomal substrate depletion and metabolite formation were performed on an Agilent series 1100 HPLC quaternary pump system (Agilent, Palo Alto, CA) equipped with a photodiode array detector (λ max 202 nm). Injections (100 µL) were made on to a Nucleosil 100 C18 (4.6 x 100 mm, 5 µm particle diameter) (Alltech, Deerfiled, IL) column with an isocratic mobile phase consisting of 55% acetonitrile and 45% water, and a flow rate of 0.4 mL/min.

Data Analysis

Initial reaction rates (pmol min^{-1}) for substrate depletion and product formation were determined by linear least-squares regression of concentration versus time data. Regressions were limited to a maximum of 20% substrate depletion and included at least three data points;

only regressions with an r^2 of at least 0.7 were considered valid. Initial reaction rates were normalized to MSP to yield initial reaction velocities (V, pmol $min^{-1}mg^{-1}$).

Substrate depletion and product formation velocities measured as a function of initial triadimefon concentration were analyzed using the Michaelis-Menten model, which expresses V as a function of initial substrate concentration ([S]):

$$V_S = \frac{V_{MAX}[S]}{K_M + [S]} \tag{3.1}$$

Values of the Michaelis constant (K_M, μM) and the maximum velocity (V_{MAX}, pmol $min^{-1}mg^{-1}$) were determined for triadimefon depletion and triadimenol formation by minimizing the sum of the squared residuals between measured velocities and the velocities calculated as a function of the triadimefon concentration using Eq. (1) (SigmaPlot, Systat Software, Point Richmond, CA). Additionally, asymptotic standard errors for K_M and V_{MAX} and the 95% confidence intervals for the regression were calculated. V_{MAX} and K_M were considered valid if the standard error of each estimate was 20% or less than the estimate itself.

A continuous mass balance was calculated as the ratio of the regression of triadimenol formation data to the regression of triadimefon depletion data across the range of initial concentrations of triadimefon.

Intrinsic Clearance Predictions

Applying the enzyme kinetic methods of Obach et al. (1997), CL_{INT} was predicted from V_{MAX} and K_M according to equation (3.2).

$$CL_{INT} = \left(\frac{V_{MAX}}{K_M}\right)\left(\frac{\text{g of liver weight}}{\text{1 kg of body weight}}\right)\left(\frac{\text{45 mg of MSP}}{\text{1 g of liver weight}}\right) \quad (3.2)$$

Liver weights used for mice and rats were 55 g/kg body weight and 34 g/kg body weight, respectively (Brown et al., 1997). Alternatively, CL_{INT} was calculated directly from *in vitro* half-life studies by applying a linear least-squares regression of natural log concentration versus time data according to methods described by Obach (1999). Only triadimefon depletion data were used in the determination of CL_{INT} by this method. Regressions that included at least four data points, had an r^2 of at least 0.8 and exhibited at least one half-life of triadimefon depletion were considered valid.

Results

Metabolite Formation

Regardless of gender or species, triadimenol was the only metabolite detected by HPLC from triadimefon under experimental conditions. The identity of triadimenol was confirmed by comparison of retention time to an authentic standard. In all studies, triadimenol accumulated and remained stable and resistant to further phase I metabolism.

A representative plot of concentration (µM) versus time (min) for the male SD rat, which demonstrates initial zero-order rates (i.e., slope) of triadimefon depletion and triadimenol formation, is shown in Figure 3.2. Initial reaction velocities (i.e., rates normalized to MSP) of triadimefon depletion and triadimenol formation were determined for each concentration of triadimefon (0 – 170 µM). In all cases, (i.e., male/female and rat/mouse), initial velocities of triadimefon depletion (Figure 3.3) and triadimenol formation (Figure 3.4) increased with increasing initial triadimefon concentration, eventually reaching a plateau at higher

concentrations. The Michaelis-Menten model (Eq.3.1) was applied to triadimefon depletion and triadimenol formation velocities as a function of initial triadimefon concentration in order to determine K_M and V_{MAX} for each of the four organisms (Table 3.1).

The percent yield of triadimenol from triadimefon depletion (Figure 3.5) differed across the organisms in this study. For all species, the ratio of triadimenol formation to triadimefon depletion varied at low concentrations, and reached a plateau at high concentrations. In the male rat, approximately 80% of the depleted triadimefon was accounted for by triadimenol formation at high initial substrate concentrations, whereas in the female rat only 10% was accounted for by triadimenol formation. In male and female mouse, approximately 40% of the depleted triadimefon was accounted for by triadimenol formation. Despite the low mass balances observed in all organisms except male rat, no metabolites other than triadimenol were observed.

In addition to the low mass balance, female rats displayed very slow rates of metabolism, which hindered the measurement of kinetic parameters. Analytical error was magnified by low metabolism velocity, resulting in a wider margin of error for this organism, and in some instances, this error invalidated the estimated kinetic parameter. A different lot of female rat microsomes was investigated in order to confirm the slow metabolism, and were observed to behave similarly (data not reported).

Michaelis Constant, K_M

Michaelis constants were calculated from both triadimefon depletion and triadimenol formation (Table 3.1, Figure 3.6). Those calculated from triadimefon depletion were similar for each of the four organisms, ranging from 40±18 µM in the female mouse to 80±25 µM in the female rat. The K_M values from triadimenol formation were more disparate, ranging from 6±1 µM in the female mouse to 78±8 µM in the female rat.

The K_M from triadimefon depletion exceeded the values calculated using triadimenol formation in both genders of mouse, whereas in male rat, the K_M calculated from triadimefon depletion was lower than that from triadimenol formation. In the female rat, the values were not significantly different.

Maximum Velocity, V_{MAX}

The maximum velocities of triadimefon depletion ranged from 7452±493 pmol $min^{-1}mg^{-1}$ in the male rat to 2824±261 pmol $min^{-1}mg^{-1}$ in male mouse (Table 3.1, Figure 3.7). In rats, the V_{MAX} of triadimefon depletion in males was nearly two-fold higher than in females (3771±589 pmol $min^{-1}mg^{-1}$). The maximum velocity of triadimefon depletion for female mouse (3956±725 pmol $min^{-1}mg^{-1}$) was only marginally higher than male mouse.

For triadimenol formation, maximum velocities were substantially lower for both species (Table 3.1, Figure 3.7). Male and female mice again had similar values of V_{MAX}, at 1052±38 pmol $min^{-1}mg^{-1}$ and 1341±52 pmol $min^{-1}mg^{-1}$, respectively. The female rat had the lowest value of V_{MAX} (344±15 pmol $min^{-1}mg^{-1}$), and the male rat was nearly sixteen-fold higher (5703±149 pmol $min^{-1}mg^{-1}$).

Intrinsic Clearance, CL_{INT}

Intrinsic clearances based upon V_{MAX} and K_M were calculated according to Eq.2, using triadimefon depletion data as well as triadimenol formation data (Table 3.1, Figure 3.8). Using triadimefon depletion data, intrinsic clearances ranged from 245 ml $min^{-1}kbw^{-1}$ for male rat, down to 72 ml $min^{-1}kbw^{-1}$ for female rat, with male and female mouse falling intermediate. For triadimenol formation, intrinsic clearances varied more widely, ranging from 531 ml $min^{-1}kbw^{-1}$ in the female mouse to 7 ml $min^{-1}kbw^{-1}$ in the female rat. In both genders of mouse, the intrinsic

clearances calculated from triadimenol formation data exceeded those determined with triadimefon depletion data, while the opposite was true in both genders of rat.

Intrinsic clearances calculated using the *in vitro* half-life method were comparable to those calculated using Michaelis-Menten data on triadimefon depletion (Table 3.1). Male rat, male mouse, and female mouse (240, 131, and 333 ml $min^{-1}kbw^{-1}$, respectively) all had clearances approximately two orders of magnitude higher than the female rat (2.0 ml $min^{-1}kbw^{-1}$). Because the *in vitro* half-life method relies on triadimefon depletion data only, comparisons to CL_{INT} derived from Michaelis-Menten regression of triadimenol formation data were not performed.

Discussion

The toxicity of triadimefon has been studied extensively, and while detailed mechanisms are not known, it has been shown to act as a neurotoxin (Crofton et al., 1988 and 1996; Moser and MacPhail, 1989; Walker et al.,1990), teratogen (Menegola et al., 2000; 2005a; 2005b), developmental toxicant (Goetz et al., 2007; Rocket et al., 2006), endocrine disruptor (Zarn et al., 2003), and carcinogen (Hurley et al., 1998; INCHEM, 1981; U.S. EPA, 1996). Triadimefon modulates expression and activity of enzymes including CYPs (Allen et al., 2006; Barton et al., 2006; Goetz et al., 2006**)**. It is unclear whether triadimefon undergoes activation or detoxification upon metabolism to triadimenol. In acute toxicity tests in rodents, both compounds possessed similar potencies (summarized in FAO/WHO 2004). In studies of conazole neurotoxicity, triadimefon and triadimenol were uniquely toxic among 1,2,4-triazoles; the authors attributed this to the ether oxygen both chemicals contain (Crofton, 1996). These findings indicate that both parent and metabolite are relevant as toxicants.

Our laboratory's approach of concomitantly measuring substrate depletion and product formation has revealed a marked difference in mass balance between rodent species: triadimenol formation was observed to account for approximately 80% of triadimefon depletion in the male rat, versus 10 – 40% in female rat and both genders of mice. The low mass balance may indicate that, in the latter organisms, triadimefon is degraded to metabolites other than triadimenol, or that subsequent metabolism of triadimenol to other alcohol and carboxylic acid derivatives is occurring, though no additional metabolites were observed by HPLC. The disparity in mass balance may also suggest that there is a difference in the activity of the enzyme responsible for triadimefon metabolism for the male rat versus the other organisms studied.

The approach of measuring both substrate depletion and product formation also underscored differences in the Michaelis constant (K_M). In studies using purified enzymes, K_M describes the dissociation constant for the enzyme substrate complex, with a high value indicating low affinity of the compound and the metabolizing enzyme, and vice versa. Microsomal metabolism kinetics are more theoretically complex than those measured in purified enzyme assays, but the measured K_M nonetheless relates to enzyme affinity. When calculated using substrate depletion values, K_M describes affinity between substrate and enzyme. K_M calculated using product formation information could plausibly be used as a surrogate measurement for a specific enzymatic pathway when the parent compound is metabolized into multiple metabolites, or immeasurable reaction intermediates. As illustrated in Figure 3.6, only in the female rat was the value of K_M unchanged regardless of source data. Additionally, it is only in male rat that the K_M derived from substrate depletion is lower than that for product formation. While the reasons for these results are unknown, it is possible that in those organisms with a poor mass balance, the unaccounted presence of additional metabolites leads to an

underestimation of K_M from product formation data, and the subsequent conclusion that there is a higher affinity between enzyme and substrate than actually exists.

Observed values of K_M for organisms in this study were in the micromolar range (6 – 80 μM); similar Michaelis constants have been reported for important pharmaceutical xenobiotic-enzyme complexes and endogenous substrate-enzyme complexes. For example, CYP subfamilies 2C and 3A, which have been implicated in triadimefon metabolism (Barton et al., 2006), have values of the Michaelis constant for the pharmaceuticals diclofenac, imipramine, and midazolam ranging from 1.0 to 22 μM (Obach and Reed-Hagen, 2002). For 11β-HSD 1 in the mouse, the Michaelis constants for the endogenous substrates cortisone and cortisol range from 184 to 340 μM (Maser and Bannenberg, 1994). These values indicate that there exists a possibility of triadimefon interfering with endogenous reactions, including competitive inhibition. For example, research by this laboratory has shown that triadimefon metabolism to triadimenol is inhibited by the presence of cortisone (Kenneke et al., 2008). Research into additional pathways of triadimefon metabolism, including phase II conjugation reactions, may clarify findings on V_{MAX} and K_M.

The influence of gender on triadimefon metabolism was most apparent between male and female rat. V_{MAX} values based on substrate depletion are two-fold higher in males, and those derived from product formation are well over an order of magnitude higher in males (Table 3.1, Figure 3.7). Intrinsic clearances were similarly disparate between male and female rats (Figure 3.8). In mice, there was a less dramatic, albeit significant, difference in intrinsic clearance values derived from product formation data. Species-mediated differences in triadimefon metabolism are underscored by comparison of maximum velocity in the male rat to both genders of mouse. Male rat V_{MAX} values for both triadimefon depletion and triadimenol formation were clearly

outliers relative to the other organisms studied (Figure 3.7). Additionally, K_M values were significantly different between all organisms when derived from triadimenol formation.

Intrinsic clearance addresses the ability of an organism to metabolize a particular chemical. In "flow limited" systems, the ability of a tissue to metabolize and clear the chemical substantially exceeds the rate at which the blood perfuses that tissue; that is, the transport of the substrate and product to and from the tissue is the rate-limiting step in chemical clearance. This minimizes the impact of variation in rates of metabolism which are well above the rate of perfusion. For male rat, male mouse, and female mouse, CL_{INT} values calculated from the kinetic constants as well as those derived from the *in vitro* half-life method are all more than an order of magnitude greater than 13 ml/min/kg, the reported value for rodent hepatic blood flow (Brown et al., 1997), indicating that these organisms would experience blood-flow limited clearance of triadimefon (Figure 3.8). CL_{INT} values derived for the female rat from classic analysis of triadimefon depletion (72 ml $min^{-1}kbw^{-1}$), triadimenol formation (7 ml $min^{-1}kbw^{-1}$), and the *in vitro* half-life method (2 ml $min^{-1}kbw^{-1}$) are all near the reported rate of rodent hepatic blood flow (13 ml/min/kg, Brown et al., 1997). Thus, in female rat, triadimefon metabolism may not be blood-flow limited and would be sensitive to variation in V_{MAX}, as can occur with enzyme induction or inhibition. Heightened sensitivity to triadimefon toxicity has been observed in female rats as compared to male rats in some studies. In studies of the neurological effects of triadimefon, it was observed that females were marginally more susceptible and recovered more slowly than male rats (Walker et al., 1990; Moser et al., 1989). Because triadimefon is known to be a developmental toxicant as well as a teratogen, slower clearance in the female rat has important implications for pregnant females. However, in the mouse the clearance in females exceeds the rate of hepatic blood flow, and exceeds the intrinsic clearance rates for the male of

the species. Ultimately, substantial differences may exist for triadimefon metabolism based on gender, a possibility that should be investigated in human microsomes as well as in *in vivo* experiments in rodents.

Clearance values from the *in vitro* half-life method are similar to those calculated from the Michaelis-Menten analyses (Table 3.1), indicating the method's utility as a screening tool. Also, as it is difficult to reliably measure substrate depletion at extreme concentrations without either increased variability in measurements (very high concentrations) or exceeding 20% substrate depletion (very low concentrations), the *in vitro* half-life method serves as an alternative method. However, there are several limitations associated with it, as compared to the generation of full Michaelis-Menten regression analyses. The *in vitro* half-life method requires that the substrate concentration be substantially lower than the K_M for the reaction. If K_M is not known, this value must be estimated, increasing uncertainty in the resulting parameters. Michaelis-Menten regressions incorporate considerably more data, necessitating more experiments, but making the resulting parameters more robust. Additionally, K_M and V_{MAX} are calculated as part of the Michaelis-Menten regression equation, whereas these numbers must be indirectly extracted from clearance values derived from the *in vitro* half-life method. The *in vitro* half-life method appears useful as an initial investigation into kinetic parameters of a chemical, or a complement to values obtained from classic methods.

While this research indicates that gender- and species-based differences exist in the metabolism kinetics of triadimefon, interpretation of these results is hindered by the dearth of mechanistic information on this chemical. In addition to elucidating possible mechanisms of toxicity and metabolism of triadimefon, this research provides kinetic parameters which can be incorporated into PBPK models for estimation of internal dosimetry. Quality experimental data

on kinetic parameters for multiple species and different genders will aide in using PBPK modeling to make more accurate extrapolations to more distant species, including humans. Experimentally measured values such as those presented here increase the accuracy and biological relevance of PBPK models by providing an alternative to mathematical curve fitting for derivation of *in silico* values.

Disclaimer

This paper has been reviewed in accordance with the U.S. Environmental Protection Agency's peer and administrative review policies and approved for publication. Mention of trade names or commercial products does not constitute endorsement or recommendation for use.

References

Allen, J.W., Wolf, D.C., George, M.H., Hester, S.D., Sun, G., Thai, S.F., Delker, D.A, Moore, T., Jones, C., Nelson, G., Roop, B.C., Leavitt, S., Winkfield, E., Ward, W.O., and Nesnow, S. (**2006**). Toxicity profiles in mice treated with hepatotumorigenic and non-hepatotumorigenic triazole conazole fungicides: propiconazole, triadimefon, and myclobutanil. *Toxicologic Pathology* **34,** 853 – 862.

Barton, H.A., Tang, J., Sey, Y.M., Stanko, J.P., Murrell, R.N., Rockett, J.C., and Dix, D.J. (**2006**). Metabolism of myclobutanil and triadimefon by human and rat cytochrome P450 enzymes and liver microsomes. *Xenobiotica* **36,** 793 – 806.

Brown, R.P., Delp, M.D., Lindstedt, S.L., Rhomberg, L.R., and Belilesi, R.P. (**1997**). Physiological parameter values for physiologically based pharmacokinetic models. *Toxicology and Industrial Health* **13**, 407 – 484.

Buchenauer, H. (**1977**). Mode of action of triadimefon in *Ustilago avenae*. *Pesticide*

Biochemistry and Physiology **7,** 309 – 320.

Crofton, K.M., Boncek, V.M., and Reiter, L.W. (**1988**). Hyperactivity induced by triadimefon, a triazole fungicide. *Fundamental and Applied Toxicology* **10,** 459 – 465.

Crofton, K.M. (**1996**). A structure-activity relationship for the neurotoxicity of triazole fungicides. *Toxicology Letters* **84,** 155 – 59.

FAO/WHO (**2004**). Pesticide Residues in Food 2004, Evaluations, FAO Plant Production and Protection Paper, **178** pp. 231 – 241. World Health Organization and Food and Agriculture Organization of the UN, Rome.

Goetz, A.K., Bao, W., Ren, H., Schmid, J.E., Tully, D.B., Wood, C., Rockett, J.C., Narotsky, M.G., Sun, G., Lambert, G.R., Thai, S.F., Wolf, D.C., Nesnow, S., and Dix, D.J. (**2006**). Gene expression profiling in the liver of CD-1 mice to characterize the hepatotoxicity of triazole fungicides. *Toxicology and Applied Pharmacology* **215,** 274 – 284.

Goetz, A.K., Ren, H., Schmid, J.E., Blystone, C.R., Thillainadarajah, I., Best, D.S., Nichols, H.P., Strader, L.F., Wolf, D.C., Narotsky, M.G., Rockett, J.C., and Dix, D.J. (**2007**). Disruption of testosterone homeostasis as a mode of action for the reproductive toxicity of triazole fungicides in the male rat. *Toxicological Sciences* **95,** 227 – 239.

Hurley, P.M., Hill, R.N., and Whiting, R.J. (**1998**). Mode of carcinogenic action of pesticides inducing thyroid follicular cell tumors in rodents. *Environmental Health Perspectives* **106,** 437 – 445.

INCHEM **1981**. Triadimefon (pesticide residues in food: 1981 evaluations) 36 pp. www.inchem.org/documents/jmpr/jmpmono/v81pr32.htm

Kenneke, J.F, Mazur, C.S., Ritger, S.E., and Sack, T.J. (**2008**). Mechanistic investigation of the

non-cytochrome P450-mediated metabolism of triadimefon to triadimenol in hepatic microsomes. *Chemical Research in Toxicology*, **21**, 1997 – 2004.

Maser, E., and Bannenberg, G. (**1994**). 11β-Hydroxysteroid dehydrogenase mediates reductive metabolism of xenobiotic carbonyl compounds. *Biochemical Pharmacology*, **47**, 1805 – 1812.

Menegola, E., Broccia, M.L., Di Renzo, F., Prati, M., and Giavini, E. (**2000**). In vitro teratogenic potential of two antifungal triazoles: triadimefon and triadimenol. *In Vitro Cell Developmental Biology* **36,** 88 – 95.

Menegola, E., Broccia, M.L., Di Renzo, F., Massa, V., and Giavini, E. (**2005**). Craniofacial and axial skeletal defects induced by the fungicide triadimefon in the mouse. *Birth Defects Research (Part B)* **74,** 185 – 195.

Menegola, E., Broccia, M.L., Di Renzo, F., Massa, V., and Giavini, E. (**2005**). Study on the common teratogenic pathway elicited by the fungicides triazole-derivatives. *Toxicology in Vitro* **19,** 737 – 748.

Mode, A. and Gustafsson, J.A. (**2006**). Sex and the liver – a journey through five decades. *Drug Metabolism Reviews* **38**, 197 – 207.

Moser, V.C. and MacPhail, R.C. (**1989**). Neurobehavioral effects of triadimefon, a triazole fungicide, in male and female rats. *Neurotoxicology and Teratology* **11,** 285 – 293.

Mugford, C.A. and Kedderis, G.L. (**1998**). Sex-dependent metabolism of xenobiotics. *Drug Metabolism Reviews* **30**, 441 – 498.

Obach, R.S., Baxter, J.G., Liston, T.E., Silber, B.M., Jones, B.C., MacIntyre, F., Rance, D.J., and

Wastall, P. (**1997**). The prediction of human pharmacokinetic parameters from preclinical and *in vitro* metabolism data. *Pharmacology and Experimental Therapeutics* **283**, 46 – 58.

Obach, R.S. (**1999**). Prediction of human clearance of twenty-nine drugs from hepatic microsomal intrinsic clearance data: an examination of in vitro half-life approach and nonspecific binding to microsomes. *Drug Metabolism and Disposition* **27,** 1350 – 1359.

Obach, R.S., and Reed-Hagen, A.E. (**2002**). Measurement of Michaelis constants for cytochrome P450-mediated biotransformation reactions using a substrate depletion approach. *Drug Metabolism and Disposition* **30**, 831 – 837.

Roberts, T. and Hutson, D. (**1999**). Triadimefon. In Metabolic Pathways of Agrochemicals Part Two: Insecticides and Fungicides. (T. Roberts and D. Hutson, Eds.), pp. 1090 – 1094. The Royal Society of Chemistry, Cambridge, UK.

Rockett, J.C., Narotsky, M.G., Thompson, K.E., Thillainadarajah, I., Blystone, C.R., Goetz, A.K., Ren, H., Best, D.S., Murrell, R.N., Nichols, H.P., Schmid, J.E., Wolf, D.C., and Dix, D.J. (**2006**). Effect of conazole fungicides on reproductive development in the female rat. *Reproductive Toxicology* **22,** 647 – 658.

Ronis, M.J.J., Ingelman-Sundberg, M., and Badger, T.M. (**1994**). Induction, suppression and inhibition of multiple hepatic cytochrome P450 isozymes in the male rat and bobwhite quail *(Colinus virginianus)* by ergosterol biosynthesis inhibiting fungicides (EBIFs). *Biochemical Pharmacology* **48,** 1953 – 1965.

United States Environmental Protection Agency. (**1996**). Triadimefon (Bayleton) pesticide tolerance. *Federal Register* **62**, 47005 – 47013.

United States Environmental Protection Agency. (**2006**). Re-registration eligibility decision for

triadimefon and triadimenol and tolerance reassessment for triadimenol. Washington D.C.: Office of Pesticide Programs, U.S. Environmental Protection Agency.

Walker, Q.D., Lewis, M.H., Crofton, K.M., and Mailman, R.B. (**1990**). Triadimefon, a triazole fungicide, induces stereotyped behavior and alters monoamine metabolism in rats. *Toxicology and Applied Pharmacology* **102,** 474 – 485.

Zarn, J.A., Bruschweiler, B.J, and Schlatter, J.R. (**2003**). Azole fungicides affect mammalian steroidogenesis by inhibiting sterol 14a-demethylase and aromatase. *Environmental Health Perspectives* **111,** 255 – 261.

Table 3.1: Kinetic Constants Derived for Triadimefon Depletion and Triadimenol Formation

Species	Gender	Source	*n*	V_{MAX} [a]	K_M [b]	R^2	CL_{INT} [c]	CL_{INT} [d]
Rat (SD)	Male	D	11	7452 ± 493	47 ± 8	0.993	245	240
		F	11	5703 ± 149	61 ± 4	0.999	142	--
	Female	D	10	3771 ± 589	80 ± 25	0.990	72	2
		F	11	344 ± 15	78 ± 8	0.999	7	--
Mouse (CD-1)	Male	D	11	2824 ± 261	45 ±11	0.986	155	131
		F	14	1052 ± 38	13 ± 2	0.995	196	--
	Female	D	13	3957 ± 725	42 ± 20	0.945	232	333
		F	12	1341 ± 52	6 ± 1	0.9923	531	--

D, triadimefon depletion; F, triadimenol formation.
[a] pmol $min^{-1}mg^{-1}$, values are the mean ± S.E.,.
[b] µM, values are the mean ± S.E.
[c] ml min^{-1} kbw^{-1}, calculated using Eq. 3.2.
[d] ml min^{-1} kbw^{-1}, calculated according to *in vitro* half-life method.

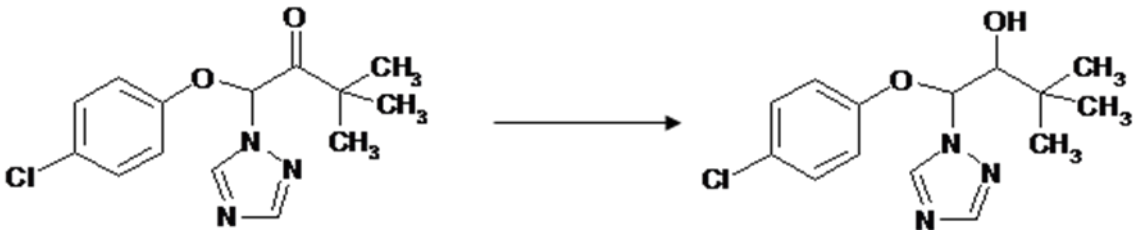

Figure 3.1: The conazole fungicide triadimefon and its primary metabolite triadimenol.

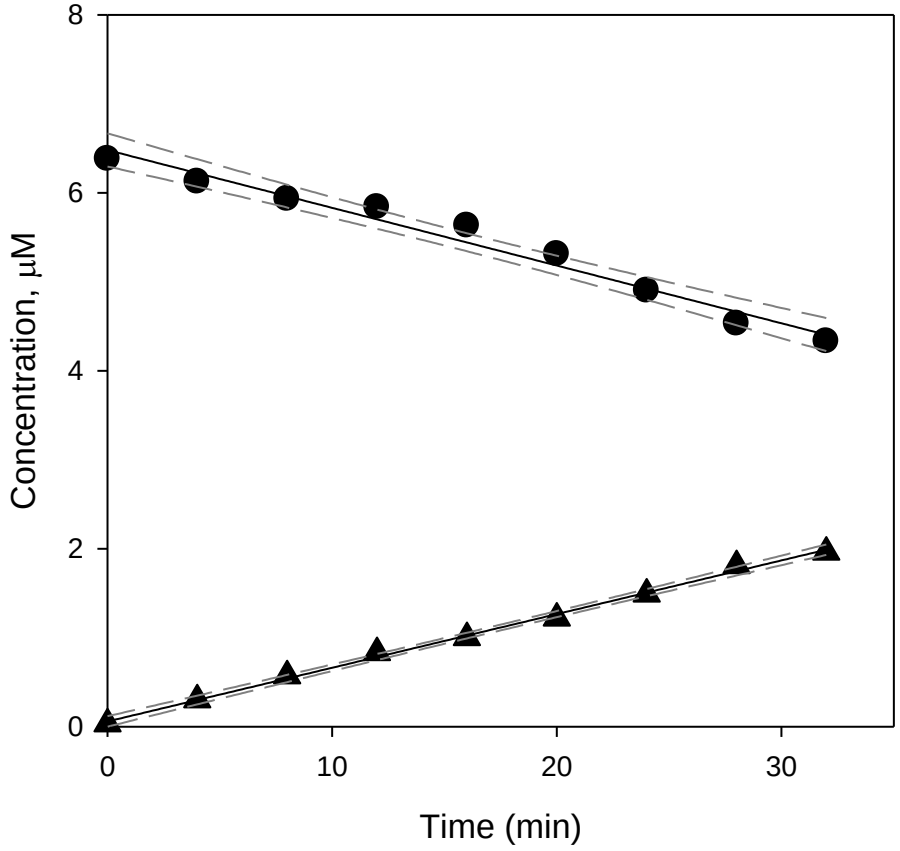

Figure 3.2: Representative time course demonstrating initial reaction rate of triadimefon depletion with time and the concurrent formation of triadimenol in male SD rat hepatic microsomes. Regressions (—) of triadimefon depletion (●) and triadimenol formation (▲) are accompanied by ±95% confidence intervals (- - -).

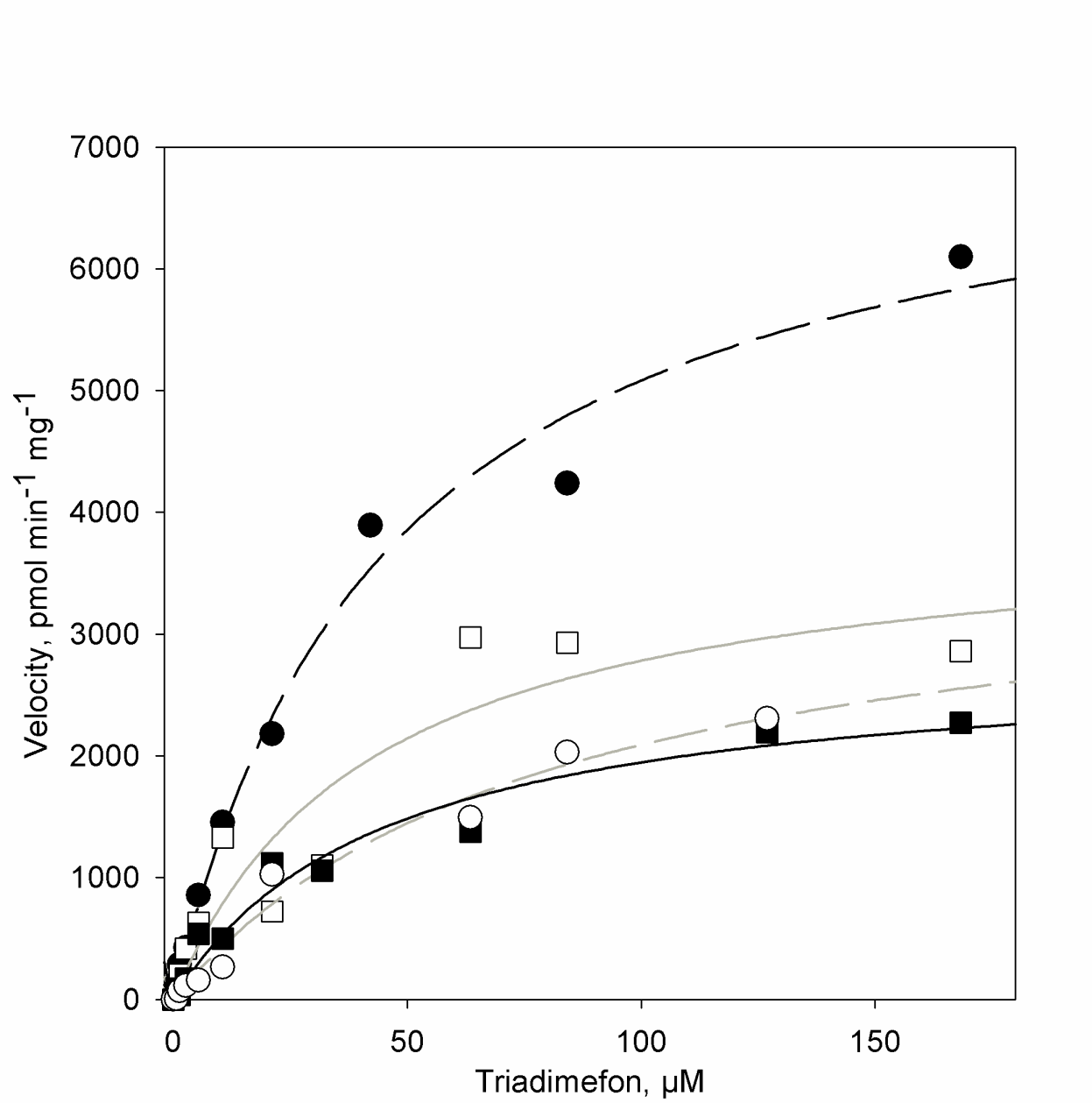

Figure 3.3: Michaelis-Menten kinetic analyses of triadimefon depletion in rodent hepatic microsomes: male SD rat (●), female SD rat (○), male CD-1 mouse (■), and female CD-1 mouse (□).

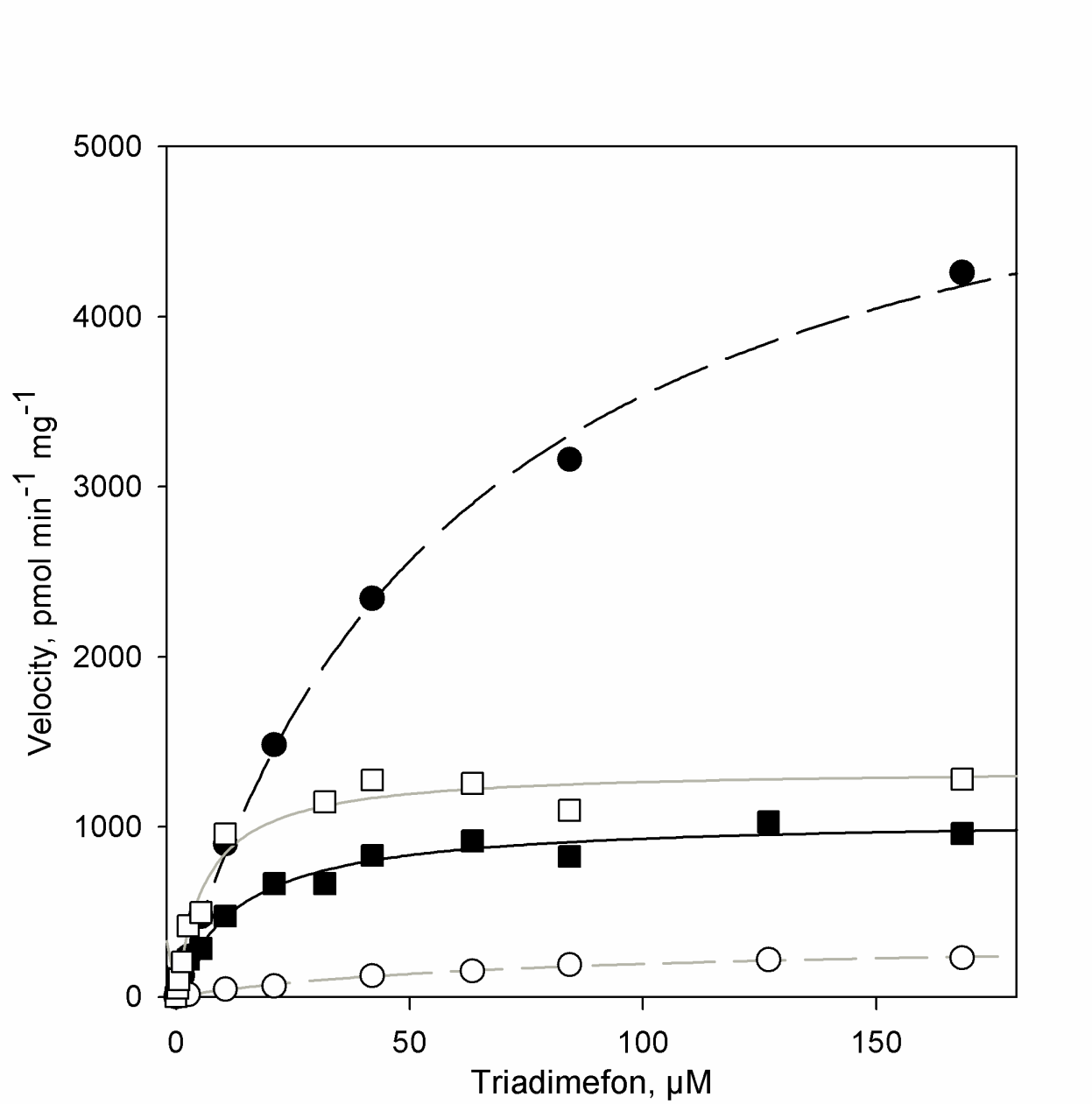

Figure 3.4: Michaelis-Menten kinetic analyses of triadimenol formation in rodent hepatic microsomes: male SD rat (●), female SD rat (○), male CD-1 mouse (■), and female CD-1 mouse (□).

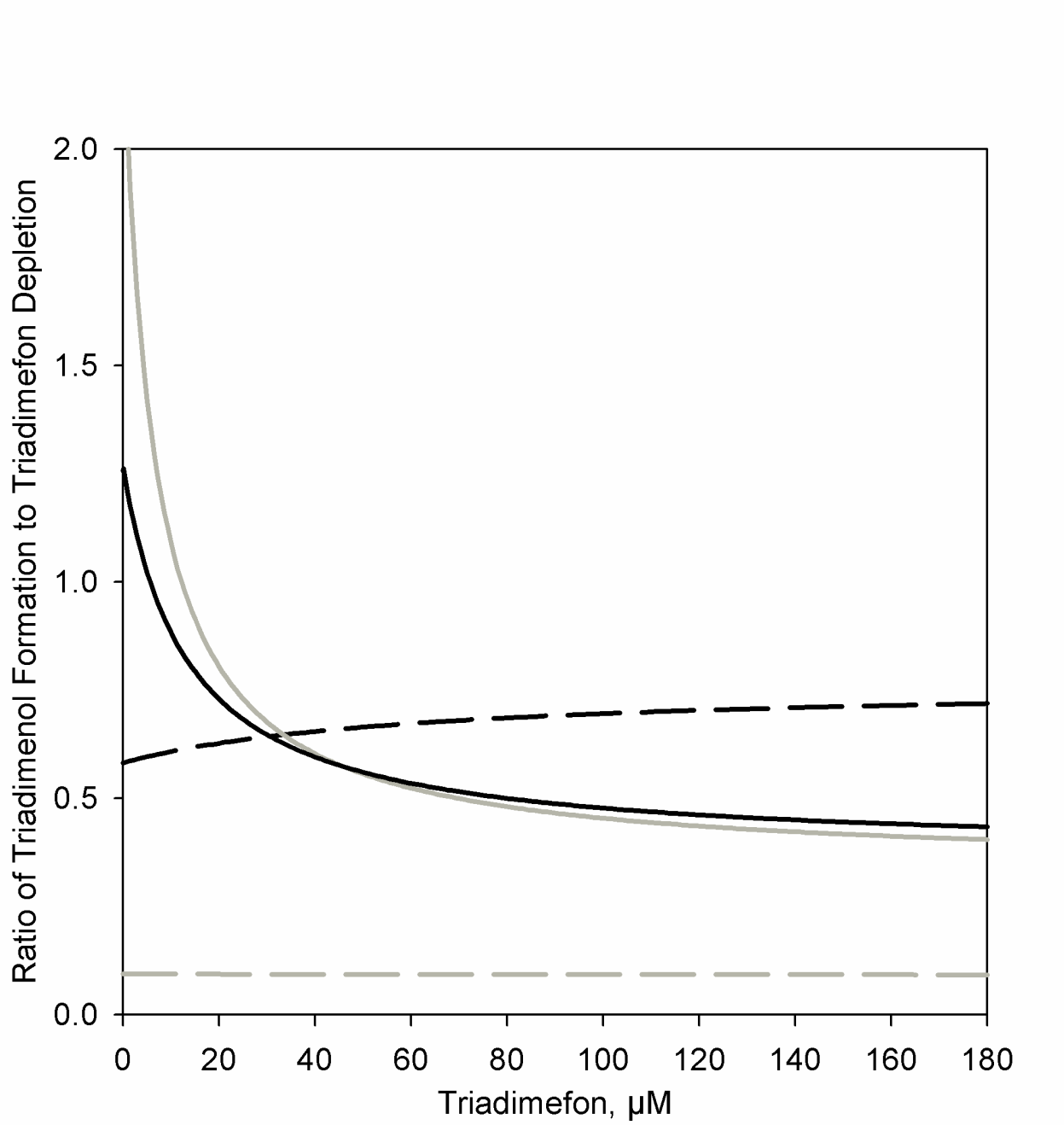

Figure 3.5: Continuous mass balance of the ratio of the Michaelis-Menten regression of triadimefon depletion to the Michaelis-Menten regression of triadimenol formation in male SD rat (- - -), female SD rat (- - -), male CD-1 mouse (—), and female CD-1 mouse (—).

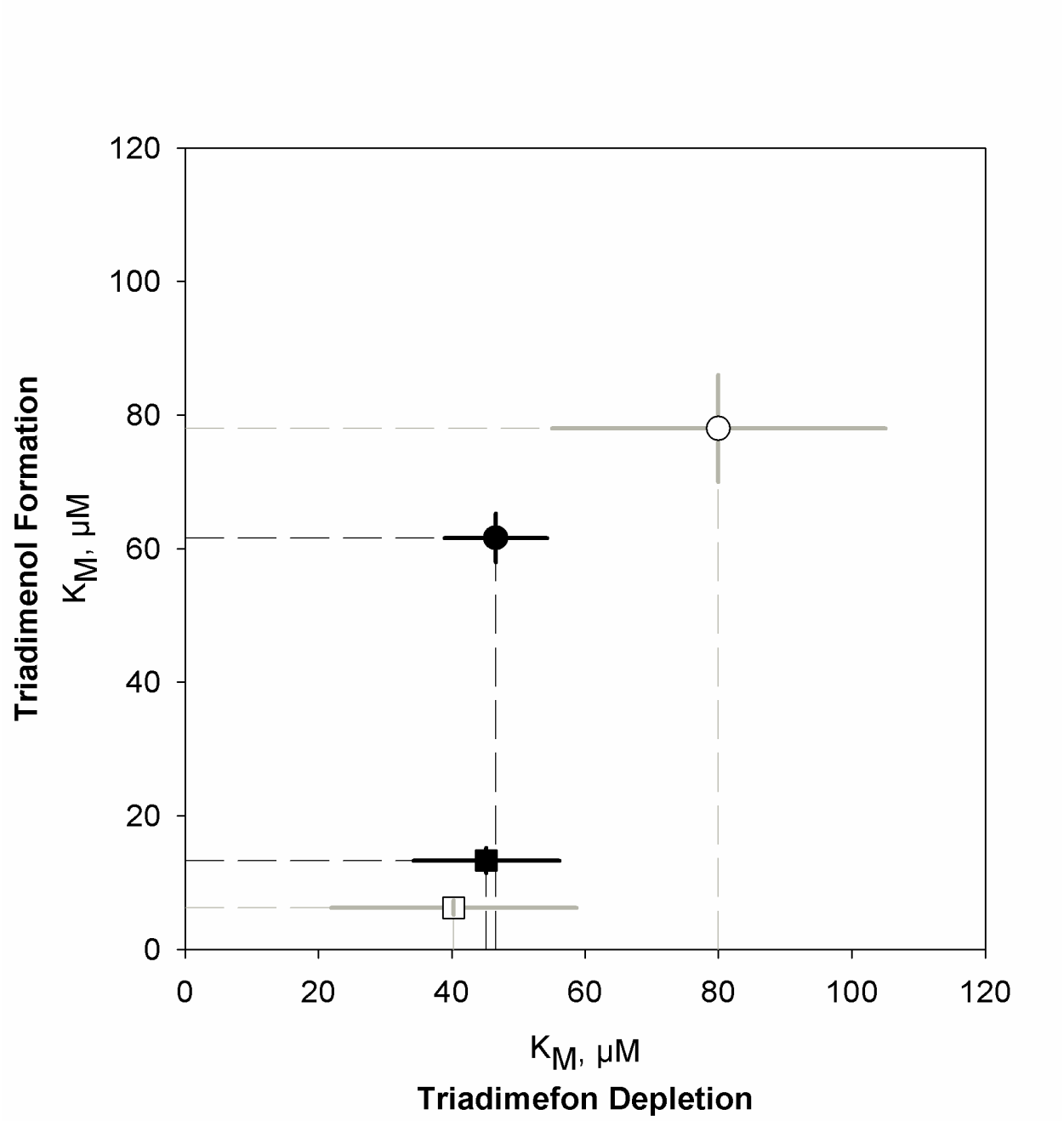

Figure 3.6: Comparison of Michaelis constants (K_M) calculated from triadimenol formation and triadimefon depletion data in male SD rat (●), female SD rat (■), male CD-1 mouse (○), and female CD-1 mouse (□), with standard error indicated by solid lines.

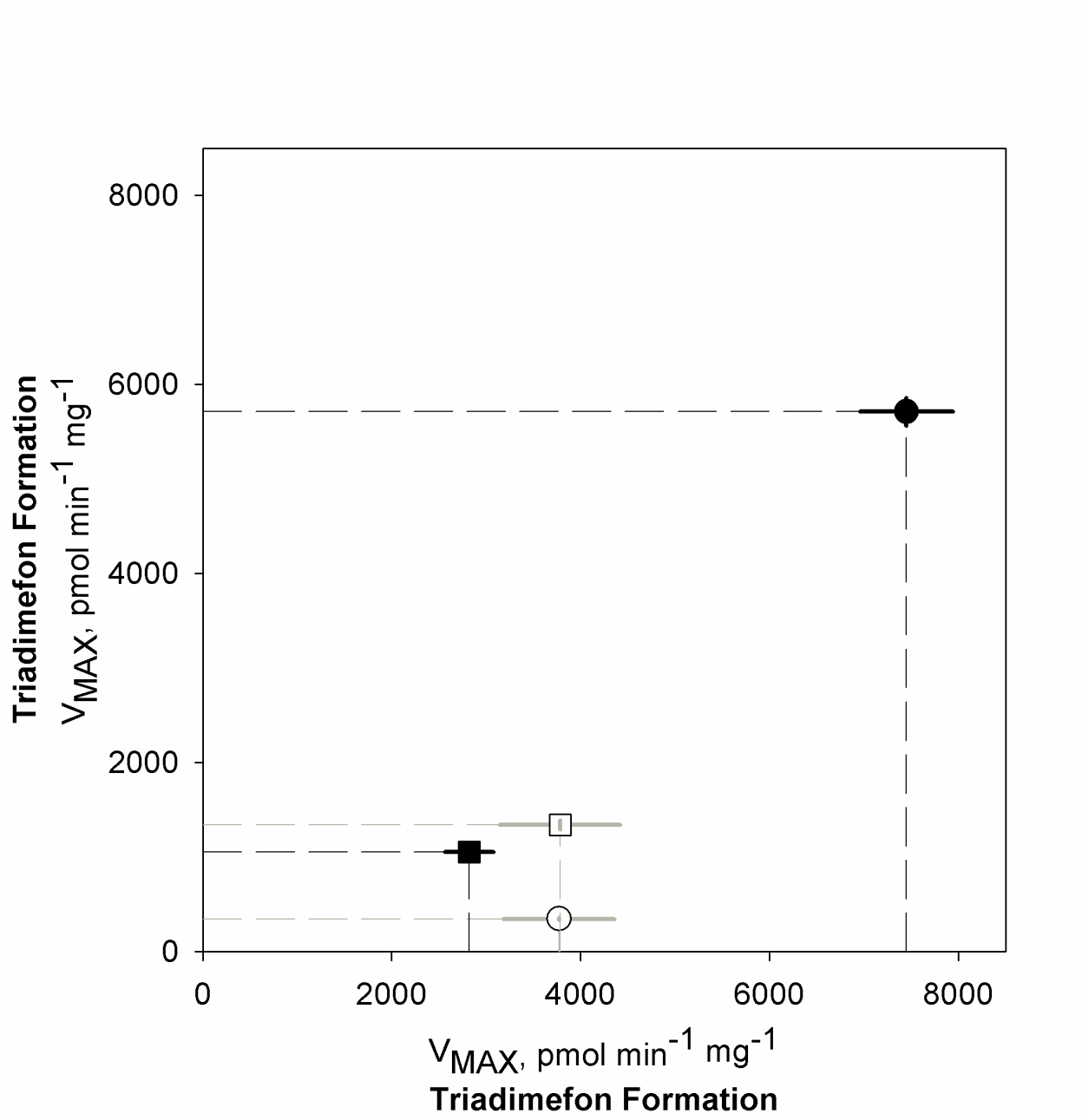

Figure 3.7: Comparison of maximum velocities (V_{MAX}) calculated from triadimenol formation and triadimefon depletion data in male SD rat (●), female SD rat (○), male CD-1 mouse (■), and female CD-1 mouse (□), with standard error indicated by solid lines.

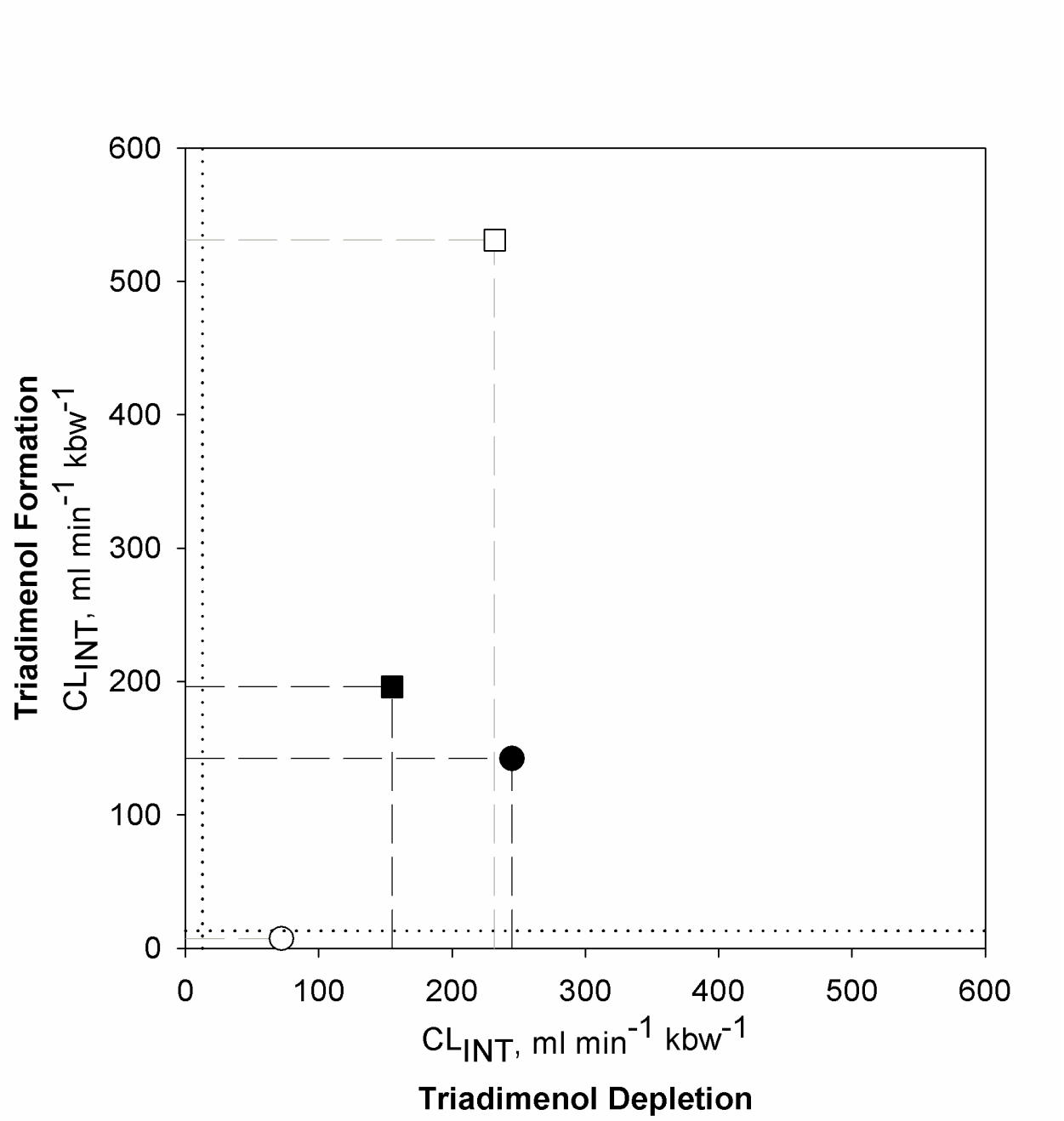

Figure 3.8: Intrinsic clearances (± S.E.) calculated from triadimefon depletion and triadimenol formation data analyzed by classic Michaelis-Menten regression in male SD rat (●), female SD rat (○), male CD-1 mouse (■), and female CD-1 mouse (□), with standard error indicated by solid lines. The rate above which clearance is mediated by the rate of blood flow is indication by dotted lines (⋯) at 13 ml $min^{-1}kbw^{-1}$ (Brown et al., 1997).

CHAPTER 4

DEVELOPMENT AND APPLICATION OF A PHYSIOLOGICALLY BASED PHARMACOKINETIC MODEL FOR TRIADIMEFON AND ITS METABOLITE TRIADIMENOL IN RATS AND HUMANS[2]

[2]Crowell, S.R., W.M. Henderson, J.F., Kenneke, and J.W. Fisher. To be submitted to *Toxicology and Applied Pharmacology*.

Abstract

A physiologically based pharmacokinetic (PBPK) model was developed for the conazole fungicide triadimefon and its primary metabolite, triadimenol. Rat tissue:blood partition coefficients and metabolic constants were measured *in vitro* for both compounds. Kinetic time course data for parent and metabolite were collected from several tissues after intravenous administration of triadimefon to male Sprague-Dawley rats. The model adequately simulated peak blood and tissue concentrations but predicted more rapid clearance of both triadimefon and triadimenol from blood and tissues. Two hypotheses were explored as possible explanations of this slow clearance: low capacity, high affinity protein binding of parent and metabolite in blood and tissues, and reverse metabolism of triadimenol to triadimefon in the liver. Model predictions were significantly improved in both cases. The original model as well as both alternate models were extrapolated to humans using *in vitro* metabolic constants measured in human hepatic microsomes. Human equivalent doses (HEDs) were calculated for all three models for a rat NOAEL dose of 11.57 µmol/kg/day using area under the concentration curve (AUC) in brain and blood for triadimefon and triadimenol as dosimetrics. All dosimetric-based HEDs were above the oral reference dose of 0.11 µmol triadimefon/kg/day.

Key Words: Triadimefon, triadimenol, PBPK, partition coefficient, human equivalent dose

Introduction

The conazole (1,2,4 triazole and imidazole) pesticides constitute approximately 40 broad spectrum fungicides with agricultural and pharmaceutical applications. The mechanism of fungicidal action is through the inhibition of 14α-lanosterol demethylase (Buchenauer, 1977), halting ergosterol synthesis and compromising the integrity and fluidity of fungal cell walls.

This biosynthetic pathway is irrelevant in vertebrates; rather, lanosterol demethylase is involved in cholesterol synthesis. Thus, it is not surprising that conazoles have been implicated in the disruption of steroid biosynthesis and related aspects of normal mammalian physiology (Zarn et al., 2003). Conazoles also modulate the expression and activity of enzymes, including many from the cytochrome P450 (CYP) family (Allen et al., 2006; Barton et al., 2006; Goetz et al.; 2006, Ronis et al. 1994), and have been observed to elicit thyroid and/or liver tumors in rodents (Hurley et al., 1998).

Triadimefon is a lipophilic, non-volatile conazole fungicide with agricultural and ornamental applications. The U.S. Environmental Protection Agency (U.S. EPA) estimates an application rate of approximately 135,000 lbs/year with an upper-end estimate of 266,000 lbs/year (U.S. EPA, 2006). In vertebrates, triadimefon undergoes carbonyl reduction to its primary metabolite, triadimenol, a reaction catalyzed by 11β-hydroxysteroid dehydrogenase type 1 (11β-HSD1) (Kenneke et al., 2008), which together with 11β-hydroxysteroid dehydrogenase type 2 is responsible for the regulation of the availability of active glucocorticoids to localized steroid receptors (Seckl and Walker, 2001). Triadimenol retains the fungicidal activity of the parent, and is itself applied as a fungicide at a rate of 24,000 lbs/year (U.S. EPA, 2006). Exposures to triadimefon and its metabolite triadimenol occur most frequently via inhalation and dermal absorption for occupational and residential handlers, as well as through oral ingestion of contaminated food products or drinking water (U.S. EPA, 2006).

A range of toxic effects have been observed subsequent to triadimefon and triadimenol exposure. Observed reproductive and developmental toxicity, as well as tumorigenicity, are held in common with other members of the conazole class. Teratogenic effects have been observed in both *in vivo* studies in mice at non-maternotoxic doses of both parent and metabolite (Menegola

et al., 2005a; 2005b) and *in vitro* studies in Sprague-Dawley rats; the latter support the hypothesized teratogenic mechanism involving triadimefon and triadimenol interaction with retinoic acid levels in the developing embryo (Di Renzo et al., 2009). Delayed reproductive development in Wistar rats subsequent to exposure to triadimefon has been attributed to the perturbation of steroid homeostasis (Goetz et al., 2007), as has reduced male/female sex ratio and female fertility index (FAO/WHO, 1985; Zarn et al., 2003). In chronic feeding studies, triadimefon has caused a dose-dependent increase in liver adenomas in male CF_1/W mice (FAO/WHO, 2004). Uniquely among conazoles, triadimefon and its metabolite cause neurotoxicity, including hyperactivity and stereotyped behavior in rodents (Crofton, 1996). Regulation of triadimefon centers upon this as the sensitive endpoint, with an oral reference dose (RfD) of 0.034 mg/kg/day. This RfD is based on a sub-chronic feeding study performed by the registrant with a no observed adverse effects level (NOAEL) dose of 3.4 mg/kg/day in Wistar rats, with an applied uncertainty factor of 100. Hyperactivity was the main effect observed at higher doses (U.S. EPA, 2006). Neurotoxicity consisting of stereotyped behavior and hyperactivity has also been observed in Sprague-Dawley rats following single administration oral gavage of 50 – 200 mg/kg triadimefon. Subsequent necropsy of the central nervous system indicated the mechanism of triadimefon induced neurotoxicity may involve alteration of monoamine (*e.g.* dopamine and/or serotonin) metabolism (Walker et al., 1990; Crofton et al., 1996), likely as a monoamine oxidase inhibitor (Gagnaire and Micillino, 2006).

Chemical risk assessment is increasingly performed with the aid of physiologically-based pharmacokinetic (PBPK) models, which facilitate interspecies extrapolations and the estimation of internal dose metrics (i.e. internal exposure to relevant tissues). They provide a quantitative alternative to uncertainty factors and thus have far reaching implications in chemical regulation.

Additionally, PBPK models often underscore unanticipated physiological complexities, based on the adequacy or inadequacy of the available resources used to create the model and its subsequent predictive ability, and thus provide an excellent means of generating future hypothesis-driven research (Clewell and Clewell, 2008).

Currently, there are no published PBPK models for any of the conazoles, and important chemical specific information, such as partition coefficients, are unavailable. Additionally, there are no published pharmacokinetic data available for triadimefon or triadimenol in any laboratory species or in humans. It is the purpose of this research to parameterize and develop a PBPK model for triadimefon and triadimenol in Sprague-Dawley rats, and then to extrapolate that model to humans. Partition coefficients for both chemicals will be measured in rat tissues, and an intravenous pharmacokinetic study undertaken in rats to provide a basis for model development and validation. The PBPK model will be used to estimate steady state oral human equivalent doses based on the rat oral NOAEL.

Materials and Methods

Animals

Male Sprague-Dawley rats (280-320 g., approximately 8-9 weeks of age) were obtained from Charles River Breeding Laboratory (Raleigh, NC). Animals were housed in isolator cages in rooms maintained at 21 ± 2°C and 50 ± 10% relative humidity with a 12-h light/dark cycle. Rats were given a minimum acclimation period of seven days before experiments began. Lab Diet Certified Rodent Chow and water were provided *ad libitum*, except during exposure. The facility is accredited by the American Association for Accreditation of Laboratory Animal Care (AAALAC). All animal protocols were approved by the Institutional Animal Care and Use

Committee at the University of Georgia and studies were performed in accordance with the National Institutes of Health (NIH) guidelines for the care and use of laboratory animals.

Chemicals

Triadimefon, triadimenol, and myclobutanil (for use as an internal standard) were obtained from the EPA National Pesticide Standard Repository (Fort Meade, MD). Phosphate buffer was purchased from Sigma Chemical Co. (St. Louis, MO). Methyl-*tert*-butyl ether (MTBE) and acetonitrile purchased from Fisher Chemicals (Fair Lawn, NJ) were of analytical grade.

Analytical

For both partition coefficient measurement and *in vivo* pharmacokinetic data, quantifications of triadimefon, triadimenol, and myclobutanil were made using an HP 6890 Series Gas Chromatograph equipped with a 5973 Mass Selective Detector and an HP 6890 Series Injector (Hewlett Packard, Avondale, PA). The injector and capillary transfer lines were both at 275°C, the MS source was at 230°C, and the quad was at 150°C. Splitless autosampler injections of 1 µl were made onto an Agilent DB-5MS column (30m x 0.25 mm x 0.25 µm) (Agilent Technologies, Santa Clara, CA), with helium carrier gas at a constant pressure (16 psi) and variable flow rate. The gas chromatograph oven temperature program began at an initial temperature of 50°C (1 min initial hold), ramped to 175°C at 27°/min, then to 250°C at 5°/min, then 10°/min to 300°C (10 min hold). The mass spectrometer was operated with the electron ionization source in selected ion monitoring mode at m/z values of 128, 181, 208, and 210 (triadimefon, retention time 14.0 min); 112, 128, 168, and 208 (triadimenol diastereomers, retention time 15.4 and 15.6 min); and 179, 206, 245, and 288 (myclobutanil, retention time 17.1 min).

Experimental

Partition coefficients were measured using methods adapted from Jepson et al. (1994). Rats were sacrificed by CO_2 asphyxiation followed by exsanguination. Blood was collected via the inferior vena cava, deposited in heparinized tubes, and stored at -80°C until use. Liver, brain, kidneys, and peri-renal fat were excised and stored separately at -80°C until use. Using a Tissue Tearor®, each tissue with the exception of blood was homogenized for ten minutes with two volumes of phosphate buffered saline (PBS) to create stock tissue slurries. Blood was vortexed with one volume of PBS to create a stock blood slurry. These stock slurries were stored at -80°C until use.

Partitioning was determined by analyzing the relative concentrations of chemical in the saline fraction and the tissue fraction of each sample, comprised of a known quantity of saline and tissue. Chemicals were dissolved in acetonitrile to create concentrated stocks, and total organic solvent in each sample was less than 1%. Tissue-free controls were prepared identically to samples.

For liver, kidney, brain, and blood, 150 µL of the appropriate tissue slurry were added to 850 µL PBS. For fat, 50 µL slurry were added to 950 µL PBS. Each sample was vortexed and then spiked with the appropriate concentration of triadimefon or triadimenol. The samples were then placed on a shaking incubator at 37°C for three (blood, liver, kidney, brain) or six (fat) hours. A time course of samples incubated for various lengths of time (30 min – 6 hours) was performed to ensure equilibration (data not shown). Samples were incubated for the shortest time necessary to reach equilibrium to prevent tissue degeneration. Each sample was then centrifuged at 1500 x *g* for 30 minutes, and 700 µL (blood, liver, kidney, brain) or 850 µL (fat) of the supernatant drawn off to a new tube. Myclobutanil was added to both the tissue and saline

fractions to a final concentration of 10 µM to act as an internal standard. Samples were vortexed for 10 minutes to allow the internal standard to mix thoroughly.

MTBE was used to extract the chemicals from each fraction of each sample. For liver, brain, blood and kidney, two volumes of MTBE were used to extract each fraction of each sample. For fat, two volumes of MTBE were used to extract the saline fraction, and four volumes of MTBE were used to extract the tissue fraction. The appropriate volume of MTBE was added to each sub-sample, and then vortexed for 30 minutes. Each sub-sample was then centrifuged at 1500 x *g* for 30 minutes, and the supernatant removed to 1.5 mL GC/MS vials, which were capped and stored at -20°C until analysis. Analyses were performed as described above.

Concentration of chemical in the saline fraction was directly determined, but because not all saline could be removed from the tissue fraction without disruption of the integrity of the pellet, concentration of chemical in the tissue fraction was calculated based on the concentration in saline, according to Equation 4.1:

$$C_T = \frac{C_{TF} * V_{TF} - C_S * (V_{TF} - V_{slurry} * C_{slurry})}{V_{slurry} * C_{slurry} * D_T}, \qquad (4.1)$$

where C_T is the concentration in tissue, C_{TF} is the measured concentration in the tissue fraction (µM), V_{TF} is the total volume of the tissue fraction (µL), C_S is the measured concentration in saline (µM), V_{slurry} is the volume of slurry used in the original sample (µL), C_{slurry} is the composition of the slurry (mg tissue/µL PBS), and D_T is the density of the tissue (g/mL).

The tissue:saline partition coefficient for each tissue was calculated according to Equation 4.2:

$$\text{Tissue:Saline} = \frac{C_T}{C_S} . \quad (4.2)$$

Tissue:blood partition coefficients were calculated by dividing the tissue:saline partition coefficients by the blood:saline partition coefficient. Mass balance for the measurement of partition coefficients was estimated by comparing the total quantity of chemical recovered in both fractions of each sample with the theoretical quantity spiked into the sample.

An intravenous (IV) pharmacokinetic study was undertaken in male Sprague-Dawley rats to aid in development and validation of a PBPK model. 66 rats were randomly assigned to ten time points (2, 15, 30, 45, 60, 120, 180, 360, 720, and 1440 minutes). A single dose of 50 mg/kg triadimefon dissolved in glycerol formal (160 mg/ml) was administered via injection at the base of the tail vein at t_0. At the appropriate end time, rats were sacrificed by CO_2 asphyxiation followed by exsanguination. Blood was collected via the inferior vena cava and then deposited in heparinized tubes and stored at -80°C until use. Liver, brain, kidneys, and peri-renal fat were excised and stored individually at -80°C until use.

For liver, brain, kidney, and fat, each tissue sample was weighed and homogenized for two minutes with two volumes of PBS using a Tissue Tearor® to create a slurry. For blood, one volume of sample was added to one volume of PBS and vortexed to create a slurry. For all tissues, 400 µL of each sample slurry was aliquoted to a microcentrifuge tube and spiked with myclobutanil, an internal standard, to a final concentration of 10 µM. Samples were vortexed for 15 minutes, and then two (blood, liver, brain, kidney) or four (fat) volumes of MTBE were added for extraction. Samples were vortexed for an additional 30 minutes, centrifuged at 1500 x *g* for 30 minutes, and the supernatant analyzed via GC/MS as described above.

PBPK Modeling

Model parameters are summarized in Tables 4.1, 4.2, and 4.3. Tissue volumes and blood flow rates were taken from Brown et al. (1997). Metabolic parameters for the carbonyl reduction of triadimefon to triadimenol for male Sprague-Dawley rats and male human were previously determined (Chapter 3; Kenneke et al., 2009). Rat tissue/blood partition coefficient values were those determined in this study. The measured kidney:saline partition coefficients for triadimefon and triadimenol were used for lumped rapidly perfused tissues and slowly perfused tissues. Rat partition coefficients were assumed to be a reasonable surrogate for human values, which were unavailable.

During development of the rat PBPK model, it became clear that the experimentally measured partition coefficients for liver and kidney were insufficient to explain the distribution of triadimefon and triadimenol to these compartments. In order to better predict partitioning into these tissues, *in vivo* distribution ratios for liver and kidney were calculated as the ratio of the area under the concentration curve (AUC) for liver and kidney data sets to the AUC for the blood data set from the pharmacokinetic study described above (Gallo et al., 1987).

The model consisted of two linked sub-models, one each for the parent (triadimefon) and the metabolite (triadimenol). Each sub-model was comprised of compartments representing blood, brain, kidney, fat, liver, and the remaining rapidly and slowly perfused tissues (Figure 4.1). All compartments except fat were described as well mixed and flow-limited; fat was described by diffusion-limited distribution. Hepatic metabolism was described using a Michaelis-Menten constant (K_M) determined *in vitro* and a calculated *in vivo* V_{MAX} value based on an *in vitro* V_{MAX} (Chapter 3; Kenneke et al., 2009) for triadimefon in the liver compartment. Clearance of triadimenol from the body was described with a simple zero order clearance term in

the blood compartment. IV exposure in the rat was simulated using study specific rates of infusion of triadimefon directly into venous blood. Uptake from food was assumed to be complete and rapid, and was incorporated into the liver compartment for both rat and human. To simulate repeated oral exposure via feeding in the rat, a constant rate of intake for twelve hours out of every 24 was used, and in the human three 30 minute meals per 24 hours, spaced five hours apart.

The terminal phase kinetics of triadimefon and triadimenol could not be described adequately with the described model structure and features. In an attempt to describe the observed kinetic behavior, two additional models were created: one with low capacity, high affinity binding of triadimefon and triadimenol in blood, liver, kidney, and brain (referred to as the "binding model"), and another with oxidation of triadimenol to triadimefon in the liver (referred to as the "reverse metabolism model").

In the binding model for Sprague-Dawley rat, parameters describing binding in blood and tissues were estimated due to the absence of data on blood or tissue binding of conazoles in the literature. For adequate description of the observed data, both parent and metabolite would bind (associate) rapidly to some biomolecule with a low binding capacity (BMaxC), and then dissociate slowly; these assumptions were used for initial visual estimation of parameters. The association constants for both triadimefon (KaTFN) and triadimenol (KaTNol) were held at a visually estimated value of 2 $\mu mol^{-1}\ hr^{-1}$, which enabled rapid binding of chemical. Slight variations in these association constants were assumed to have minimal influence on predicting tissue concentrations of either conazole. Tissue specific BMaxC and dissociation constant (Kd, µmol/hr) values were optimized as discussed below. Binding capacities were scaled to tissue volume, and association and dissociation constants were not scaled.

In the reverse metabolism model for Sprague-Dawley rat, triadimenol to triadimefon metabolism was assumed to be catalyzed by 11β HSD1 in the liver compartment. This enzyme, which is also responsible for the metabolism of triadimefon to triadimenol, has been illustrated to catalyze both oxidation and reduction reactions of endogenous metabolites (Diederich et al., 2000; Seckl and Walker, 2001). In one study, the kinetic parameters for the introconversion of the native substrates cortisone and cortisol by human liver microsomes were characterized (Diederich et al., 2000). It was reported that the ratio of the V_{MAX} of the reduction reaction to that of the oxidation reaction was approximately 2.0, while the ratio of the K_M of the reduction reaction to that of the oxidation reaction was approximately 1.5. These ratios were applied to the kinetic parameters for the reduction of triadimefon to arrive at values to characterize the reverse reaction (Table 4.3) (Diederich et al., 2000).

Model parameters neither available in the literature nor measured in this study were optimized using acslX Parameter Estimation version 2.5.0.6 (Aegis Technologies, Huntsville, AL). Optimizations were performed iteratively, based on their influence on the model. First, the clearance of metabolite from blood (CLbld2C) of rats was optimized to fit the rat IV data set. Subsequently, diffusion into and out of adipose tissue for triadimefon (PAFatC) and triadimenol (PAFat2C) were sequentially optimized. For the formulation of the model that included blood and tissue binding, each tissue was fitted to its terminal time course data (1-24hrs) for the tissue specific parameters BmaxC and Kd. Optimizations were repeated in the described manner until no change in value was observed to ensure that the resulting estimates were as accurate as possible. Optimized binding parameters appear in Table 4.3.

Extrapolation of the original model from rats to humans was performed by the inclusion of human *in vitro* metabolic constants for the conversion of triadimefon to triadimenol. For the

model with blood and tissue binding, extrapolation to humans was undertaken by incorporating *in vitro* metabolic constants and by scaling the rat binding parameters so that the peak blood concentration of triadimefon and the ratios of bound chemical to free chemical achieved by the rat model in each compartment were maintained in the human model. For the reverse metabolism model, *in vitro* metabolic constants for the conversion of triadimefon to triadimenol were included, and were also used as the basis for estimation of the metabolic constants for the conversion of triadimenol to triadimefon.

Rat and human model parameter sensitivity under steady-state conditions was quantitatively analyzed using normalized sensitivity coefficients (NSCs), which represent a fractional change in output corresponding to a fractional change in the parameter (Clewell et al., 2000). Based on the regulatory endpoint of neurotoxicity for triadimefon and triadimenol, steady state 24 hour area under the curve (AUC) for triadimefon and triadimenol in brain were chosen as the relevant model outputs. Because these are not readily measured, steady state 24 hour AUCs in blood were also used as dosimetrics for both chemicals. For the model with blood and tissue binding, unbound rather than total triadimefon and triadimenol were considered. Global sensitivity was assessed for each of the three models (original, binding, and reverse metabolism) in both rats and humans. Model parameters were increased by 10% and the model executed using rat NOAEL (11.57 umol/kg/day) oral intakes. The NSCs were calculated according to equation 4.3:

$$NSC = \frac{(A - B)/B}{(C - D)/D}, \qquad (4.3)$$

where A equals the model prediction with a 10% increase in parameter value, B is model prediction with original parameter value, C is parameter value increased by 10%, and D is

original parameter value. Each parameter was designated as having low ($|NSC|<0.15$), medium ($0.15<|NSC|<0.5$), or high sensitivity ($|NSC|>0.5$). Parameters with medium or high sensitivity were considered sufficient to influence dose or route extrapolations and thus have an impact on risk assessment.

Human equivalent doses (HEDs) were calculated for comparison to regulatory limits for human exposure derived via default approaches. The HED is the human oral triadimefon exposure (μmol/kg/day) resulting in identical dose metrics elicited in the rat following simulation of chronic NOAEL exposure concentration (11.57 μmol/kg/day). The effects of tissue binding of triadimefon and triadimenol, as well as reverse metabolism of triadimenol to triadimefon on these HEDs were also assessed.

All simulations and parameter fitting were conducted using AcslX version 2.5.0.6 (Aegis Technologies, Huntsville, AL). The Gear algorithm was used for integration of double precision variables. Parameter fitting was performed using the relative error model (variance is assumed to be proportional to the measured value across the range of measured values, or heteroskedasticity = 2), and the Nelder-Mead algorithm. The fitting criterion was maximization of the log-likelihood function. Model code appears in the appendix.

Results

Experimental

Values of experimentally measured tissue:saline and tissue:blood partition coefficients are recorded in Table 4.4. During model development, it became apparent that the partition coefficients for liver:blood and kidney:blood inadequately described the observed data. Comparisons of the area under the concentration curve (AUC) for each tissue data set to that of

the blood data set were undertaken to verify the accuracy of the measured partition coefficients. It was found that the computational approach yielded estimates similar to (*i.e.* not less than half nor more than twice) those measured experimentally in all cases except for the distribution of triadimenol in liver and kidney. The calculated *in vivo* distribution coefficients for liver and kidney were unexpectedly higher than the experimental partition coefficients, and similar to or higher than the experimental and computational values for fat. This indicated that there were physiological complexities unaccounted for by simple partitioning, and thus the computational *in vivo* distribution coefficients were used in these instances in place of measured values.

Data from the pharmacokinetic study appear in Figures 4.2, 4.3, and 4.4, alongside model simulations.

PBPK Modeling

Following IV bolus exposure to triadimefon, prediction of blood and tissue initial and peak concentrations of triadimefon and triadimenol by the original model were generally in close agreement with observed data, but predictions of concentrations during the terminal clearance phase were substantially lower than observed data. Under-prediction was more pronounced for triadimefon than triadimenol. The addition of blood and tissue binding or of reverse metabolism to the hypothesized alternate models resulted in significant improvement in the fidelity of model predictions to the observed data (Figures 4.2 – 4.4).

Blood concentrations of triadimefon and triadimenol were predicted with high accuracy for initial time points (0-3 hours) by the original model, after which clearance of each from blood was predicted to occur more rapidly than observed data suggested (Figure 4.2). The under-prediction was more marked for triadimefon, for which the simulation continued dropping rapidly to approximately 0.01 µM, while the data lingered near 1 µM until the end of the study.

While blood levels of triadimenol were modestly under-predicted, the shape of the curve was better simulated than for triadimefon. The model with blood and tissue binding simulated blood concentrations of both triadimefon and triadimenol with high fidelity for the duration of the data sets, accurately predicting peak concentrations as well as distribution and clearance behavior. The model with reverse metabolism over-predicted triadimefon concentrations in blood but predicted triadimenol concentrations with great accuracy (Figure 4.2).

Peak concentrations and several hours of redistribution and clearance of triadimefon in brain and kidney were predicted with high fidelity by the original model, while in liver the model began to under-predict triadimefon concentration within the first hour (Figure 4.3). Simulation of triadimefon concentrations in all tissue compartments except fat dropped lower and more rapidly than observed data indicated, so that the model insufficiently predicted the nature of the data set. Original model prediction of triadimefon concentration in fat was excellent for the duration of the pharmacokinetic data set. The binding model predicted triadimefon concentrations in all tissues with high fidelity for the entirety of the data set. While the reverse metabolism model predictions constituted a marked improvement in comparison to original model predictions for liver, kidney, and brain compartments, the model tended to over-predict concentrations at early time points and under-predict later time points. For prediction of triadimefon concentration in fat, the original model and the binding model yielded nearly identical and highly accurate predictions, while the reverse metabolism model modestly over-predicted concentration (Figure 4.3).

Peak liver concentrations of triadimenol were slightly over-predicted by the original model, whereas peak kidney concentrations were slightly under-predicted. In brain, the observed data suggested the concentration of triadimenol peaked at one hour, whereas the simulation by

the original model suggested the peak occurred much more rapidly. The addition of blood and tissue binding vastly improved the fit of the clearance phase of the simulations for liver, kidney, and brain to the observed data. The reverse metabolism model under-predicted clearance phase concentrations of triadimenol in liver, kidney, and brain, albeit more modestly than did the original model. Triadimenol in fat was well predicted in all three models, with the addition of binding causing a slight decrease in clearance rate, and the addition of reverse metabolism effecting negligible changes compared to the original model (Figure 4.4).

The results of the global sensitivity analyses for each of the rat and human PBPK models are presented in Tables 4.5 and 4.6, respectively. NSCs were determined for all model parameters which could logically vary, and those with medium or high sensitivity were considered sufficiently sensitive to warrant further discussion. Of the parameters tested in the original model, only six were found to be sensitive: body weight (BW), brain:blood partition coefficients for triadimefon and triadimenol (PBrn and PBrn2), the capacity for metabolism of triadimefon to triadimenol (VMaxC), the Michaelis constant for triadimefon to triadimenol (KM), and the rate of clearance of triadimenol from the blood (CLBld2C). In both rat and human models, all of these except for body weight were highly sensitive parameters, with NSCs ranging from 0.9 to 1.0 in rats, and 0.9 to 1.1 in humans. The highest NSCs were for CLBld2C; in the human model, the values of 1.1 indicated that error in this value may be amplified by the model.

In the rat model with blood and tissue binding of triadimefon and triadimenol, thirteen model parameters were found to have at least medium sensitivity: BW, brain volume (VBrnC), PBrn, PBrn2, VMaxC, KM, CLBld2C, the association constants for triadimefon and triadimenol binding (KaTFN and KaTNol), the maximum binding capacities for triadimefon and triadimenol

in the brain (BMaxBrnC and BMaxBrn2C), and the dissociation constants for triadimefon and triadimenol from the brain tissue (KdBrn and KdBrn2). In the human binding model, the maximum binding capacity of triadimenol in blood (BMaxBld2C) and the dissociation constant for triadimenol from blood (KdBld2) were sensitive in addition to all the sensitive parameters from the rat model. In rat, all parameters were highly sensitive except for KaTFN, BMaxBrnC, and KdBrn; in the human, all parameters were highly sensitive except for KaTFN. Additionally, in rat, no parameters had NSCs in excess of 1.0, whereas in human, NSCs for BW, KaTNol, and BMaxBld2C all exceeded 1.0 and thus may cause amplification of error in the human binding model.

In the rat model with reverse metabolism of triadimenol to triadimefon, ten model parameters were found to have at least medium sensitivity: cardiac output (QCC), blood flow to the liver (QLivC), BW, PBrn, PBrn2, VMaxC, KM, the capacity for metabolism of triadimenol to triadimefon (VMax2C), the Michaelis constant for triadimenol to triadimefon (KM2), and ClBld2C. In the human reverse metabolism model, the same parameters were sensitive with the exception of QCC and QLivC.. QCC, QlivC, and BW in the rat model, and BW in the human model had medium sensitivity, whereas the other parameters were highly sensitive. In neither the rat nor the human reverse metabolism models did any of the NSCs exceed 1.0, indicating no expectation of amplification of error.

The HEDs for the rat NOAEL of 11.57 umol/kg/day triadimefon appear in Table 4.7. Using the original model, the HED for the AUC of triadimefon in both blood and brain was 0.45 µmol/kg/day; the HED for the AUC of triadimenol in blood was 1.4 µmol/kg/day, and the HED for the AUC of triadimenol in brain was 0.32 µmol/kg/day. The addition of blood and tissue binding to the rat and human models had the effect of increasing the human exposure required to

achieve equivalent dose metrics to the rat. The HEDs for the blood and tissue binding model were 1.1 µmol/kg/day and 0.64 µmol/kg/day for the AUC of triadimefon in blood (unbound) and brain, respectively, and 7.9 µmol/kg/day and 0.78 µmol/kg/day for the AUC of triadimenol in blood (unbound) and brain, respectively. The addition of reverse metabolism of triadimenol to triadimefon to the rat and human models had the effect of reducing the human exposure required to achieve equivalent dose metrics to the rat, as well as increasing the steady state AUCs. The HEDs for the reverse metabolism model were 2.8 µmol/kg/day for the AUC of triadimefon in blood and in brain, and 3.0 µmol/kg/day for the AUC of triadimenol in blood and brain.

Discussion

The present study constitutes the first attempt to develop a PBPK model for triadimefon and triadimenol or any other conazole fungicides. While PBPK models of chemically unrelated pesticides have been developed, none have focused on this important class of agriculturally and medicinally relevant compounds. This study also provides the first detailed pharmacokinetic (PK) data set of triadimefon and triadimenol.

The PBPK model for triadimefon and triadimenol as it was originally constructed failed to capture the nature of the PK data, which indicated that parent and metabolite lingered in all tissue compartments rather than clearing rapidly, as the model predicted. Two alternate models were constructed to explore the observed clearance kinetics: the binding model and the reverse metabolism model. Possible effects of the inclusion of blood and tissue binding of parent and metabolite were illustrated, as were the effects of the inclusion of reverse metabolism of triadimenol to triadimefon. Other physiological processes that could potentially explain the unexpectedly long residence time include active transport of triadimefon and triadimenol into

tissues, or enterohepatic recirculation of one or both compounds, though the possibilities explored in this study are the most consistent with the observed data and the available literature.

While the binding model best described the observed rat PK data set, the considerable number of parameters optimized to the PK data limits the basis for extrapolation of this model. That is, the binding model may be overly fitted to and reliant on the PK data set. Additionally, because unique binding capacities and dissociation constants were employed in each tissue compartment, this model is the least parsimonious of those presented in this study.

The reverse metabolism model provided a marked improvement in model prediction compared to the original model, and is consistent with the available literature on the reversibility of the enzyme responsible for triadimefon reduction (Kenneke et al., 2008). However, both forward (triadimefon reduction) and reverse (triadimenol oxidation) metabolism were oversimplified in the PBPK models presented in this study. While 11β HSD1 has been illustrated to reduce triadimefon to triadimenol in liver microsomes, this enzyme is expressed in a variety of other tissues, and it is not known if the activity is the same across tissues. 11β HSD1 catalyzes both oxidation and reduction reactions for endogenous substrates (Seckl and Walker, 2001), but its ability to oxidize triadimenol has not been investigated; therefore the assumption that the relative kinetics of these reactions are comparable between endogenous ligands and xenobiotics may or may not hold true. Further complicating the case for introconversion of triadimefon and triadimenol is 11β HSD2. This enzyme, expressed primarily in the kidney, is responsible for the oxidation of active glucocorticoids and has been illustrated to catalyze oxidation of xenobiotics (Diederich et al., 2000; Seckl and Walker, 2001). 11β HSD2 is highly specific: the Michaelis constants for its native substrates are in the nanomolar range (Seckl and Walker, 2001). Thus, it is unclear if it would have a significant impact on the metabolism of

triadimenol. In any case, triadimenol oxidation should be investigated for each of these enzymes, and in tissues other than liver, in order to clarify the potential role of introconversion between triadimefon and triadimenol in their pharmacokinetics.

Though no human data sets were available for the validation of the extrapolated human PBPK models, human equivalent doses (HEDs) were calculated based on the rat NOAEL of 11.57 μmol/kg/day used for the derivation of the oral reference dose for triadimefon (0.11 μmol/kg/day). HEDs for the original model were generally the lowest, while those for the reverse metabolism model tended to be higher. The binding model had the greatest disparity between HEDs for the four dosimetrics. These HEDs, and the dosimetrics they are derived for, reflect the peculiarities of the predictions discussed for each of the models. That is, the original model predicts lower concentrations, begetting lower dosimetrics, in turn begetting lower HEDs; the opposite is true for the reverse metabolism model. It is notable that the HEDs for several of the dosimetrics for both the original and the binding models are within an order of magnitude of the oral RfD for triadimefon exposure in humans (0.11 μmol/kg/day). Though the extrapolated human models could not be validated, further research into the pharmacokinetics of triadimefon and triadimenol is certainly indicated.

Extrapolation of each of the proposed models to humans is fraught with assumptions, and none can currently be validated in humans. Additionally, the rat models on which the human models rely were developed and validated with a single PK data set. Thus, it could be considered imprudent to undertake even theoretical applications of these models to questions of risk assessment. However, limitations aside, these models provide a more scientific basis for extrapolation of the behavior of triadimefon and triadimenol between rats and humans than the

generic uncertainty factors generally employed in the risk assessment process, and encourage hypothesis driven research into data gaps uncovered by the models presented here.

PBPK modeling of triadimefon and triadimenol could be vastly improved by experimental measurement of diffusion rates into and out of adipose tissue, as well as by elucidation of clearance kinetics for both parent and metabolite. Clearance of triadimenol directly from blood was assumed to be the only route of excretion in the models presented here; this simplification was employed rather than separate routes of excretion from liver (representing fecal excretion) and kidney (representing urinary excretion) compartments because of the unavailability of sufficiently detailed data on excretion of parent or metabolite. While radiolabeling studies performed by the registrant describe the relative contributions of several routes of excretion for triadimenol, only total radiolabel excreted is reported, without identification of excreted compounds or associated time course (FAO/WHO, 1989). Additional PK studies, including urinary and fecal excretion, for different routes of administration and/or in different laboratory species would eliminate the reliance on a single data set, making the models more robust.

References

Allen, J.W., Wolf, D.C., George, M.H., Hester, S.D., Sun, G., Thai, S.F., Delker, D.A, Moore, T., Jones, C., Nelson, G., Roop, B.C., Leavitt, S., Winkfield, E., Ward, W.O., and Nesnow, S. (2006). Toxicity profiles in mice treated with hepatotumorigenic and non-hepatotumorigenic triazole conazole fungicides: propiconazole, triadimefon, and myclobutanil. *Toxicologic Pathology* 34, 853 – 862.

Barton, H.A., Tang, J., Sey, Y.M., Stanko, J.P., Murrell, R.N., Rockett, J.C., and Dix, D.J.

(2006). Metabolism of myclobutanil and triadimefon by human and rat cytochrome P450 enzymes and liver microsomes. *Xenobiotica* 36, 793 – 806.

Brown, R.P., M.D. Delp, S.L. Lindstedt, L.R. Rhomberg, R.P. Beliles (1997). Physiological parameter values for physiologically based pharmacokinetic models. *Toxicology and Industrial Health* **13**, 407 – 484.

Buchenauer, H. (1977). Mode of action of triadimefon in *Ustilago avenae*. *Pesticide Biochemistry and Physiology* 7, 309 – 320.

Clewell, H.J., P.R. Gentry, T.R. Covington, and J.M. Gearheart (2000). Development of a physiologically based pharmacokinetic model of trichloroethylene and its metabolites for use in risk assessment. *Environmental Health Perspectives Supplement 2: Trichloroethylene Health Risks – State of the Science* **108**, 283 – 305.

Crofton, K.M. (1996). A structure-activity relationship for the neurotoxicity of triazole fungicides. *Toxicology Letters* 84, 155 – 59.

Di Renzo, F., E. Corsin, M.L. Broccia, M. Marinovich, C.L.Galli, E. Giavini, and E. Menegola (2009). Molecular mechanisms of teratogenic effects induced by the fungicide triadimefon: study of the expression of TGF-β mRNA and TGF-β and CRABPI proteins during rat *in vitro* development. *Toxicology and Applied Pharmacology* 234, 107 – 116.

Diederich, S., C. Grossman, B. Hanke, M. Quinkler, M. Herrmann, V. Bahr, and W. Oelkers (2000). In the search for specific inhibitors of human 11β-hydroxysteroid-dehydrogenases (11β-HSDs): chenodeoxycholic acid selectively inhibits 11β-HSD-1. *European Journal of Endocrinology* **142**, 200 – 207.

FAO/WHO (1985). Pesticide Residues in Food: 1985 evaluations. http://www.inchem.org/documents/jmpr/jmpmono/v85pr18.htm

FAO/WHO (1989). Pesticide Residues in Food: 1989 evaluations. http://www.inchem.org/documents/jmpr/jmpmono/v89pr14.htm

FAO/WHO (2004). Pesticide Residues in Food 2004, Evaluations, FAO Plant Production and Protection Paper, 178 pp. 231 – 241. World Health Organization and Food and Agriculture Organization of the UN, Rome.

Gagnaire, F. and J.C. Micillino (2006). Effects of triadimefon on extracellular dopamine, DOPAC, HVA and 5-HIAA in adult rat striatum. *Toxicology* 217, 91 – 104.

Goetz, A.K., Bao, W., Ren, H., Schmid, J.E., Tully, D.B., Wood, C., Rockett, J.C., Narotsky, M.G., Sun, G., Lambert, G.R., Thai, S.F., Wolf, D.C., Nesnow, S., and Dix, D.J. (2006). Gene expression profiling in the liver of CD-1 mice to characterize the hepatotoxicity of triazole fungicides. *Toxicology and Applied Pharmacology* 215, 274 – 284.

Goetz, A.K., Ren, H., Schmid, J.E., Blystone, C.R., Thillainadarajah, I., Best, D.S., Nichols, H.P., Strader, L.F., Wolf, D.C., Narotsky, M.G., Rockett, J.C., and Dix, D.J. (2007). Disruption of testosterone homeostasis as a mode of action for the reproductive toxicity of triazole fungicides in the male rat. *Toxicological Sciences* 95, 227 – 239.

Hurley, P.M., Hill, R.N., and Whiting, R.J. (1998). Mode of carcinogenic action of pesticides inducing thyroid follicular cell tumors in rodents. *Environmental Health Perspectives* 106, 437 – 445.

Jepson, G.W., D.K. Hoover, R.K. Black, J.D. McCafferty, D.A. Mahle, and J.M. Gearhart (1994). A partition coefficient determination method for nonvolatile chemicals in biological tissues. *Fundamental and Applied Toxicology* 22, 519 – 524.

Kenneke, J.F, Mazur, C.S., Ritger, S.E., and Sack, T.J. (2008). Mechanistic investigation of the

non-cytochrome P450-mediated metabolism of triadimefon to triadimenol in hepatic microsomes. *Chemical Research in Toxicology*, 21, 1997 – 2004.

Kenneke, J.F…..2009

Menegola, E., Broccia, M.L., Di Renzo, F., Massa, V., and Giavini, E. (2005). Craniofacial and axial skeletal defects induced by the fungicide triadimefon in the mouse. *Birth Defects Research (Part B)* 74, 185 – 195.

Menegola, E., Broccia, M.L., Di Renzo, F., Massa, V., and Giavini, E. (2005). Study on the common teratogenic pathway elicited by the fungicides triazole-derivatives. *Toxicology in Vitro* 19, 737 – 748.

Ronis, M.J.J., Ingelman-Sundberg, M., and Badger, T.M. (1994). Induction, suppression and inhibition of multiple hepatic cytochrome P450 isozymes in the male rat and bobwhite quail *(Colinus virginianus)* by ergosterol biosynthesis inhibiting fungicides (EBIFs). *Biochemical Pharmacology* 48, 1953 – 1965.

Seckl, J.R. and B.R. Walker (2001). Minireview: 11β-hydroxysteroid dehydrogenase type 1 – a tissue-specific amplifier of glucocorticoid action. *Endocrinology* **142**, 1371 – 1376.

United States Environmental Protection Agency (2006). Re-registration eligibility decision for triadimefon and triadimenol and tolerance reassessment for triadimenol. Washington D.C.: Office of Pesticide Programs, U.S. Environmental Protection Agency.

Walker, Q.D., Lewis, M.H., Crofton, K.M., and Mailman, R.B. (1990). Triadimefon, a triazole fungicide, induces stereotyped behavior and alters monoamine metabolism in rats. *Toxicology and Applied Pharmacology* 102, 474 – 485.

Zarn, J.A., Bruschweiler, B.J, and Schlatter, J.R. (2003). Azole fungicides affect mammalian

steroidogenesis by inhibiting sterol 14a-demethylase and aromatase. *Environmental Health Perspectives* 111, 255 – 261.

Table 4.1. Model Physiological Parameters

Parameter[a]	Symbol	Rat	Human
Body weight (kg)	BW	0.307[b]	70[c]
Cardiac output (L/h/kg$^{0.75}$)	QCC	15.0	16.5[d]
Blood flows (fraction of cardiac output)			
Fat	QFatC	0.07	0.052[d]
Liver	QLivC	0.174	0.24[e]
Kidney	QKidC	0.141	0.175
Brain	QBrnC	0.02	0.114
Rapidly perfused[f]	QRapC	0.7	0.7
Slowly perfused[f]	QSlwC	0.3	0.3
Tissue volumes (fraction of body weight)			
Blood	VBldC	0.074	0.079
Fat	VFatC	0.075	0.214[d]
Fraction of fat as blood	VFatBldC	0.02	0.02
Liver	VLivC	0.0366	0.026[d]
Kidney	VKidC	0.0073	0.0044
Brain	VBrnC	0.0057	0.02
Rapidly perfused	VRapC	0.09	0.09
Slowly perfused	VSlwC	0.82	0.82

[a]Parameter values taken from Brown et al. (1997) unless otherwise noted.
[b]Study specific.
[c]ICRP Reference Man.
[d]Clewell et al. (2000).
[e]Fisher, Mahle, & Abbas (1998).
[f]Clewell et al. 2005.

Table 4.2. Measured chemical specific model parameters

	Rat Model		Human Model	
Parameter	TFN	TNL	TFN	TNL
Partition Coefficients[a]				
Fat:Blood	13.58	4.54	--	--
Liver:Blood	1.25	6.98[b]	--	--
Brain:Blood	0.96	1.18	--	--
Kidney:Blood	1.33	2.76[b]	--	--
Rapidly Perfused:Blood[c]	1.33	2.76	--	--
Slowly Perfused:Blood[c]	1.33	2.76	--	--
V_{MAX} (μmol/h/kg$^{0.75}$)	556.4	--	547.2	--
K_M (μmol/L)	47.3	--	132.7	--

TFN, triadimefon; TNL, triadimenol.
[a]Rat values used directly in human model (unitless).
[b]*In vivo* distribution coefficient, calculated as the ratio of the area under the curve of the pharmacokinetic dataset for tissue to that for blood.
[c]Assumed equal to value for kidney.

Table 4.3. Estimated parameters for PBPK models of triadimefon and triadimenol

Parameter	Units	Rat Model TFN	Rat Model TNL	Human Model TFN	Human Model TNL
	Original Model				
Clearance from blood[a]	L/h-kg	--	0.84	--	--
Diffusion into / out of fat[a]	L/h-kg	0.025	0.044	--	--
	Binding Model				
Clearance from blood[a]	L/h-kg	--	1.1	--	--
Diffusion into / out of fat[a]	L/h-kg	0.025	0.049	--	--
Association constant[b]	$\mu mol^{-1}hr^{-1}$	2	2	0.02	0.02
Dissociation constant[a]	hr^{-1}				
Blood		0.13	0.18	--	--
Liver		0.076	0.044	--	--
Kidney		0.12	0.17	--	--
Brain		0.089	0.067	--	--
Maximum binding capacity	µM				
Blood		1.7	7.9	1.5[c]	12.6[c]
Liver		21.0	19.0	89.5[c]	152[c]
Kidney		13.9	37.6	4.2[c]	94.6[c]
Brain		10.2	39.5	1.25[c]	85.0[c]
	Reverse Metabolism Model				
V_{MAX}, TNL oxidation	$\mu mol/h/kg^{0.75}$	--	278.2	--	273.5
K_M, TNL oxidation	µmol/L	--	31.5	--	88.5
Clearance from blood[a]	L/h-kg	--	0.79	--	--
Diffusion into / out of fat[a]	L/h-kg	0.025	0.063	--	--

TFN, triadimefon; TNL, triadimenol; values are estimated using AcslX Parameter Estimation except where otherwise noted.
[a]Rat value used directly in human model.
[b]Visually estimated.
[c]Estimated based on maintenance of ratio of bound to free chemical between rat and human models.

Table 4.4. Partition coefficients for triadimefon and triadimenol in Sprague-Dawley rats

Tissue	Tissue:Saline	Tissue:Blood[a]	Tissue:Blood[b]
Triadimefon			
Blood	11.79	--	--
Liver	14.68	1.25	2.56
Fat	158.8	13.47	9.84
Brain	11.45	0.97	1.68
Kidney	15.58	1.32	1.61
Triadimenol			
Blood	12.24	--	--
Liver	17.58	1.44	6.98
Fat	55.62	4.54	2.89
Brain	14.46	1.18	1.5
Kidney	12.85	1.05	2.76

[a]Determined by tissue:saline divided by blood:saline.
[b]Determined by dividing area under the curve of pharmacokinetic data sets for each tissue by that for blood.

Table 4.5. Normalized sensitivity coefficients for PBPK model prediction of steady state area under the curve for triadimefon in blood (AUC_{BLD}) and brain (AUC_{BRN}), and triadimenol in blood (AUC_{BLD2}) and brain (AUC_{BRN2}) in rat subsequent to oral exposure to 11.57 µmol/kg/day triadimefon.[a]

Parameter	AUC_{BLD}	AUC_{BRN}	AUC_{BLD2}	AUC_{BRN2}
		Original Model		
BW	0.24	0.24	0.24	0.24
PBrn	--	1.0	--	--
VMaxC	-0.91	-0.91	--	--
KM	1.0	1.0	--	--
PBrn2	--	--	--	1.0
ClBld2C	--	--	1.1	1.1
		Binding Model		
BW	0.24	0.53	0.20	0.86
VBrnC	--	0.28	--	0.65
PBrn	--	1.0	--	--
PBrn2	--	--	--	0.98
VMaxC	-0.91	-0.91	--	--
KM	1.0	1.0	--	--
ClBld2C	--	--	-0.97	-0.97
KaTFN	--	0.28	--	--
KaTNol	--	--	--	0.61
BMaxBrnC	--	0.28	--	--
KdBrn	--	-0.26	--	--
BMaxBrn2C	--	--	--	0.67
KdBrn2	--	--	--	-0.61
		Reverse Metabolism Model		
QCC	-0.17	-0.17	--	--
QLivC	-0.20	-0.20	--	--
BW	0.24	0.24	0.24	0.24
PBrn	--	1.0	--	--
PBrn2	--	--	--	1.0
VMaxC	-0.92	-0.92	--	--
KM	1.0	1.0	--	--
VMax2C	0.95	0.95	--	--
KM2	-0.84	-0.84	--	--
ClBld2C	-0.67	-0.67	-0.96	-0.96

[a]Units for AUCs are mg-hr/L. --, less than 0.15 in absolute value.

Table 4.6. Normalized sensitivity coefficients for PBPK model prediction of steady state area under the curve for triadimefon in blood (AUC_{BLD}) and brain (AUC_{BRN}), and triadimenol in blood (AUC_{BLD2}) and brain (AUC_{BRN2}) in human subsequent to oral exposure to 11.57 µmol/kg/day triadimefon.[a]

Parameter	AUC_{BLD}	AUC_{BRN}	AUC_{BLD2}	AUC_{BRN2}
		Original Model		
BW	0.25	0.25	0.24	0.24
PBrn	--	1.0	--	--
VMaxC	-0.90	-0.90	--	--
KM	1.0	1.0	--	--
PBrn2	--	--	--	1.0
ClBld2C	--	--	1.1	1.1
		Binding Model		
BW	0.24	0.71	-1.1	-0.22
VBrnC	--	0.49	--	0.75
PBrn	--	0.94	--	--
PBrn2	--	--	--	0.79
VMaxC	-0.89	-0.86	--	--
KM	1.0	0.96	--	--
ClBld2C	--	--	-0.68	-0.55
KaTFN	--	0.49	--	--
KaTNol	--	--	-1.2	-0.32
BMaxBldC	--	--	--	--
KdBld	--	--	--	--
BMaxBld2C	--	--	-1.6	-1.4
KdBld2	--	--	0.52	0.41
BMaxBrnC	--	0.56	--	--
KdBrn	--	-0.44	--	--
BMaxBrn2C	--	--	--	0.97
KdBrn2	--	--	--	-0.70
		Reverse Metabolism Model		
BW	0.24	0.24	0.24	0.24
PBrn	--	1.0	--	--
PBrn2	--	--	--	1.0
VMaxC	-0.91	-0.91	--	--
KM	1.0	1.0	--	--
VMax2C	0.85	0.85	--	--
KM2	-0.71	-0.71	--	--
ClBld2C	-0.62	-0.62	-0.95	-0.95

[a]Units for AUCs are mg-hr/L. --, less than 0.15 in absolute value.

Table 4.7. Human equivalent doses for rat oral exposure to 11.57 μmol/kg/day TFN determined using PBPK models

	Original		Binding		Reverse Metabolism	
Dose Metric	AUC	HED	AUC	HED	AUC	HED
TFN in Blood	0.73	0.45	0.73[a]	1.1	10.8	2.8
TFN in Brain	0.70	0.45	0.99	0.64	10.4	2.8
TNL in Blood	9.7	1.4	7.2[a]	7.9	10.3	3.0
TNL in Brain	11.4	0.32	25.7	0.78	12.2	3.0

AUC, steady state daily area under the curve (μmol/L·hr); HED, Human equivalent dose (μmol/kg/day); TFN, triadimefon; TNL, triadimenol.
[a]Unbound chemical.

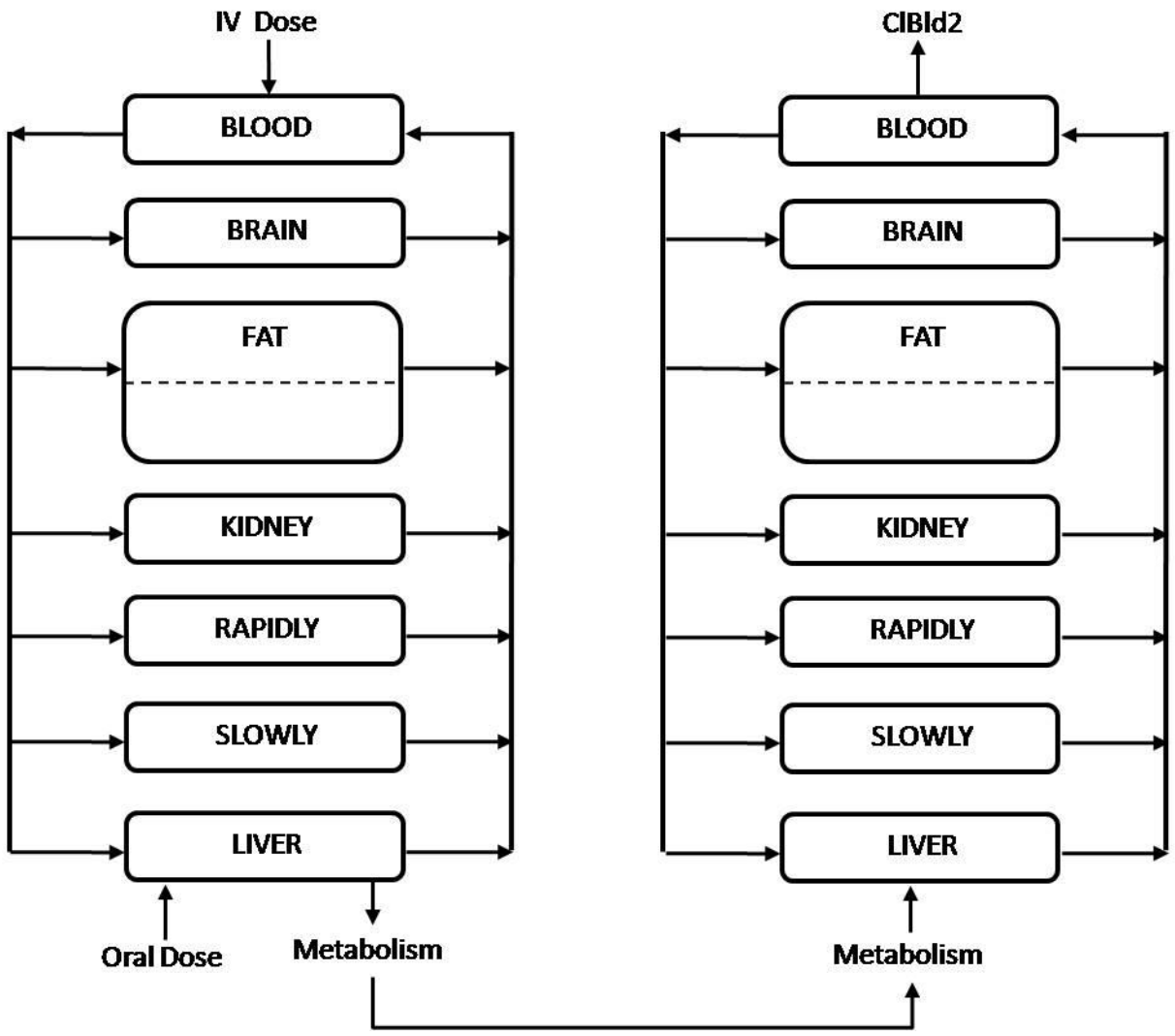

Figure 4.1. Physiologically based pharmacokinetic model used to describe the disposition of triadimefon and its metabolite triadimenol in rats and humans after oral consumption or intravenous injection (IV) of triadimefon.

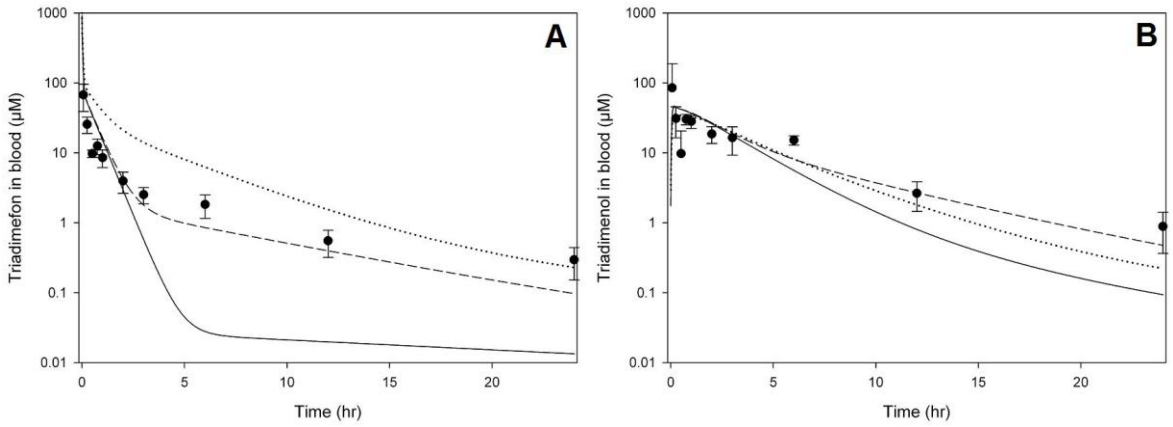

Figure 4.2. Triadimefon (TFN) and Triadimenol (TNL) in Rat Blood Pharmacokinetic data (●), original model simulations (—), binding model simulations (---), and reverse metabolism model simulations (⋯) of the (a) concentration of TFN in blood and (b) concentration of TNL in blood of male Sprague-Dawley rats administered TFN by intravenous injection at 50 mg/kg.

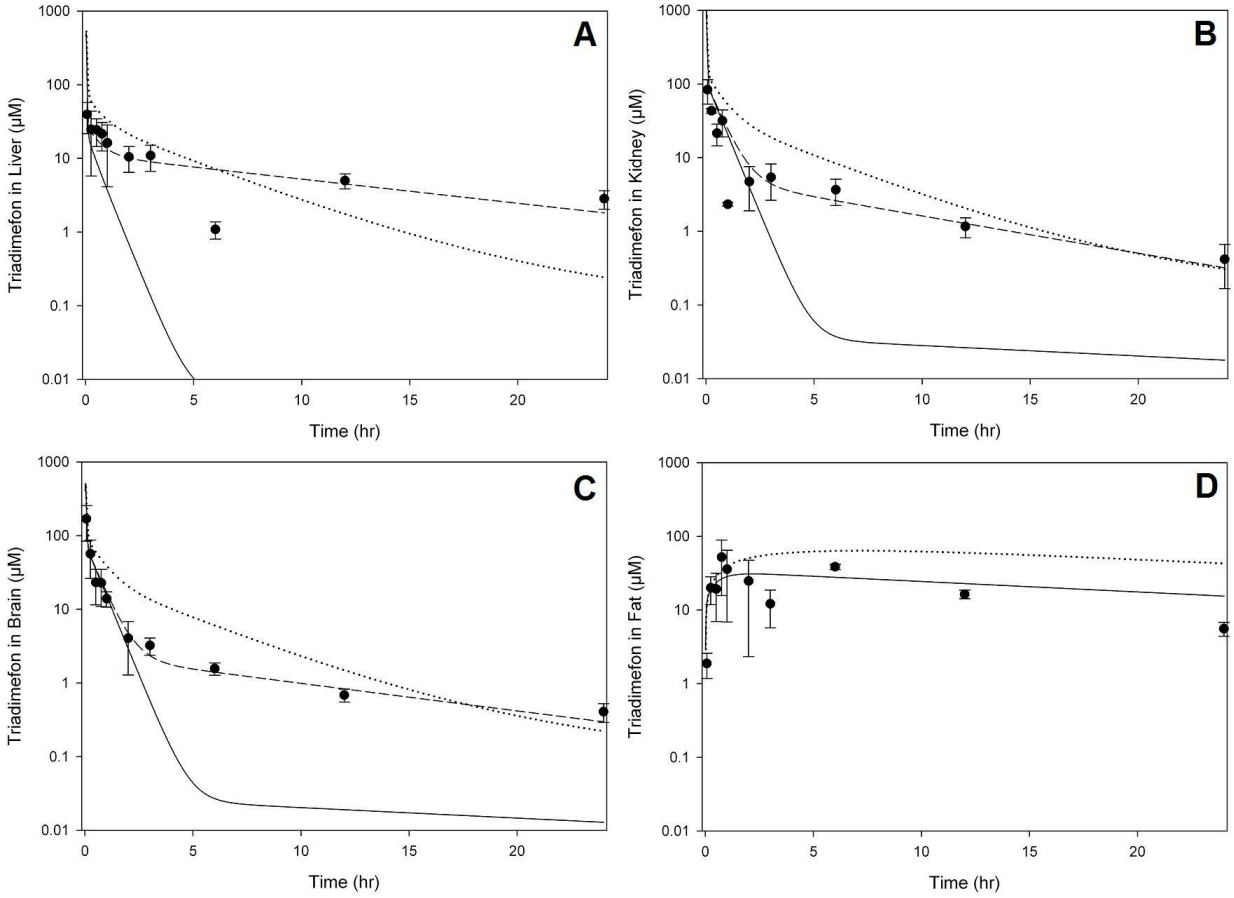

Figure 4.3. Triadimefon (TFN) in Rat Tissues. Pharmacokinetic data (●), original model simulations (—), binding model simulations (---), and reverse metabolism model simulations (⋯) of the concentration of TFN in (a) liver, (b) kidney, (c) brain, and (d) fat of male Sprague-Dawley rats administered TFN by intravenous injection at 50 mg/kg.

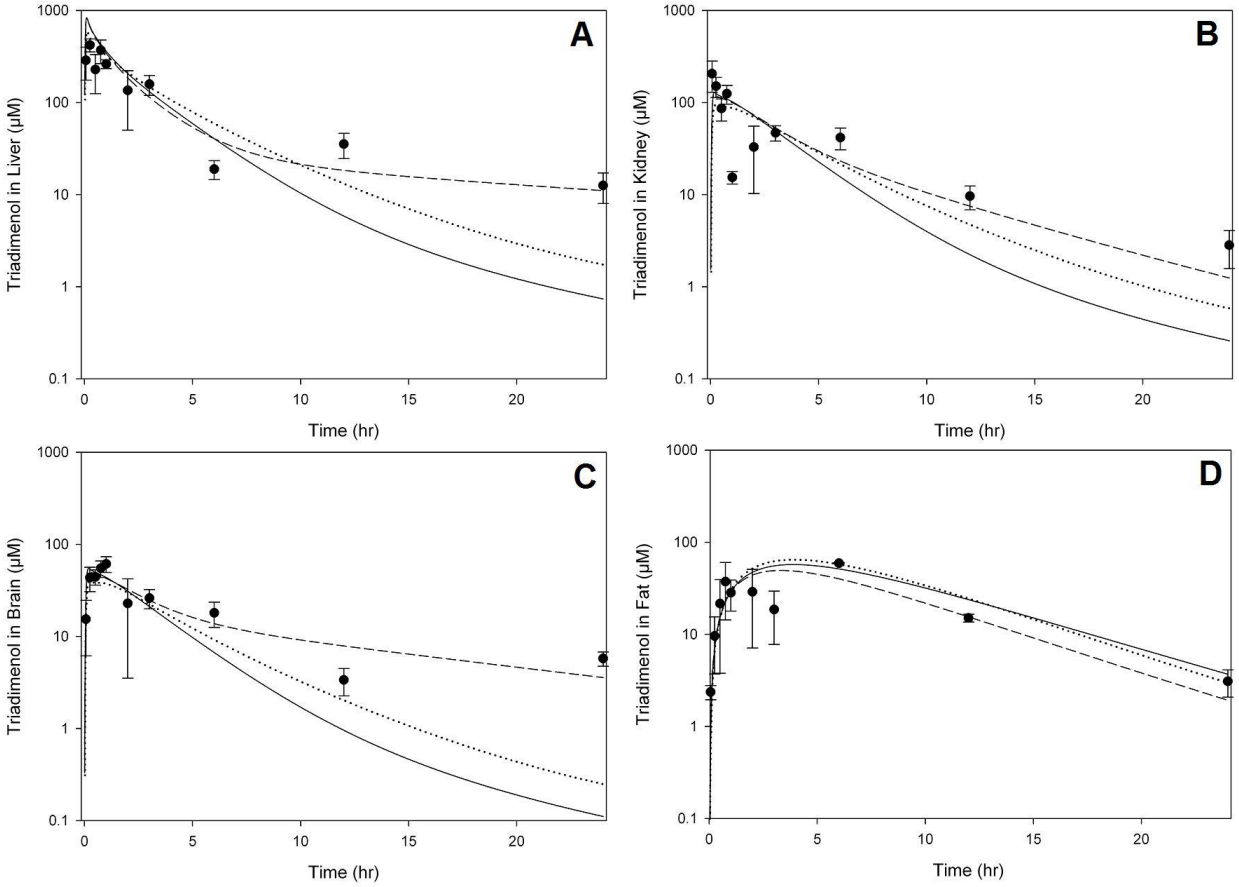

Figure 4.4. Triadimenol (TNL) in Rat Tissues. Pharmacokinetic data (●), original model simulations (—), binding model simulations (---), and reverse metabolism model simulations (⋯) of the concentration of TNL in (a) liver, (b) kidney, (c) brain, and (d) fat of male Sprague-Dawley rats administered TNL by intravenous injection at 50 mg/kg.

CHAPTER 5

COMPARISON OF THREE METHODS TO DETERMINE PARTITION COEFFICIENT VALUES: CASE STUDY WITH TRIADIMEFON AND TRIADIMENOL

[3]Crowell, S.R., W.M. Henderson, J.F. Kenneke, and J.W. Fisher. To be submitted to *Toxicology Letters.*

Abstract

The partitioning of the conazole fungicides triadimefon and triadimenol was estimated using three different methods. Partition coefficients were measured *in vitro* in male Sprague-Dawley rat tissues, calculated using an algorithm that incorporates tissue composition and log K_{OW} information, and calculated as a ratio of area under the concentration curve (AUC) in tissue and in blood from a pharmacokinetic data set in Sprague-Dawley rats subsequent to intravenous dosing of triadimefon. Values measured *in vitro* were generally lower than calculated partition coefficients, while those calculated by algorithm were substantially higher than those obtained by other methods. Partition coefficient values were used in a previously published physiologically based pharmacokinetic (PBPK) model to illustrate the consequences of determination method choice on model outcome.

Introduction

Partition coefficients describe the distribution of chemical between two adjacent phases at equilibrium. In the realm of pharmacokinetics, they often describe the ratio of distribution between blood and tissue, or blood and air. Partition coefficients are an indispensable facet of physiologically based pharmacokinetic (PBPK) models, which describe the internal distribution of a chemical or chemicals of interest within a physiological system and facilitate interspecies, route-to-route, and high-dose to low-dose extrapolations. There are a variety of methods available for the measurement or estimation of partition coefficients, the validity of which in regards to volatile compounds have been previously discussed (Payne and Kenny, 2002). For volatile chemicals, vial equilibration headspace analysis is an accepted method of *in vitro* partition coefficient measurement that has been used in a plethora of PBPK models. For this

method, the chemical of interest is allowed to reach equilibrium in tissue or tissue homogenate and the air above in a closed vial. The air is then sampled and analyzed and the distribution of the chemical in the two phases or three, if saline is used, is calculated based on mass balance (Gargas et al., 1989).

In vitro partition coefficient measurement may also be performed for chemicals with insufficient volatility for the vial equilibration headspace method. This is accomplished by measuring tissue:saline equilibrium distribution through physical separation of phases and subsequent analysis of the saline phase, according to method of Jepson and colleagues (1994). Compared to the relatively simple and elegant method for volatile compounds, there are more opportunities for the introduction of error in the measurement of partition coefficients for non-volatiles, as phases must be physically separated, sampled, extracted, and analyzed. This method for partition coefficient determination has been used in PBPK models for ethylene glycol and its metabolites (Corley et al., 2005), the metabolites of trichloroethylene (Fisher, 1998), and bisphenol A (Kawamoto et al., 2007). In the latter study, the researchers increased the measured liver:blood partition coefficient by a factor of more than 300 in order to achieve reasonable prediction of observed data, attributing the difference to physicochemical affinity and active transport of chemical into the liver.

Another oft-used method for the estimation of chemical partition coefficients is calculation by an algorithm incorporating tissue composition information and chemical specific octanol-water partition coefficients (K_{OW}) values (Poulin and Krishnan, 1996). In addition to water and octanol solubility, species- and tissue-specific measurements of water, neutral lipid, and phospholipid content are necessary for each partition coefficient calculated using the algorithm. This method has been used to calculate partition coefficients for a number of PBPK

models for pesticides, including for aldicarb (Pelekis 2009), molinate (Campbell 2009), chlorpyrifos and diazinon (Timchalk and Poet, 2007), and carbofuran (Zhang 2000). An assessment of the accuracy of this method in comparison to the vial equilibrium method for volatile compounds by Payne and Kenny (2002) revealed that the algorithm often overestimated rat tissue:blood partition coefficients, potentially because of the underestimation of solubility in blood due to possible interaction with proteins. Kidney:air and brain:air partition coefficients in particular were overestimated by approximately a factor of two, and when coupled with underestimation of blood:air partitioning, the error in tissue:blood partition coefficients was especially problematic in these tissues. The authors also found that the use of solubility in vegetable oil rather than octanol yielded partition coefficients that were in better agreement with experimentally measured values (Payne and Kenny, 2002); however, this information is not readily available for most chemicals.

If *in vivo* pharmacokinetic data sets are available, a ratio of area under the concentration curve (AUC) in tissue to AUC in blood, referred to as *in vivo* distribution coefficients, can also be used as an empirical proxy for partition coefficients (Gallo et al., 1987; King et al., 1983; Lam et al., 1981; Mirfazaelian et al., 2006). Advantages of this method include the lack of disruption of normal tissue architecture and physiology; however, it is impossible to measure *in vivo* distribution coefficients for most chemicals in humans using this method due to ethical considerations. Additionally, residual blood in *in vivo* tissues may introduce error into the resulting estimates (Khor and Mayersohn, 1991).

The conazoles are an important family of agriculturally and medicinally relevant fungicides. Currently, there are no published calculated or measured tissue:blood partition coefficients for any of the conazole family of fungicides. This work compares three methods of

partition coefficient estimation for triadimefon and its primary metabolite triadimenol: *in vitro* measurement, calculation by algorithm, and calculation by AUC ratio of *in vivo* distribution.

Methods and Materials

In Vitro *Measurement*

The methods of Jepson *et al*. (1994) were adapted for *in vitro* partition coefficient determination as previously described in Chapter 4. In short, partitioning was determined via GC/MS analysis of the relative concentrations of chemical in the saline fraction and the tissue fraction of a physically separated saline:tissue homogenate that had been spiked with a known quantity of chemical and allowed to come to equilibrium. More specifically, a known quantity of tissue homogenized using a Tissue Tearor® was added to a volume of phosphate buffered saline (PBS, pH 7.4), and then either triadimefon or triadimenol was added at known concentrations to the tissue-saline mixture. Triplicate samples were prepared for both parent and metabolite. Samples were placed in a shaking incubator at 37°C until equilibrium was reached (3 – 6 hours). Subsequent to incubation, samples were centrifuged at 1500 x *g* for 30 minutes, and a known volume constituting 75 - 90% of the total saline fraction removed. Myclobutanil was added to both the tissue and saline fractions of each sample to act as an internal standard. Samples were vortexed for 10 minutes to allow the internal standard to mix thoroughly. Samples were then extracted with methyl-*tert*-butyl ether (MTBE) at a volumetric ratio of 1:2 for saline and tissue fractions for tissues other than adipose, and 1:4 for adipose tissue fractions. Subsequent to the addition of MTBE, each sample fraction was vortexed for an additional 30 minutes, and then centrifuged at 1500 x *g* for 30 minutes. The MTBE was drawn off each sample into 1.5 mL glass vials and stored at -20°C until analysis by GC/MS.

Quantifications of triadimefon, triadimenol, and myclobutanil were made using an HP 6890 Series Gas Chromatograph equipped with a 5973 Mass Selective Detector and an HP 6890 Series Injector (Hewlett Packard, Avondale, PA). The injector and capillary transfer lines were both at 275°C, the MS source was at 230°C, and the quad was at 150°C. Splitless autosampler injections of 1 µl were made onto an Agilent DB-5MS column (30m x 0.25 mm x 0.25 µm) (Agilent Technologies, Santa Clara, CA), with helium carrier gas at a constant pressure (16 psi) and variable flow rate. The gas chromatograph oven temperature program began at an initial temperature of 50°C (1 min initial hold), ramped to 175°C at 27°/min, then to 250°C at 5°/min, then 10°/min to 300°C (10 min hold). The mass spectrometer was operated with the electron ionization source in selected ion monitoring mode at m/z values of 128, 181, 208, and 210 (triadimefon, retention time 14.0 min); 112, 128, 168, and 208 (triadimenol diastereomers, retention time 15.4 and 15.6 min); and 179, 206, 245, and 288 (myclobutanil, retention time 17.1 min).

Subsequent to GC/MS analysis, the concentrations in the saline and tissue fractions were calculated. Concentration of chemical in the saline fraction was directly determined, but because not all saline could be removed from the tissue fraction without disruption of the pellet, concentration of chemical in the tissue fraction was calculated based on the concentration in saline, according to Equation 5.1:

$$C_T = \frac{C_{TF} * V_{TF} - C_S * (V_{TF} - V_{slurry} * C_{slurry})}{V_{slurry} * C_{slurry} * D_T}, \qquad (5.1)$$

where C_T is the concentration in tissue, C_{TF} is the calculated concentration in the tissue fraction (µM), V_{TF} is the total volume of the tissue fraction (µL), C_S is the measured concentration in

saline (μM), V_{slurry} is the volume of slurry used in the original sample (μL), C_{slurry} is the composition of the slurry (mg tissue/μL PBS), and D_T is the density of the tissue (g/mL). The tissue:saline partition coefficient for each tissue was calculated according to Equation 5.2:

$$\text{Tissue:Saline} = \frac{C_T}{C_S} . \quad (5.2)$$

Tissue:blood partition coefficients were calculated by dividing the tissue:saline partition coefficients by the blood:saline partition coefficient.

In Vivo *Distribution Coefficient Calculation*

For calculation of *in vivo* distribution coefficients based on the ratio of the AUC for chemical in tissue to the AUC for chemical in blood, a pharmacokinetic data set in male Sprague-Dawley rats was used for calculation of AUCs. The pharmacokinetic data, described in detail in Chapter 4, was obtained after intravenous (IV) dosing with triadimefon; triadimefon and triadimenol were measured at ten time points over 24 hours in blood, liver, fat, brain, and kidney. AUC for concentration of triadimefon or triadimenol was determined for each data set as the area under the line connecting the measured concentrations in the tissue of interest at each time point. The *in vivo* distribution coefficient of each chemical was then determined according to Equation 5.3:

$$\text{Tissue:Blood} = \frac{AUC_T}{AUC_B} , \quad (5.3)$$

where AUC_T is the AUC in the tissue of interest, and AUC_B is the AUC in blood.

Algorithm Calculation

Tissue:blood partition coefficients for triadimefon and triadimenol were calculated for liver, adipose, brain, and kidney of Sprague-Dawley rat according to the algorithm published by Poulin and Krishnan (1995). Tissue composition information (Poulin and Theil, 2002) was incorporated in Equation 5.4:

$$\text{Tissue:Blood} = \frac{K_{OW}(V_{NT} + 0.3V_{PT}) + (V_{WT} + 0.7V_{PT})}{K_{OW}(V_{NB} + 0.3V_{PB}) + (V_{WB} + 0.7V_{PB})}, \quad (5.4)$$

(Poulin and Krishnan, 1995), where K_{OW} is the octanol:water partition coefficient, V_{NT} is the fractional volume of neutral lipids in the tissue, V_{PT} is the fractional volume of phospholipids in the tissue, V_{WT} is the fractional volume of water in the tissue, V_{NB} is the fractional volume of neutral lipids in the blood, V_{PB} is the fractional volume of phospholipids in the blood, and V_{WB} is the fractional volume of water in the blood. Log K_{OW} for triadimefon was 3.18, and 3.14 for triadimenol (individual pesticide reports from www.ars.usda.gov).

PBPK Model Comparison of Partition Coefficients

A previously described PBPK model for triadimefon and triadimenol in Sprague-Dawley rats (Chapter 4) was employed for assessment of the partition coefficients developed from the three different methods. One of several possibilities presented, the PBPK model employed here features bidirectional metabolism of triadimefon to triadimenol, and vice versa (Chapter 4). The partition coefficients were incorporated into this model, yielding three distinct model formulations, subsequently referred to as A (*in vitro* measured partition coefficients), B (*in vivo* distribution coefficients), and C (algorithm calculated partition coefficients). For each, the parameters for which published values were unavailable were estimated using acslX Parameter

Estimation version 2.5.0.6 (Aegis Technologies) and the previously described pharmacokinetic data. Optimizations were performed iteratively, based on the parameter's influence on the model. First, the clearance of triadimenol from blood (ClBld2C) was optimized to fit the data from all tissues; subsequently, diffusion into and out of adipose tissue for triadimefon (PAFatC) and triadimenol (PAFat2C) were sequentially optimized to the data describing triadimefon and triadimenol in adipose, respectively. Optimized model parameters for each of the model formulations appear in Table 5.2.

Subsequent to parameter estimation, models A, B, and C were used to simulate the exposure situation of the pharmacokinetic data set: 50 mg/kg body weight triadimefon administered via an intravenous bolus dose. Visual assessments of model predictions were used as the basis of comparison for each model formulation in order to illustrate the consequences of the utilization of each partition coefficient determination method.

Results

Partition Coefficients

Values of tissue:blood partition coefficients for triadimefon and triadimenol can be found in Table 5.1. Generally, *in vitro* partition coefficients and *in vivo* distribution coefficients were similar, while partition coefficients calculated by the algorithm were substantially (1.4 – 139 fold) higher.

The *in vitro* and *in vivo* methods resulted in partition coefficients that were within a factor of two of each other, with the exception of liver:blood and kidney:blood partition coefficients for triadimenol. The liver:blood partition coefficient for triadimenol from the *in vitro* method was 1.44, versus 6.98 for the *in vivo* method. The kidney:blood partition coefficient for triadimenol from the *in vitro* method was 1.05, versus 2.76 for the *in vivo* method.

The partition coefficients determined with the *in vitro* method were all lower than those determined by the *in vivo* method, with the exception of adipose:blood partition coefficients for both parent and metabolite, at 13.5 and 4.5, respectively; *in vivo* distribution coefficients for adipose:blood were 8.7 and 2.6, respectively. The algorithm method yielded adipose:blood partition coefficients for triadimefon and triadimenol that were 25 to 130 fold higher than estimates by other methods, at 347.6 and 340.4 respectively.

PBPK Modeling

Overall, model predictions of blood and tissue data were nearest the observed data for models A and B; model C simulations were often well above or below observed data, and in nearly all cases, the shape of the simulation was also inconsistent (Figure 5.1 – 5.5).

Model prediction of triadimefon and triadimenol in blood can be found in Figure 5.1. For triadimefon, models A and B had greater fidelity to the shape and values of the data than did model C. For A and B, concentration of triadimefon was over-predicted for much of the dataset, but the shape of the curves resembled the dataset. The prediction by model C substantially over-predicted early time points, and under-predicted terminal time points, failing to capture the shape of the data. For triadimenol, again models A and B provided predictions with high fidelity to the data, while the prediction of model C was well below the data and had an unreasonable shape.

Model prediction of triadimefon in other tissues was best for A and B, while model C generally failed to predict tissue concentration (Figure 5.2). Models A and B modestly over-predicted tissue concentration for liver, brain, and kidney, but the shape of the simulations was very similar to that of the data. For liver, brain, and kidney, model C vastly over-predicted early time points, and vastly under-predicted late time points, once again failing to capture the nature

of the data. All three models predicted triadimefon concentrations in fat with nearly identical high fidelity.

Triadimenol in tissues other than blood was generally predicted with slightly less sufficiency than triadimefon by each of the three models (Figure 5.3). Model B provided the best prediction of liver and kidney concentrations, falling at or near observed data through hour 12. Model A under-predicted liver and kidney concentrations for the majority of the time courses, but had reasonable shapes. Model C displayed an unreasonably rapid clearance of triadimenol from each of these compartments. For triadimenol in brain, models A and B provided similar and adequate predictions through hour 12, while model C over-predicted peak concentration and clearance. For triadimefon in fat, models A and B once again provided adequate predictions; the prediction by model C was reasonable through hour 6, at which point the clearance is under-estimated.

Discussion

Each of the three methods for partition coefficient determination presented here are useful for developing chemical specific parameters for PBPK modeling efforts. For triadimefon and triadimenol, the algorithm method was the least resource intensive of the three methods assessed, but also yielded values which were often dissimilar to those achieved with other methods. The *in vitro* and *in vivo* methods were both more labor and resource intensive, but resulted in values that were not only in relatively good agreement with one another, but also model predictions that were sufficiently near observed data points.

The observed inadequacies of the algorithm method for determining rat partition coefficients for triadimefon and triadimenol may be related to the caveats discussed by Payne

and Kenny (2002) in their analysis of the method for prediction of partition coefficients for volatile compounds. The authors asserted that possible binding to proteins and macromolecules in blood, and less importantly, in tissues, might cause an over-estimation of tissue:blood partition coefficients. Another possibility put forth by Payne and Kenny (2002) was that for brain and kidney in particular, overestimation was hypothesized to occur because some of the adipose within these tissues could be unavailable as a lipid sink. The apparent overestimation of partition coefficients for triadimefon and triadimenol had the effect of reducing the predictive capability of model C. Even with substantial changes in the values of optimized distribution and clearance parameters, the observed data could not be adequately simulated with the model C.

While the *in vitro* and *in vivo* approaches to partition coefficient determination generally resulted in similar values, there are advantages associated with each. Use of the *in vitro* method reduces model reliance on often scarce pharmacokinetic data sets, thereby increasing model robustness and contributing to a strong basis for model extrapolation. The *in vivo* method generates distribution coefficients that will account for physiological processes other than passive equilibration that might contribute to chemical distribution between tissues. Additionally, because physiological structure and integrity are maintained, complexities that might be missed *in vitro* will be accounted for by the *in vivo* method. Indeed, the kidney:blood and liver:blood distribution coefficients for triadimenol determined by the *in vivo* method may illustrate the latter point as they are significantly higher than those determined by the *in vitro* method, and higher than the adipose:blood partition coefficient for triadimenol determined in the same manner, which is unexpected based on the physicochemical properties of triadimenol.

By the same token, *in vivo* distribution coefficients are also the most vulnerable to variation depending on unforeseen or uninvestigated physiological factors. That the

adipose:blood partition coefficients are low relative to expectations may indicate that triadimefon and triadimenol were not in equilibrium in this physiological compartment, i.e. that triadimefon and triadimenol had not finished loading into adipose tissue. Upon extrapolation to humans, *in vivo* distribution coefficients may underestimate the true partitioning of a chemical, because the larger compartment volume relative to rats or laboratory animals used in PK data sets may magnify any inadequacies in these values. For instance, whereas in rats compartment size and blood flow generally support the assumption that a chemical reaches rapid and complete equilibrium in a blood flow limited compartment, this same assumption may not hold in humans.

In conclusion, the comparison of partition coefficient determination method for triadimefon and triadimenol presented here revealed that *in vitro* and *in vivo* methods result in similar values, while the algorithm method generally yielded higher values. Triadimefon and triadimenol are only two members of the conazole family of pesticides, and despite structural and physicochemical similarity, the results of this study should be only cautiously applied to other conazoles. Additional research into partition coefficients for conazole pesticides, as well as non-volatile chemicals in general, is certainly warranted by these results.

References

Campbell, A. (2009). Development of PBPK model of molinate and molinate sulfoxide in rats and humans. *Regulatory Toxicology and Pharmacology* 53, 195-204.

Corley, R.A., M.J. Bartels, E.W. Carney, K.K. Weitz, J.J.Soelberg, R.A. Gies, and K.D. Thrall (2005). Development of a physiologically based pharmacokinetic model for ethylene glycol and its metabolite, glycolic acid, in rats and humans. *Toxicological Sciences* 85, 476 – 490.

Fisher, J.W., D. Mahle, and R. Abbas (1998). A human physiologically based pharmacokinetic model for trichloroethylene and its metabolites, trichloroacetic acid and free trichloroethanol. *Toxicology and Applied Pharmacology* 152, 339 – 359.

Gallo, J.M., F.C. Lam, and D.G. Perrier (1987). Area method for the estimation of partition-coefficients for physiological pharmacokinetic models. *Journal of Pharmacokinetics and Biopharmaceutics* 15, 271 – 280.

Gargas, M.L., R.J. Burgess, D.E. Voisard, G.H. Cason, and M.E. Andersen (1989). Partition coefficients of low-molecular-weight volatile chemicals in various liquids and tissues. *Toxicology and Applied Pharmacology* 98, 87 – 99.

Jepson, G.W., D.K. Hoover, R.K. Black, J.D. McCafferty, D.A. Mahle, and J.M. Gearhart (1994). A partition coefficient determination method for nonvolatile chemicals in biological tissues. *Fundamental and Applied Toxicology* 22, 519 – 524.

Kawamoto, Y., W. Matsuyama, M. Wada, J. Hishikawa, M.P.L. Chan, A. Nakayama, and S. Morisawa (2007). Development of a physiologically based pharmacokinetic model for bisphenol A in pregnant mice. *Toxicology and Applied Pharmacology* 224, 182 – 191.

Khor, S.P., and M. Mayersohn (1991). Potential error in the measurement of tissue to blood distribution coefficients in physiological pharmacokinetic modeling: residual tissue blood. I. Theoretical considerations. *Drug Metabolism and Disposition* 19, 478 – 485.

King, F.G., R.L. Dedrick, J.M. Collins, H.B. Matthews, and L.S. Birnbaum (1983). Physiological model for the pharmacokinetics of 2,3,7,8-tetrachlorodibenzofuran in several species. *Toxicology and Applied Pharmacology* 67, 390 – 400.

Lam, G., M. Chen, and W.L. Chiou (1981). Determination of tissue to blood partition

coefficients in physiologically-based pharmacokinetic studies. *Journal of Pharmaceutical Sciences* 71, 454 – 456.

Payne, M.P. and L.C. Kenny (2002). Comparison of models for the estimation of biological partition coefficients. *Journal of Toxicology and Environmental Health, Part A* **65**, 897 – 931.

Pelekis, M. and C. Emond (2009). Physiological modeling and derivation of the rat to human toxicokinetic uncertainty factor for the carbamate pesticide aldicarb. *Environmental Toxicology and Pharmacology* 28, 179 – 191.

Poulin, P. and Krishnan, K. 1995. An Algorithm for Predicting Tissue:Blood Partition Coefficients of Organic Chemicals from n-Octanol:Water Partition Coefficient Data. *Journal of Toxicology and Environmental Health*, 46:117-129.

Poulin, P. and K. Krishnan (1996). A tissue composition-based algorithm for predicting tissue:air partition coefficients of organic chemicals. *Toxicology and Applied Pharmacology* 136, 126 – 130.

Poulin, P. and Theil, F.P. 2002. Prediction of Pharmacokinetics Prior to *In Vivo* Studies. 1. Mechanism-Based Prediction of Volume of Distribution. *Journal of Pharmaceutical Sciences*, 91(1):129-156.

Timchalk, C. and T.S. Poet (2007). Development of a physiologically based pharmacokinetic and pharmacodynamic model to determine dosimetry and cholinesterase inhibition for a binary mixture of chlorpyrifos and diazinon in the rat. *Neurotoxicology* 29, 428 – 443.

Zhang, X., A.M. Tsang, M.S. Okino, F.W. Power, J.B. Knaak, L.S. Harrison, and C.C. Dary

(2000). A physiologically based pharmacokinetic/pharmacodynamic model for carbofuran in Sprague-Dawley rats using the exposure-related dose estimating model. *Toxicological Sciences* 100, 345 – 359.

Table 5.1. Partition coefficients for triadimefon and triadimenol developed using three methods.

Partition Coefficient	*In vitro*	*In vivo*	Algorithm
TFN Adipose:Blood	13.47	8.67	347.60
TFN Brain:Blood	0.97	1.68	22.69
TFN Kidney:Blood	1.32	1.61	8.69
TFN Liver:Blood	1.25	2.56	9.52
TNL Adipose:Blood	4.54	2.64	340.36
TNL Brain:Blood	1.18	1.50	22.00
TNL Kidney:Blood	1.05	2.76	8.53
TNL Liver:Blood	1.44	6.98	9.16

TFN, Triadimefon; TNL, Triadimenol.

Table 5.2. Optimized PBPK model parameters for triadimefon and triadimenol

Parameter	A	B	C
ClBld2c	0.69	0.70	2.46
PAFatC	0.012	0.014	0.015
PAFat2C	0.044	0.058	0.058

A, model with measured *in vitro* partition coefficients; B, model with *in vivo* area under the curve (AUC) ratio distribution coefficients; C, model with algorithm-based partition coefficients.

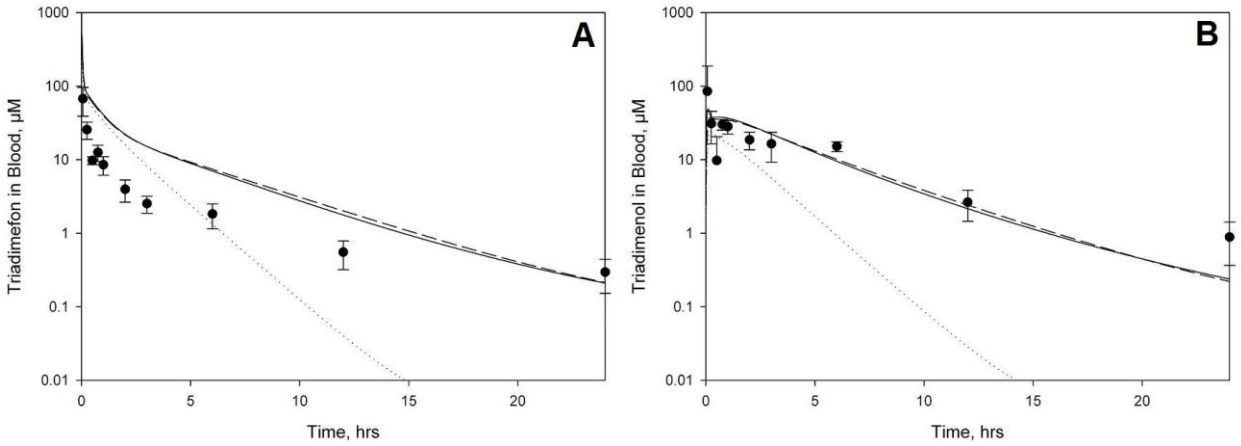

Figure 5.1. Comparison of PBPK model predictions of (A) triadimefon and (B) triadimenol in blood using three different methods of determining partition coefficients: *in vitro* measurement (—), *in vivo* distribution ratios (---), and calculation by algorithm (····).

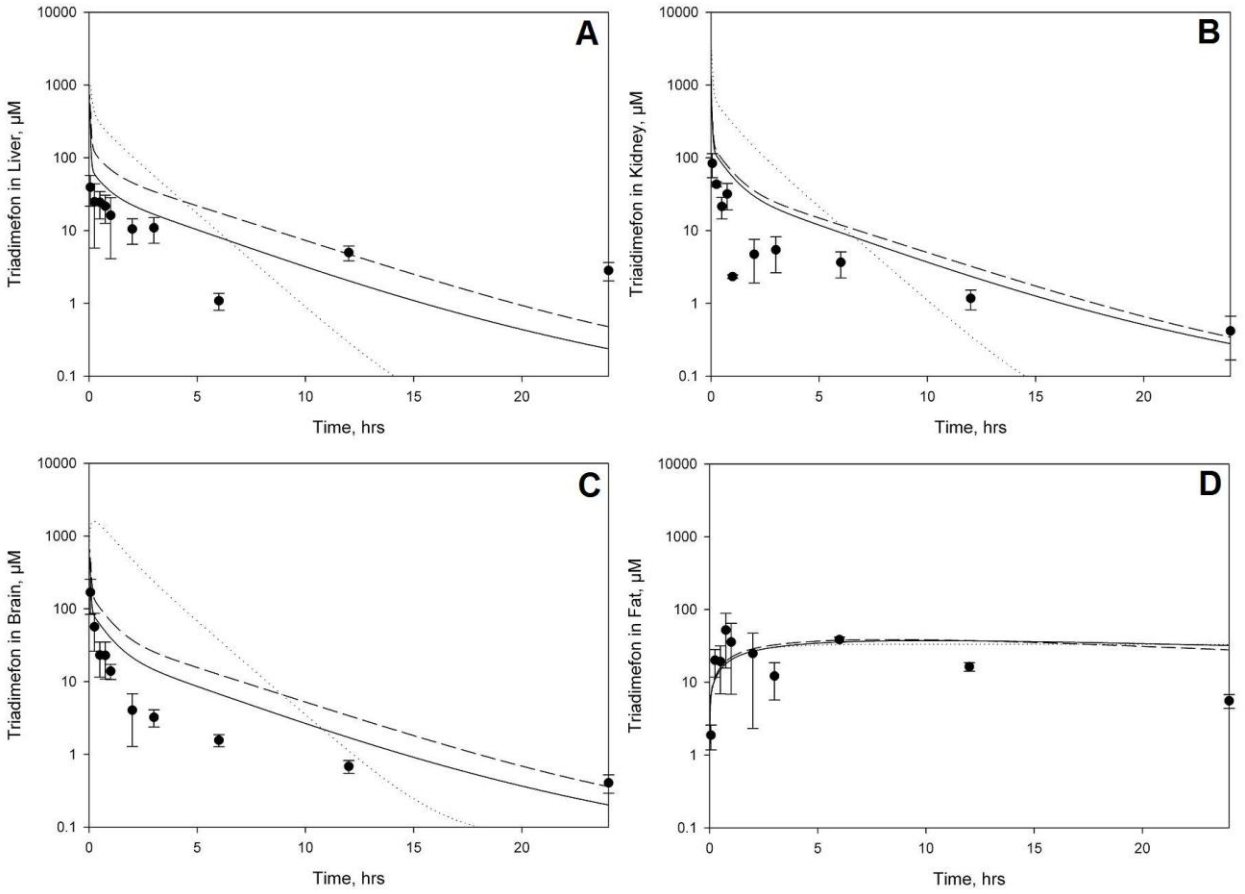

Figure 5.2. Comparison of PBPK model predictions of triadimefon in (A) liver, (B) kidney, (C) brain, and (D) fat using three different methods of determining partition coefficients: *in vitro* measurement (—), *in vivo* distribution ratios (---), and calculation by algorithm (····).

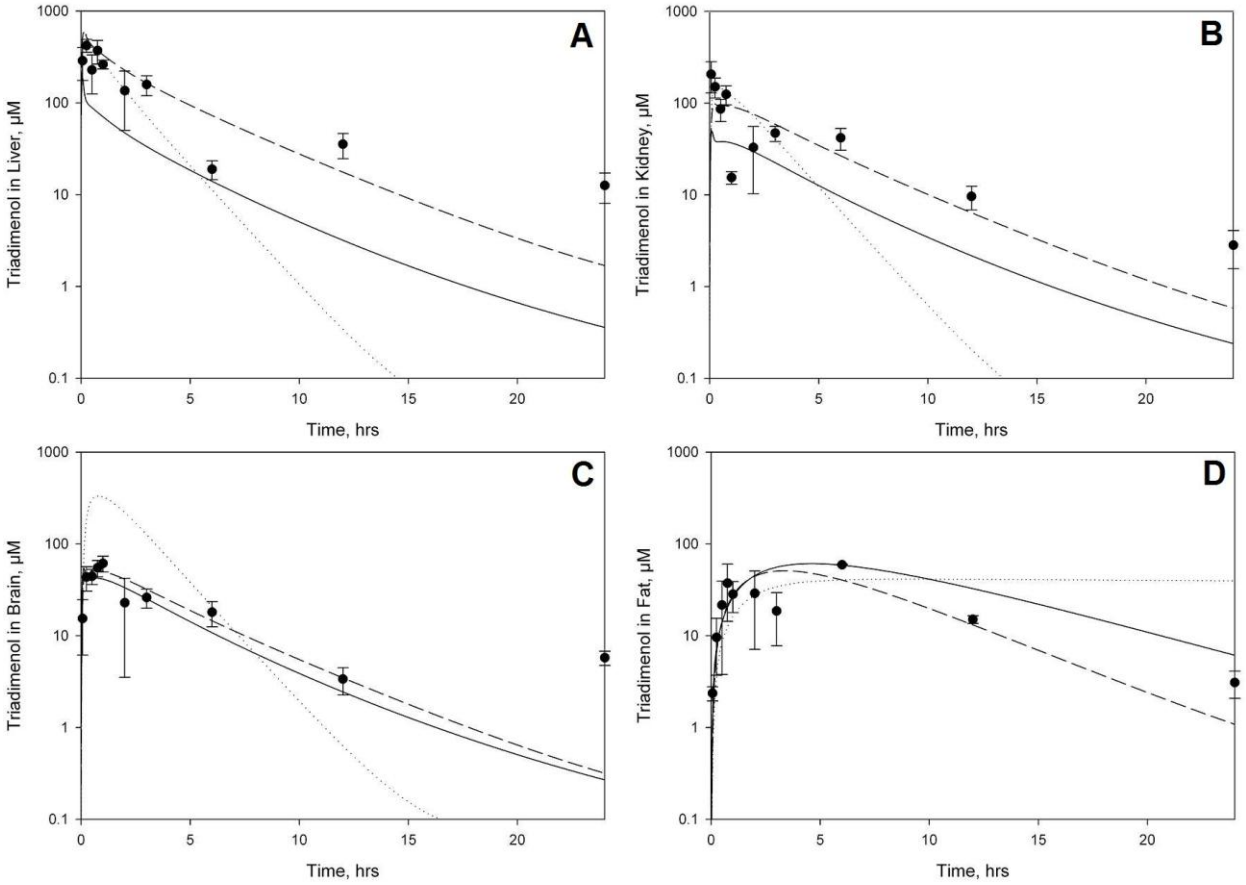

Figure 5.3. Comparison of PBPK model predictions of triadimenol in (A) liver, (B) kidney, (C) brain, and (D) fat using three different methods of determining partition coefficients: *in vitro* measurement (—), *in vivo* distribution ratios (---), and calculation by algorithm (····).

CHAPTER 6

CONCLUSIONS

Physiologically based pharmacokinetic (PBPK) modeling is often conducted as a separate enterprise from experimental characterization of chemicals, and as such, both endeavors suffer from inefficiency. This body of research focuses on the experimental description and computational modeling of triadimefon and its primary metabolite, triadimenol. Through the synthesis of these approaches, we were able to illustrate the benefits of pursuing both ends simultaneously: increasingly robust models and the generation of hypothesis-driven research.

In Vitro Metabolism Study

The reduction of triadimefon to triadimenol was investigated in hepatic microsomes of male and female Sprague-Dawley rats and CD-1 mice to determine the kinetics of the reaction. Results from this study suggest that triadimefon is reduced most rapidly by male rats, and least rapidly by female rats. Male and female mice had intermediate rates of metabolism which were very similar to one another. Michaelis constants for all reactions were in the micromolar range, indicating that interference, such as competitive inhibition, with metabolism of endogenous substrates might occur. This study also focused on the utility of the *in vitro* half life method for determination of xenobiotic clearance; results indicated this approach to be a useful screening tool. This study provided invaluable kinetic parameters for inclusion in PBPK models such as the one described subsequently.

Triadimefon and Triadimenol PBPK Model

Experimental measurement of partition coefficients and a pharmacokinetic time course for triadimefon and triadimenol generated as part of this research constitute the first such information available on any of the conazole fungicides. The PBPK model as it was originally constructed was unable to adequately predict observed data, but served as a foundation for the generation of hypotheses about triadimefon and triadimenol disposition.

Blood and tissue binding of triadimefon and triadimenol, as well as bidirectional metabolism (i.e. triadimefon reduction to triadimenol, and triadimenol oxidation to triadimefon) were hypothesized and explored in alternate PBPK models. While the resulting binding model provided excellent simulations of the pharmacokinetic data, the model contained numerous parameters that were fit to the same data set; that is, the degree of parameter estimation caused the model to be more empirical than is desirable for a PBPK model, reducing the basis for extrapolation. Additionally, the use of unique binding parameters for each compartment reduced model parsimony, casting further doubt on the validity of this alternate model for triadimefon and triadimenol ADME. The alternate model with bidirectional metabolism yielded vast improvements over the original model, though some discrepancy remained between model predictions and observed data. Despite its shortcomings, the physiological explanation was elegant and reasonable based on the available literature, and certainly warrants further exploration.

Partition Coefficient Determination Method Comparison

A number of approaches have been used historically for the measurement of partition coefficients, though the validity of most approaches has only been assessed for volatile compounds. This study sought to address three methods of partition coefficient determination

for triadimefon and triadimenol: *in vitro* measurement ("*in vitro"),* calculation from *in vivo* distribution using area under the concentration curve ("AUC"), and calculation by algorithm based on species-specific tissue composition data and information on chemical solubility in water and octanol ("algorithm"). Partition coefficients were determined for parent and metabolite, and the previously discussed PBPK model used to illustrate the effects of method choice for these chemicals. The partition coefficients determined using the *in vitro* and AUC methods were generally similar, while those determined by the algorithm method were substantially higher for most tissues. Incorporation into the PBPK model underscored this fact, as model simulations relying on partition coefficients derived from *in vitro* and AUC methods adequately described the observed data, while the simulations incorporating algorithm-derived partition coefficients failed to predict the concentrations of triadimefon and triadimenol in blood and tissues.

Conclusions and Future Directions

Experimentally measured chemical-specific parameters on metabolism and partitioning provide an invaluable anchor for the development of robust PBPK models. The PBPK model for triadimefon and triadimenol revealed interesting and important data gaps, and aided in the generation and evaluation of hypotheses for their explanation. Not only does this research underscore the importance of future research on the potential for metabolic introconversion between triadimefon and triadimenol, it also explicates the necessity of that research to be designed to provide parameters for use in this or other models. Additionally, this work reveals the necessity of additional and varied pharmacokinetic data, in other laboratory species and via other routes of administration. While data in humans is currently unavailable, the recent

inclusion of triadimefon and triadimenol into the National Health and Nutrition Examination Survey (NHANES) may lead to the development of biomonitoring data for these chemicals.

Taken together, the findings of the research presented here constitute a foundation for subsequent forays in PBPK modeling of conazole pesticides, and for triadimefon and triadimenol specifically. The model can easily be altered to reflect advancements in understanding of metabolism and other physiological processes.

APPENDIX A

The acslX (version 2.5.0.6) .csl file for triadimefon and triadimenol PBPK model (Chapter 4) is contained within this Appendix. Model code is structured as follows: first section contains physiological parameters and compound-specific constants. Second section includes scaled parameters and is followed by model code, first for triadimefon, and then triadimenol. Finally, the last section contains mass balance equations.

```
PROGRAM: Triadimefon and Triadimenol rat model

INITIAL

!-------------------------PHYSIOLOGICAL PARAMETERS--------------------------------------
!Rat Blood flows (fraction of cardiac output)
     CONSTANT     QCC = 15            ! Brown 97 via TCE report on TERA
     CONSTANT  QBrnC = 0.02          ! Brown 97
     CONSTANT  QFatC = 0.07          ! Brown 97
     CONSTANT  QLivC = 0.174         ! Brown 97
     CONSTANT  QKidC = 0.141         ! Brown 97
     CONSTANT  QRapC = 0.7           !solvent code
     CONSTANT  QSlwC = 0.3           !solvent code

!Rat Tissue Volumes (fraction of body weight, kg=L)
     CONSTANT       BW = 0.307         ! average from study (kg)
     CONSTANT    VBrnC = 0.0057        ! Brown 97, F344
     CONSTANT    VFatC = 0.075         ! Brown 97, SD
     CONSTANT    VLivC = 0.0366        ! Brown 97, F344
     CONSTANT    VKidC = 0.0073        ! Brown 97, SD
     CONSTANT    VRapC = 0.09          ! solvent code
     CONSTANT    VSlwC = 0.82          ! solvent code
     CONSTANT    VBldC = 0.074         ! Brown 97
     CONSTANT VFatBldC = 0.02          ! fat as blood, Human value, Brown 97

!-------------------------CHEMICAL SPECIFIC PARAMETERS---------------------------------
!Rat TFN Metabolism Parameters
     CONSTANT  VMaxC = 556.374    ! Max rxn rate, TFN-->Tnol, measured (umol/hr)
     CONSTANT     KM = 47.3       ! TFN-->TNol, measured (umol/L)

!Rat TFN Tissue/Blood Partition Coefficients
     CONSTANT   PBrn = 0.96      ! Brain, measured
     CONSTANT   PFat = 13.58     ! Fat, measured
     CONSTANT   PLiv = 1.25      ! Liver, measured
```

```
     CONSTANT   PKid = 1.333     ! Kidney, measured
     CONSTANT   PRap = 1.33      ! Rapidly Perfused, = Kidney
     CONSTANT   PSlw = 1.33      ! Slowly Perfused, = Kidney

!Rat TNol Tissue/Blood Partition Coefficients
     CONSTANT   PBrn2 = 1.18       ! Brain, measured
     CONSTANT   PFat2 = 4.54       ! Fat, measured
     CONSTANT   PLiv2 = 6.98       ! Liver, AUC
     CONSTANT   PKid2 = 2.76       ! Kidney, AUC
     CONSTANT   PRap2 = 2.76       ! Rapidly Perfused, = kidney
     CONSTANT   PSlw2 = 2.76       ! Slowly Perfused, = kidney

!Rat Uptake and Clearance Parameters - Estimated - Turn on one set
     !CONSTANT  ClBld2C = 0.840      ! Clearance of TNol from blood (L/hr-kg), optimized
     !CONSTANT   PAFatC = 0.0245     ! Diffusion of TFN into fat (L/h-kg), optimized
     !CONSTANT  PAFat2C = 0.0443     ! Diffusion of TNol into fat (L/hr-kg), optimized

     CONSTANT ClBld2C = 1.099         ! BINDING MODEL
     CONSTANT  PAFatC = 0.0245        ! BINDING MODEL
     CONSTANT PAFat2C = 0.04912       ! BINDING MODEL

!Rat Tissue Binding Parameters - Estimated
     CONSTANT    KaTFN = 2            ! RAT association rate constant, (1/umol*hr)
     CONSTANT   KaTNol = 2            ! RAT; set KAs to 0 to turn off binding
     CONSTANT    KdBld = 0.1326       ! dissociation rate constant, (umol/hr), optimized
     CONSTANT    KdBrn = 0.08857      ! umol/hr, optimized
     CONSTANT    KdLiv = 0.07598      ! umol/hr, optimized
     CONSTANT    KdKid = 0.1207       ! umol/hr, optimized
     CONSTANT   KdBld2 = 0.1820       ! umol/hr, optimized
     CONSTANT   KdBrn2 = 0.0666       ! umol/hr, optimized
     CONSTANT   KdLiv2 = 0.04345      ! umol/hr, optimized
     CONSTANT   KdKid2 = 0.1697       ! umol/hr, optimized
```

```
     CONSTANT  BMaxBldC = 1.663        ! RAT uM, max binding capacity of TFN in blood
     CONSTANT  BMaxBrnC = 10.117       ! RAT uM, optimized
     CONSTANT  BMaxLivC = 21.004       ! RAT uM, optimized
     CONSTANT  BMaxKidC = 13.89        ! RAT uM, optimized
     CONSTANT BMaxBld2C = 7.877        ! RAT uM, max binding capacity of TNol in blood
     CONSTANT BMaxBrn2C = 39.487       ! RAT uM, optimized
     CONSTANT BMaxLiv2C = 19.033       ! RAT uM, optimized
     CONSTANT BMaxKid2C = 37.63        ! RAT uM, optimized

!Dosing Parameters - IV (turn on IV or oral!)
     !CONSTANT   IVc_TFN = 171.39      ! IV Dose, umol/kg (50mg/kg / 291.73ug/umol)
     !CONSTANT   IVc_TFN = 109.7       ! IV for human binding ratio fitting
     !CONSTANT    IVtime = 0.00833     ! hrs, length of time for IV infusion.  (30sec)

!Dosing Parameters - ORAL
     CONSTANT   bwMeals = 0.01          ! hrs, time bw meals (RAT continuous ingestion)
     CONSTANT  MealTime = 0.01          ! hrs, time meal lasts (RAT continuous ingestion)
     CONSTANT AwakeTime = 12       ! hrs, length of time rat is awake (RAT)

     CONSTANT   OralDose = 11.57        ! Oral Dose, umol/kg/day   (3.4 mg/kg/day)
          TotMealTime = MealTime*AwakeTime/bwMeals

!Simulation Control Parameters
     CONSTANT StartDs = 0.0        ! Time first dose is given (hrs)
     CONSTANT  StopDs = 0.0        ! Time last dose is given (hrs), 0 means no repeat
     dosing
     CONSTANT   TStop = 24         ! Time simulation ends (hrs)

!------------------------SCALED PARAMETERS----------------------------------------
!Scaled Bloodflows (L/Hr)
       QC = QCC * (BW**0.75)
     QBrn = QBrnC * QC
     QFat = QFatC * QC
     QLiv = QLivC * QC
```

```
      QKid = QKidC * QC
      QRap = QRapC * QC - QLiv - QKid
      QSlw = QSlwC * QC - QFat - QBrn

!Scaled Tissue Volumes (L)
      VBld = VBldC * BW
      VBrn = VBrnC * BW
      VFat = VFatC * BW
      VLiv = VLivC * BW
      VKid = VKidC * BW
      VRap = VRapC * BW - VLiv - VKid
      VSlw = VSlwC * BW - VFat - VBrn
      VFatBld = VFatBldC * VFat            ! Fat blood volume (L)

! Tissue Mass Balance - should equal bw of rat (0.307 kg)
      TV = VBld + VBrn + VFat + VLiv + VKid + VRap + VSlw

!Blood flow mass balance - should equal QC
      TQ = QBrn + QFat + QLiv + QKid + QRap + QSlw

!Scaled Metabolism Parameters
      VMax = VMaxC * (BW**0.75)

!Scaled Clearance Rates
      ClBld2 = ClBld2C * (BW**0.75)
      PAFat = PAFatC * QFat
      PAFat2 = PAFat2C * QFat

!Scaled Binding capacities
      BMaxBld = BMaxBldC * VBld                    ! Max binding capacity, umol
      BMaxBrn = BMaxBrnC * VBrn
      BMaxLiv = BMaxLivC * VLiv
      BMaxKid = BMaxKidC * VKid
      BMaxBld2 = BMaxBld2C * VBld
```

```
     BMaxBrn2 = BMaxBrn2C * VBrn
     BMaxLiv2 = BMaxLiv2C * VLiv
     BMaxKid2 = BMaxKid2C * VKid

!Initialize Starting Values
     CInt = 0.01        ! Communication Interval
     TotDose = 0.0

END ! INITIAL

DYNAMIC

ALGORITHM IALG = 2                    !Gear stiff method

DERIVATIVE
! use either ORAL or IV

!ORAL
     Meal    = Pulse(0.,bwMeals,MealTime)         ! 30 min meals every 6 hours
     Awake   = Pulse(0.,24,AwakeTime)             ! awake for 12 hours out of 24
     Eat     = Meal*Awake
     PDose   = OralDose*BW                       ! umol/day)

!IV
     !IVR     = IVon*IVdose/IVtime
     !DoseIV  = integ(IVR, 0)
     !Dose_hr = DoseIV/IVtime
     !IVon    = Pulse(0, 24, IVtime)
     !IVdose  = IVc_TFN*BW                                    !umol

     DISCRETE
     END !DISCRETE
```

```
!-------------------------TFN Model-----------------------------------------------

! Amount in Arterial Blood (umol)
     RABldFree = QC*(CVen - CBldFree) + KDBld*ABldBound - KaTFN*BMaxBldRemain*ABldFree
     ABldFree = INTEG(RABldFree, 0)
     CBldFree = ABldFree / VBld

     RABldBound = RABldBind - RABldUnbind
     ABldBound = INTEG(RABldBound, 0.0)
     CBldBound = ABldBound / VBld
     ABld = ABldFree + ABldBound
     CBld = ABld / VBld
     AUCCBld = INTEG(CBld, 0.0)
     AUCCBldFree = INTEG(CBldFree, 0.0)

     RABldBind = KaTFN * BMaxBldRemain * ABldFree
     RABldUnbind = KDBld * ABldBound
     BMaxBldRemain = BMaxBld - ABldBound

! Amount in Brain (umol)
     RABrnFree = QBrn * (CBldFree - CVBrn) - RABrnBound
     ABrnFree = INTEG (RABrnFree,0)
     CBrnFree = ABrnFree / VBrn
     CVBrn = CBrnFree / PBrn

     RABrnBound = RABrnBind - RABrnUnbind
     ABrnBound = INTEG(RABrnBound, 0.0)
     CBrnBound = ABrnBound / VBrn

     RABrnBind = KaTFN*BMaxBrnRemain*ABrnFree
     RABrnUnbind = KDBrn*ABrnBound
     BMaxBrnRemain = BMaxBrn - ABrnBound

     ABrn = ABrnFree + ABrnBound
```

```
      CBrn = ABrn / VBrn
      AUCCBrn = INTEG(CBrn, 0.0)

! Amount in Fat (umol)
      RAFat = PAFat * (CVFat - CFat / PFat)
      AFat = INTEG(RAFat, 0)
      CFat = AFat / VFat
      AUCCFat = INTEG(CFat,0.0)

! Amount in Fat blood (umol)
      RAFatBld = QFat * (CBldFree - CVFat) + PAFat * (CFat/PFat - CVFat)
      AFatBld = INTEG(RAFatBld, 0)
      CVFat = AFatBld / VFatBld

! Amount in Liver tissue (umol)
      !RALivFree = QLiv * (CBldFree - CVLiv) - RALivBound - RAMet                    !IV
      RALivFree = QLiv * (CBldFree - CVLiv) - RALivBound - RAMet + RIntake         !Oral
      ALivFree = INTEG (RALivFree, 0)
      CLivFree = ALivFree / VLiv
      CVLiv = CLivFree / PLiv

      RALivBound = RALivBind - RALivUnbind
      ALivBound = INTEG(RALivBound, 0)
      CLivBound = ALivBound / VLiv

      RALivBind = KaTFN*BMaxLivRemain*ALivFree
      RALivUnbind = KDLiv*ALivBound
      BMaxLivRemain = BMaxLiv - ALivBound

      ALiv = ALivFree + ALivBound
      CLiv = ALiv / VLiv
      AUCCLiv = INTEG(CLiv, 0.0)

      ! Oral ingestion into Liver - turn off for IV
```

```
          RIntake = Eat*Pdose/TotMealTime
          Intake  = INTEG(RIntake,0)

     ! Amount Metabolized in Liver -- Saturable (umol)
          RAMet = (VMax * CVLiv) / (KM + CVLiv)
          AMet = INTEG(RAMet, 0.0)

! Amount in Kidney tissue (umol)
     RAKidFree = QKid * (CBldFree - CVKid) - RAKidBound
     AKidFree = INTEG (RAKidFree, 0)
     CKidFree = AKidFree / VKid
     CVKid = CKidFree / PKid

     RAKidBound = RAKidBind - RAKidUnbind
     AKidBound = INTEG(RAKidBound, 0.0)
     CKidBound = AKidBound / VKid

     RAKidBind = KaTFN*BMaxKidRemain*AKidFree
     RAKidUnbind = KDKid*AKidBound
     BMaxKidRemain = BMaxKid - AKidBound

     AKid = AKidFree + AKidBound
     CKid = AKid / VKid
     AUCCKid = INTEG(CKid, 0.0)

! Amount in Rapidly Perfused Tissue (umol)
     RARap = QRap * (CBldFree - CVRap)
     ARap = INTEG(RARap, 0)
     CRap = ARap / VRap
     CVRap = CRap / PRap

! Amount in Slowly Perfused Tissue (umol)
     RASlw = QSlw * (CBldFree - CVSlw)
     ASlw = INTEG(RASlw, 0)
```

```
     CSlw = ASlw / VSlw
     CVSlw = CSlw / PSlw

! Concentration in Mixed Venous Blood (umol/L)
!CVen = (QBrn*CVBrn+QFat*CVFat+QLiv*CVLiv+QKid*CVKid+QRap*CVRap+QSlw*CVSlw+IVR)/QC !IV
 CVen = (QBrn*CVBrn+QFat*CVFat+QLiv*CVLiv+QKid*CVKid+QRap*CVRap+QSlw*CVSlw)/QC   !ORAL
 AVen = INTEG(CVen,0.0)

!------------------------TNol Model-----------------------------------------------------

! Amount in Arterial Blood (umol)
RABldFree2 = QC*(CVen2-CBldFree2+KDBld2*ABldBound2-KaTNol*BMaxBldRemain2*ABldBound2...
     ...-RAClBld2
     ABldFree2 = INTEG(RABldFree2, 0)
     CBldFree2 = ABldFree2 / VBld

     RABldBound2 = RABldBind2 - RABldUnbind2
     ABldBound2 = INTEG(RABldBound2, 0.0)
     CBldBound2 = ABldBound2 / VBld
     ABld2 = ABldFree2 + ABldBound2
     CBld2 = ABld2 / VBld                        ! total concentration in blood
     AUCCBld2 = INTEG(CBld2, 0.0)
     AUCCBldFree2 = INTEG(CBldFree2, 0.0)        ! free in blood

     RABldBind2 = KaTNol * BMaxBldRemain2 * ABldFree2
     RABldUnbind2 = KDBld2 * ABldBound2
     BMaxBldRemain2 = BMaxBld2 - ABldBound2

     ! Clearance from blood (umol)
          RAClBld2 = ClBld2 * CVen2
           AClBld2 = INTEG(RAClBld2, 0.0)

! Amount in Brain (umol)
```

```
      RABrnFree2 = QBrn * (CBldFree2 - CVBrn2) - RABrnBound2
      ABrnFree2 = INTEG(RABrnFree2, 0)
      CBrnFree2 = ABrnFree2 / VBrn
      CVBrn2 = CBrnFree2 / PBrn2

      RABrnBound2 = RABrnBind2 - RABrnUnbind2
      ABrnBound2 = INTEG(RABrnBound2, 0.0)
      CBrnBound2 = ABrnBound2 / VBrn

      RABrnBind2 = KaTNol * BMaxBrnRemain2 * ABrnFree2
      RABrnUnbind2 = KDBrn2 * ABrnBound2
      BMaxBrnRemain2 = BMaxBrn2 - ABrnBound2

      ABrn2 = ABrnFree2 + ABrnBound2
      CBrn2 = ABrn2 / VBrn
      AUCCBrn2 = INTEG (CBrn2, 0)

! Amount in Fat blood (umol)
      RAFatBld2 = QFat * (CBldFree2 - CVFat2) + PAFat2 * (CFat2/PFat2 - CVFat2)
      AFatBld2 = INTEG(RAFatBld2, 0)
      CVFat2 = AFatBld2 / VFatBld

! Amount in Fat tissue (umol)
      RAFat2 = PAFat2 * (CVFat2 - CFat2 / PFat2)
      AFat2 = INTEG(RAFat2, 0)
      CFat2 = AFat2 / VFat
      AUCCFat2 = INTEG(CFat2,0)

! Amount in Liver (umol)
      RALivFree2 = QLiv * (CBldFree2 - CVLiv2) - RALivBound2 + RAMet
      ALivFree2 = INTEG(RALivFree2, 0)
      CLivFree2 = ALivFree2 / VLiv
      CVLiv2 = CLivFree2 / PLiv2
```

```
      RALivBound2 = RALivBind2 - RALivUnbind2
      ALivBound2 = INTEG(RALivBound2, 0.0)
      CLivBound2 = ALivBound2 / VLiv

      RALivBind2 = KaTNol * BMaxLivRemain2 * ALivFree2
      RALivUnbind2 = KDLiv2 * ALivBound2
      BMaxLivRemain2 = BMaxLiv2 - ALivBound2

      ALiv2 = ALivFree2 + ALivBound2
      CLiv2 = ALiv2 / VLiv
      AUCCLiv2 = INTEG (CLiv2, 0)

! Amount in Kidney (umol)

      RAKidFree2 = QKid * (CBldFree2 - CVKid2) - RAKidBound2
      AKidFree2 = INTEG(RAKidFree2, 0)
      CKidFree2 = AKidFree2 / VKid
      CVKid2 = CKidFree2 / PKid2

      RAKidBound2 = RAKidBind2 - RAKidUnbind2
      AKidBound2 = INTEG(RAKidBound2, 0.0)
      CKidBound2 = AKidBound2 / VKid

      RAKidBind2 = KaTNol * BMaxKidRemain2 * AKidFree2
      RAKidUnbind2 = KDKid2 * AKidBound2
      BMaxKidRemain2 = BMaxKid2 - AKidBound2

      AKid2 = AKidFree2 + AKidBound2
      CKid2 = AKid2 / VKid
      AUCCKid2 = INTEG (CKid2, 0)

! Amount in Rapidly Perfused Tissue (umol)
      RARap2 = QRap * (CBldFree2 - CVRap2)
      ARap2 = INTEG(RARap2, 0)
```

```
     CRap2 = ARap2 / VRap
     CVRap2 = CRap2 / PRap2

! Amount in Slowly Perfused Tissue (umol)
     RASlw2 = QSlw * (CBldFree2 - CVSlw2)
     ASlw2 = INTEG(RASlw2, 0)
     CSlw2 = ASlw2 / VSlw
     CVSlw2 = CSlw2 / PSlw2

! Concentration in Mixed Venous Blood (umol/L)
     CVen2 = (QBrn*CVBrn2+QFat*CVFat2+QLiv*CVLiv2+QKid*CVKid2+QRap*CVRap2+QSlw*CVSlw2)/QC
     AVen2 = INTEG(CVen2,0.0)

!-----------------Mass Balance---------------------------------------------------------
     !TDose = INTEG(IVR, 0.0)                    ! IV
     TDose = INTEG(RIntake, 0.0)                ! Oral
TFN = ABldFree+ABldBound+AFat+ALivFree+ALivBound+AKidFree+AKidBound+ARap+ASlw+AFatBld
TNL = ABldFree2+ABldBound2+AFat2+ALivFree2+ALivBound2+AKidFree2+AKidBound2...
     ...+ARap2+ASlw2+AFatBld2
     !PerEx = AClBld2/IVDose * 100
     Perex = AClBld2/Pdose * 100

TERMT(T.GT.TStop, 'Simulation Finished')

END ! DERIVATIVE
END ! DYNAMIC
!TERMINAL
!END ! TERMINAL
END ! PROGRAM
```

APPENDIX B

The acslX (version 2.5.0.6) .m file for rat PBPK model simulations of triadimefon concentration in blood and tissues (Chapter 4) is contained within this appendix. Code to display pharmacokinetic data is followed by commands used to generate simulations of triadimefon concentration in blood and tissues subsequent to the exposure scenario of the pharmacokinetic data and code to generate dosimetrics used for calculation of human equivalent doses.

```
%M File for simulation of TFN concentrations in tissues of Rat

%time in hrs, TFN in uM, TNol in uM
RatLiv = [0.067    39.511    287.147
0.250    24.832    421.615
0.500    24.399    228.392
0.750    21.592    371.533
1.000    16.269    262.156
2.000    10.482    135.829
3.000    10.903    158.045
6.000    01.086    018.913
12.00    04.990    035.430
24.00    02.838    012.552];

%time in hrs, TFN in uM, TNol in uM
RatFat = [0.067    01.880    02.360
0.250    20.028    09.577
0.500    19.279    21.544
0.750    52.152    37.306
1.000    35.816    28.337
2.000    24.813    28.972
3.000    12.156    18.562
6.000    38.610    59.369
12.00    16.373    15.066
24.00    05.580    03.086];

%time in hrs, TFN in uM, TNol in uM
RatBld = [0.067    67.41487718    84.97011671
0.250    25.70349426    30.91374583
0.500    09.74675369    09.7616430
0.750    12.52958257    30.22047723
1.000    08.56557746    28.21581189
2.000    03.96634196    18.60690974
3.000    02.52507091    16.43837312
```

```
6.000    01.82701153    15.20864159
12.00    00.55176395    02.64689812
24.00    00.29671826    00.88786814];

%time in hrs, TFN in uM, TNol in uM
RatBrn = [0.067    169.021    15.376
0.250    056.629    43.463
0.500    023.162    44.462
0.750    022.857    54.913
1.000    013.934    61.254
2.000    004.054    22.873
3.000    003.234    26.106
6.000    001.569    17.997
12.00    000.686    03.365
24.00    000.407    05.749];

%time in hrs, TFN in uM, TNol in uM
RatKid = [0.067    83.735    205.783
0.250    43.259    150.402
0.500    21.485    086.186
0.750    31.819    124.579
1.000    02.332    015.430
2.000    04.724    032.816
3.000    05.429    046.987
6.000    03.674    041.683
12.00    01.170    009.620
24.00    00.417    002.825];

TSTOP=24
CInt=0.01
output @clear
prepare @clear @all
start @NoCallback
```

```
livx=[0.067 0.25 0.5 0.75 1 2 3 6 12 24];
livy=[39.511 24.832 24.399 21.592 16.269 10.482 10.903 1.086 4.99 2.838]% error centers
live=[17.797 19.079 9.986 9.023 12.162 4.017 4.222 0.286 1.137 0.801]% error size
livh = errorbar(livx,livy,live)                          % Generate error bars
liv=plot(livh,1,_t,_cliv,RatLiv(:,1),RatLiv(:,2),'+')    % Overlay simulated results
settabtitle(liv,'Liver')

fatx=[0.067 0.25 0.5 0.75 1 2 3 6 12 24];
faty=[1.88 20.028 19.279 52.152 35.816 24.813 12.156 38.61 16.373 5.58]% error centers
fate=[0.705 8.22 12.302 36.476 28.951 22.489 6.457 3.182 2.199 1.189]% error size
fath = errorbar(fatx,faty,fate)                          % Generate error bars
fat=plot(fath,1,_t,_cfat,RatFat(:,1),RatFat(:,2),'+')    % Overlay simulated results
settabtitle(fat,'Fat')

venx=[0.067 0.25 0.5 0.75 1 2 3 6 12 24];
veny=[67.415 25.703 9.747 12.53 8.566 3.966 2.525 1.827 0.552 0.297]% error centers
vene=[28.354 6.754 1.156 3.124 2.427 1.33 0.657 0.672 0.232 0.145]% error size
venh = errorbar(venx,veny,vene)                           % Generate error bars
%ven=plot(venh,1,_t,_cven,RatBld(:,1),RatBld(:,2),'+')    % Overlay simulated results
ven=plot(venh,1,_t,_cbld,RatBld(:,1),RatBld(:,2),'+')
settabtitle(ven,'Blood')

brnx=[0.067 0.25 0.5 0.75 1 2 3 6 12 24];
brny=[169.021 56.629 23.162 22.857 13.934 4.054 3.234 1.569 0.686 0.407]% error centers
brne=[85.273 30.413 11.665 12.003 3.271 2.771 0.851 0.294 0.138 0.115]% error size
brnh = errorbar(brnx,brny,brne)                           % Generate error bars
brn=plot(brnh,1,_t,_cbrn,RatBrn(:,1),RatBrn(:,2),'+')     % Overlay simulated results
settabtitle(brn,'Brain')

kidx=[0.067 0.25 0.5 0.75 1 2 3 6 12 24];
kidy=[83.735 43.259 21.485 31.819 2.332 4.724 5.429 3.674 1.17 0.417]% error centers
kide=[30.553 3.237 7.032 12.673 0.132 2.822 2.797 1.437 0.354 0.25]% error size
kidh = errorbar(kidx,kidy,kide)                           % Generate error bars
```

```
kid=plot(kidh,1,_t,_ckid,RatKid(:,1),RatKid(:,2),'+')      % Overlay simulated results
settabtitle(kid,'Kidney')
```

APPENDIX C

The acslX (version 2.5.0.6) .m file for rat IV exposure PBPK model simulations of triadimenol concentration in blood and tissues (Chapter 4) is contained within this appendix. Code to display pharmacokinetic data is followed by commands used to generate simulations of triadimenol concentration in blood and tissues subsequent to the exposure scenario of the pharmacokinetic data.

```
%M File for simulation of TFN concentrations in tissues of Rat

%time in hrs, TFN in uM, TNol in uM
RatLiv = [0.067    39.511    287.147
0.250    24.832    421.615
0.500    24.399    228.392
0.750    21.592    371.533
1.000    16.269    262.156
2.000    10.482    135.829
3.000    10.903    158.045
6.000    01.086    018.913
12.00    04.990    035.430
24.00    02.838    012.552];

%time in hrs, TFN in uM, TNol in uM
RatFat = [0.067    01.880    02.360
0.250    20.028    09.577
0.500    19.279    21.544
0.750    52.152    37.306
1.000    35.816    28.337
2.000    24.813    28.972
3.000    12.156    18.562
6.000    38.610    59.369
12.00    16.373    15.066
24.00    05.580    03.086];

%time in hrs, TFN in uM, TNol in uM
RatBld = [0.067    67.41487718    84.97011671
0.250    25.70349426    30.91374583
0.500    09.74675369    09.7616430
0.750    12.52958257    30.22047723
1.000    08.56557746    28.21581189
2.000    03.96634196    18.60690974
3.000    02.52507091    16.43837312
```

```
6.000    01.82701153    15.20864159
12.00    00.55176395    02.64689812
24.00    00.29671826    00.88786814];

%time in hrs, TFN in uM, TNol in uM
RatBrn = [0.067    169.021    15.376
0.250    056.629    43.463
0.500    023.162    44.462
0.750    022.857    54.913
1.000    013.934    61.254
2.000    004.054    22.873
3.000    003.234    26.106
6.000    001.569    17.997
12.00    000.686    03.365
24.00    000.407    05.749];

%time in hrs, TFN in uM, TNol in uM
RatKid = [0.067    83.735    205.783
0.250    43.259    150.402
0.500    21.485    086.186
0.750    31.819    124.579
1.000    02.332    015.430
2.000    04.724    032.816
3.000    05.429    046.987
6.000    03.674    041.683
12.00    01.170    009.620
24.00    00.417    002.825];
TSTOP=24
CInt=0.01
output @clear
prepare @clear @all

start @NoCallback
```

```
liv2x=[0.067 0.25 0.5 0.75 1 2 3 6 12 24];
liv2y=[287.147 421.615 228.392 371.533 262.156 135.829 158.045 18.913 35.43 12.552]
liv2e=[112.208 67.825 103.788 106.874 28.702 85.861 38.701 4.411 10.839 4.569]
liv2h = errorbar(liv2x,liv2y,liv2e)                          % Generate error bars
liv2=plot(liv2h,1,_t,_cliv2,RatLiv(:,1),RatLiv(:,3),'+')   % Overlay simulated results
settabtitle(liv2,'Liver2')

fat2x=[0.067 0.25 0.5 0.75 1 2 3 6 12 24];
fat2y=[2.36 9.577 21.544 37.306 28.337 28.972 18.562 59.369 15.066 3.086]
fat2e=[0.412 5.862 17.762 22.982 10.532 21.859 10.797 0.751 1.426 1.012]
fat2h = errorbar(fat2x,fat2y,fat2e)                          % Generate error bars
fat2=plot(fat2h,1,_t,_cfat2,RatFat(:,1),RatFat(:,3),'+')   % Overlay simulated results
settabtitle(fat2,'Fat2')

ven2x=[0.067 0.25 0.5 0.75 1 2 3 6 12 24];
ven2y=[84.97 30.914 9.762 30.22 28.216 18.607 16.438 15.209 2.647 0.888]
ven2e=[101.932 14.528 10.856 5.055 5.84 5.002 7.145 2.316 1.197 0.524]
ven2h = errorbar(ven2x,ven2y,ven2e)                          % Generate error bars
ven2=plot(ven2h,1,_t,_cbld2,RatBld(:,1),RatBld(:,3),'+')   % Overlay simulated results
settabtitle(ven2,'Blood2')

brn2x=[0.067 0.25 0.5 0.75 1 2 3 6 12 24];
brn2y=[15.376 43.463 44.462 54.913 61.254 22.873 26.106 17.997 3.365 5.749]
brn2e=[9.215 12.894 8.397 11.191 11.894 19.355 6.155 5.508 1.11 1.012]
brn2h = errorbar(brn2x,brn2y,brn2e)                          % Generate error bars
brn2=plot(brn2h,1,_t,_cbrn2,RatBrn(:,1),RatBrn(:,3),'+')   % Overlay simulated results
settabtitle(brn2,'Brain2')

kid2x=[0.067 0.25 0.5 0.75 1 2 3 6 12 24];
kid2y=[205.783 150.402 86.186 124.579 15.43 32.816 46.987 41.683 9.62 2.825]
kid2e=[76.707 37.003 23.41 28.942 2.412 22.573 8.878 11.126 2.786 1.256]
kid2h = errorbar(kid2x,kid2y,kid2e)                          % Generate error bars
kid2=plot(kid2h,1,_t,_ckid2,RatKid(:,1),RatKid(:,3),'+')   % Overlay simulated results
settabtitle(kid2,'Kidney2')
```

APPENDIX D

The acslX (version 2.5.0.6) .m file for human oral exposure simulations by the PBPK model of triadimefon and triadimenol (Chapter 4) is contained within this appendix. The .m file contains first human physiological and chemical specific parameters, followed by code to generate the appropriate dosimetrics for the calculation of human equivalent doses. The code facilitates use of the original model, the binding model, or the reverse metabolism model based on which physiological parameters are enabled.

```
% Human Blood flows
QCC = 16.5        % Clewell et al. 2000
QBRNC = 0.114         % Brown et al. 1997
QFATC = 0.052         % Clewell et al. 2000
QLIVC = 0.24            % Fisher, Mahle, & Abbas, 1998
QKIDC = 0.175         % Brown et al., 1997
QRAPC = 0.7       % Clewell et al. 2005
QSLWC = 0.3       % Clewell et al. 2005

% Human Tissue volumes
BW = 70            % EPA Default
VBRNC = 0.02       % Brown et al. 1997
VFATC = 0.214      % Clewell et al. 2000
VLIVC = 0.026      % Clewell et al. 2000
VKIDC = 0.0044     % Brown et al. 1997
VRAPC = 0.09       % Solvent code
VSLWC = 0.82       % Solvent code
VBLDC = 0.0869      % Brown et al. 1997
VFATBLDC = 0.02     % Brown et al. 1997

% Human TFN Metabolism Parameters
VMAXC = 547.153
KM = 132.74

% Human dosing parameters
BWMEALS = 6           % hrs, length of time between meals (HUMAN)
MEALTIME = 0.5        % hrs, length of time meal lasts (HUMAN)
AWAKETIME = 18        % hrs, length of time man is awake (HUMAN)

%--------------ORIGINAL MODEL-----------------
VMAX2C = 0            % turns off reverse metabolism
KM2 = 0               % turns off reverse metabolism
KATFN = 0             % turns off binding
KATNOL = 0            % turns off binding
```

```
%--------------BINDING MODEL--------------------
% Human Binding Parameters
%KATFN = 0.02
%KATNOL = 0.02
%BMAXBLDC = 1.49
%BMAXBRNC = 4.2
%BMAXLIVC = 89.5
%BMAXKIDC = 1.25
%BMAXBLD2C = 12.59
%BMAXBRN2C = 94.6
%BMAXLIV2C = 151.6
%BMAXKID2C = 85

%--------------REVERSE METABOLISM MODEL---------
%VMAX2C = 273.5
%KM2 = 88.5
%KATFN = 0              % turns off binding
%KATNOL = 0             % turns off binding

%-----------------------------------------------
TSTOP=1848
CINT=0.01
output @clear
prepare @clear
prepare @all

start @NoCallback

display auccbldfree
display auccbldfree2
display auccbrn
display auccbrn2
```

APPENDIX E

The acslX (version 2.5.0.6) .m file for comparison of simulations using partition coefficients determined by three methods by the PBPK model of triadimefon and triadimenol (Chapter 5) is contained within this appendix. The .m file contains first human physiological and chemical specific parameters, followed by code to generate the appropriate dosimetrics for the calculation of human equivalent doses. The code facilitates use of the original model, the binding model, or the reverse metabolism model based on which physiological parameters are enabled.

```
%time in hrs, TFN in uM, TNol in uM
RatLiv = [0.067    39.511    287.147
0.250    24.832    421.615
0.500    24.399    228.392
0.750    21.592    371.533
1.000    16.269    262.156
2.000    10.482    135.829
3.000    10.903    158.045
6.000    01.086    018.913
12.00    04.990    035.430
24.00    02.838    012.552];

%time in hrs, TFN in uM, TNol in uM
RatFat = [0.067    01.880    02.360
0.250    20.028    09.577
0.500    19.279    21.544
0.750    52.152    37.306
1.000    35.816    28.337
2.000    24.813    28.972
3.000    12.156    18.562
6.000    38.610    59.369
12.00    16.373    15.066
24.00    05.580    03.086];

%time in hrs, TFN in uM, TNol in uM
RatBld = [0.067    67.41487718    84.97011671
0.250    25.70349426    30.91374583
0.500    09.74675369    09.7616430
0.750    12.52958257    30.22047723
1.000    08.56557746    28.21581189
2.000    03.96634196    18.60690974
3.000    02.52507091    16.43837312
6.000    01.82701153    15.20864159
12.00    00.55176395    02.64689812
```

```
24.00    00.29671826    00.88786814];

%time in hrs, TFN in uM, TNol in uM
RatBrn = [0.067    169.021    15.376
0.250    056.629    43.463
0.500    023.162    44.462
0.750    022.857    54.913
1.000    013.934    61.254
2.000    004.054    22.873
3.000    003.234    26.106
6.000    001.569    17.997
12.00    000.686    03.365
24.00    000.407    05.749];

%time in hrs, TFN in uM, TNol in uM
RatKid = [0.067    83.735    205.783
0.250    43.259    150.402
0.500    21.485    086.186
0.750    31.819    124.579
1.000    02.332    015.430
2.000    04.724    032.816
3.000    05.429    046.987
6.000    03.674    041.683
12.00    01.170    009.620
24.00    00.417    002.825];

%----------------------In Vitro--------------------
    PLIV = 1.25
    PFAT = 13.58
    PKID = 1.333
    PBRN = 0.96
    PLIV2 = 1.44
    PFAT2 = 4.54
    PKID2 = 1.05
```

```
    PBRN2 = 1.18
    CLBLD2C = 0.69
    PAFATC = 0.012
    PAFAT2C = 0.044

%---------------------In Vivo-----------------------
    %PLIV = 2.56
    %PFAT = 8.67
    %PKID = 1.61
    %PBRN = 1.68
    %PLIV2 = 6.98
    %PFAT2 = 2.64
    %PKID2 = 2.76
    %PBRN2 = 1.50
    %CLBLD2C = 0.7
    %PAFATC = 0.014
    %PAFAT2C = 0.058

%---------------------Algorithm--------------------
    %PLIV = 9.52
    %PFAT = 347.6
    %PKID = 8.69
    %PBRN = 22.69
    %PLIV2 = 9.16
    %PFAT2 = 340.36
    %PKID2 = 8.53
    %PBRN2 = 22.0
    %CLBLD2C = 2.5
    %PAFATC = 0.015
    %PAFAT2C = 0.058

TSTOP=24
CINT=0.01
output @clear
```

```
prepare @clear
prepare @all
start @NoCallback

livx=[0.067 0.25 0.5 0.75 1 2 3 6 12 24];
livy=[39.511 24.832 24.399 21.592 16.269 10.482 10.903 1.086 4.99 2.838]
live=[17.797 19.079 9.986 9.023 12.162 4.017 4.222 0.286 1.137 0.801]
livh = errorbar(livx,livy,live)                              % Generate error bars
liv=plot(livh,1,_t,_cliv,RatLiv(:,1),RatLiv(:,2),'+')    % Overlay simulated results
settabtitle(liv,'Liver')

fatx=[0.067 0.25 0.5 0.75 1 2 3 6 12 24];
faty=[1.88 20.028 19.279 52.152 35.816 24.813 12.156 38.61 16.373 5.58]
fate=[0.705 8.22 12.302 36.476 28.951 22.489 6.457 3.182 2.199 1.189]
fath = errorbar(fatx,faty,fate)                               % Generate error bars
fat=plot(fath,1,_t,_cfat,RatFat(:,1),RatFat(:,2),'+')     % Overlay simulated results
settabtitle(fat,'Fat')

venx=[0.067 0.25 0.5 0.75 1 2 3 6 12 24];
veny=[67.415 25.703 9.747 12.53 8.566 3.966 2.525 1.827 0.552 0.297]
vene=[28.354 6.754 1.156 3.124 2.427 1.33 0.657 0.672 0.232 0.145]
venh = errorbar(venx,veny,vene)                               % Generate error bars
ven=plot(venh,1,_t,_cven,RatBld(:,1),RatBld(:,2),'+')      % Overlay simulated results
settabtitle(ven,'Blood')

brnx=[0.067 0.25 0.5 0.75 1 2 3 6 12 24];
brny=[169.021 56.629 23.162 22.857 13.934 4.054 3.234 1.569 0.686 0.407]
brne=[85.273 30.413 11.665 12.003 3.271 2.771 0.851 0.294 0.138 0.115]
brnh = errorbar(brnx,brny,brne)                               % Generate error bars
brn=plot(brnh,1,_t,_cbrn,RatBrn(:,1),RatBrn(:,2),'+')      % Overlay simulated results
settabtitle(brn,'Brain')

kidx=[0.067 0.25 0.5 0.75 1 2 3 6 12 24];
kidy=[83.735 43.259 21.485 31.819 2.332 4.724 5.429 3.674 1.17 0.417]
```

```
kide=[30.553 3.237 7.032 12.673 0.132 2.822 2.797 1.437 0.354 0.25]
kidh = errorbar(kidx,kidy,kide)                                % Generate error bars
kid=plot(kidh,1,_t,_ckid,RatKid(:,1),RatKid(:,2),'+')      % Overlay simulated results
settabtitle(kid,'Kidney')

liv2x=[0.067 0.25 0.5 0.75 1 2 3 6 12 24];
liv2y=[287.147 421.615 228.392 371.533 262.156 135.829 158.045 18.913 35.43 12.552]
liv2e=[112.208 67.825 103.788 106.874 28.702 85.861 38.701 4.411 10.839 4.569]
liv2h = errorbar(liv2x,liv2y,liv2e)                            % Generate error bars
liv2=plot(liv2h,1,_t,_cliv2,RatLiv(:,1),RatLiv(:,3),'+')   % Overlay simulated results
settabtitle(liv2,'Liver2')

fat2x=[0.067 0.25 0.5 0.75 1 2 3 6 12 24];
fat2y=[2.36 9.577 21.544 37.306 28.337 28.972 18.562 59.369 15.066 3.086]
fat2e=[0.412 5.862 17.762 22.982 10.532 21.859 10.797 0.751 1.426 1.012]
fat2h = errorbar(fat2x,fat2y,fat2e)                            % Generate error bars
fat2=plot(fat2h,1,_t,_cfat2,RatFat(:,1),RatFat(:,3),'+')   % Overlay simulated results
settabtitle(fat2,'Fat2')

ven2x=[0.067 0.25 0.5 0.75 1 2 3 6 12 24];
ven2y=[84.97 30.914 9.762 30.22 28.216 18.607 16.438 15.209 2.647 0.888]
ven2e=[101.932 14.528 10.856 5.055 5.84 5.002 7.145 2.316 1.197 0.524]
ven2h = errorbar(ven2x,ven2y,ven2e)                            % Generate error bars
ven2=plot(ven2h,1,_t,_cven2,RatBld(:,1),RatBld(:,3),'+')   % Overlay simulated results
settabtitle(ven2,'Blood2')

brn2x=[0.067 0.25 0.5 0.75 1 2 3 6 12 24];
brn2y=[15.376 43.463 44.462 54.913 61.254 22.873 26.106 17.997 3.365 5.749]
brn2e=[9.215 12.894 8.397 11.191 11.894 19.355 6.155 5.508 1.11 1.012]
brn2h = errorbar(brn2x,brn2y,brn2e)                            % Generate the error bars
brn2=plot(brn2h,1,_t,_cbrn2,RatBrn(:,1),RatBrn(:,3),'+')   % Overlay the simulated
results
settabtitle(brn2,'Brain2')
```

```
kid2x=[0.067 0.25 0.5 0.75 1 2 3 6 12 24];
kid2y=[205.783 150.402 86.186 124.579 15.43 32.816 46.987 41.683 9.62 2.825]
kid2e=[76.707 37.003 23.41 28.942 2.412 22.573 8.878 11.126 2.786 1.256]
kid2h = errorbar(kid2x,kid2y,kid2e)                          % Generate the error bars
kid2=plot(kid2h,1,_t,_ckid2,RatKid(:,1),RatKid(:,3),'+')   % Overlay the simulated
results
settabtitle(kid2,'Kidney2')
```